



VYSOKÉ UČENÍ TECHNICKÉ V BRNĚ
BRNO UNIVERSITY OF TECHNOLOGY



FAKULTA STROJNÍHO INŽENÝRSTVÍ
ÚSTAV MECHANIKY TĚLES, MECHATRONIKY A
BIOMECHANIKY

FACULTY OF MECHANICAL ENGINEERING
INSTITUTE OF SOLID MECHANICS, MECHATRONICS AND
BIOMECHANICS

DEVELOPMENT OF A VARIABLE ROLLER PUMP AND EVALUATION OF ITS POWER SAVING POTENTIAL AS A CHARGE PUMP IN HYDROSTATIC DRIVETRAINS

NÁVRH REGULAČNÍHO HYDROGENERÁTORU S VÁLEČKY V DRÁŽKÁCH
ROTORU A OHODNOCENÍ JEHO POTENCIÁLU ÚSPORY VÝKONU V
HYDROSTATICKÝCH POHONECH

DOCTORAL THESIS

DIZERTAČNÍ PRÁCE

AUTHOR

AUTOR

Ing. PETER ZAVADINKA

SUPERVISOR

VEDOUCÍ PRÁCE

doc. Ing. ROBERT GREPL, Ph.D.

BRNO 2015

STATUTORY DECLARATION

With this statement I claim, that this thesis is my genuine authorial thesis, which was created under leadership of my supervisors and with usage of mentioned references.

Peter Zavadinka, Brno, 2015

BIBLIOGRAPHIC CITATION

ZAVADINKA, P. *Development of a Variable Roller Pump and Evaluation of its Power Saving Potential as a Charge Pump in Hydrostatic Drivetrains*. Brno: Brno University of Technology, Faculty of Mechanical Engineering, 2015. 142 p.
Supervisor doc. Ing. Robert Grepl, Ph.D..

ACKNOWLEDGMENT

First of all, I would like to sincerely thank my supervisors doc. Ing. Robert Grepl, Ph.D. and doc. Ing. Peter Krissak, Ph.D. My thanks go to whole Institute of Solid Mechanics, Mechatronics and Biomechanics. I also would like to thank my managers Dr. Andreas Schumacher and Dr. Robert Rahmfeld for their great support regarding this work and all related articles.

My further thanks go to my work colleagues. Especially, Ing. Miroslav Chmatil, Ing. Andrej Babusa, Ing. Peter Urbanek and their group, who supported my work and brought an initial idea to deal with this topic in my doctoral thesis. Next to this, I would like to mention my colleagues in the simulation team and my former colleague Dr. Oliver Meincke. Also I thank to test lab engineers for their support during measurements and my friends Ing. Boris Novosad and Ing. Peter Stanak, Ph.D. for their help.

A special thank is dedicated to my parents: Milan and Zdenka and my whole family who support me in a perfect way all my life. Finally, I would like to express sincere gratitude to my wife Steffi, for her great patience and support.

ABSTRACT

Presented doctoral thesis deals with an extensive hydraulic variable roller pump analysis and the power saving prediction of hydrostatic drivetrains in the mobile machines achieved with a variable roller charge pump implementation.

At the first part of the work, the roller pump functionality was described and the theory of a 1-D simulation model was developed. Based on this developed simulation model is suitable for pressure profile prediction, roller force prediction and cross port leakage prediction which has a direct impact on the total volumetric efficiency. The simulation model was successfully used as a tool for optimization of the port plates, which was confirmed by measurements. The first part of the work includes the pump control force analysis validated by measurements and also the basic pressure compensator controls comparison. Developed control force prediction could help to improve the control performance. The measurements confirmed that the variable roller charge pump is able to successfully work in transmissions with measured types of the control.

The second part of the work analyzed the power saving potential of a variable charge pump for two selected typical mobile applications: telehandler (9 ton) and combine harvester (20 ton). This part required a 1-D drivetrain simulation model together with thermal behaviour of the hydrostatic transmission. Two different modifications of the charging systems were compared with the conventional charging system in simulations performed for the working and transporting mode. The drivetrain simulation of the variable roller charge pump with a bypass orifice confirms higher power savings only in cases when the pump speed was significantly higher than normal speeds and a relatively constant flushing flow through the bypass orifice to the pump case still ensures suitable cooling. The highest power savings were achieved with variable flushing flows, where the demand for charging flow was adjusted according to the hydrostatic transmission cooling requirements. At the end of the second part, this thesis deals with a variable charge pump sizing.

Keywords: variable roller charge pump, port plate optimization, 1-D simulation model, hydrostatic transmission drivetrain, flushing system, power saving potential, pressure regulation, telehandler, combine harvester.

ABSTRAKT

Predložená doktorandská dizertačná práca (ďalej len práca) sa zaoberá rozsiahlou analýzou valčekového hydrogenerátora s premenlivým geometrickým objemom a predikciou výkonových úspor dosiahnutých aplikáciou navrhnutého valčekového hydrogenerátora s premenlivým geometrickým objemom v hydrostatickom pohone vybraných mobilných pracovných strojov.

Teoretický rozbor princípov fungovania valčekového hydrogenerátora a teória jednorozmerného simulačného modelu sú popísané v prvej časti práce. Na základe odvodennej teórie je vytvorený simulačný model, ktorý je vhodný na predikciu priebehu tlaku v komorách valčekového hydrogenerátora, síl pôsobiacich na valček a na predikciu vnútorných únikov vzniknutých skratovaním rozvodovej dosky, ktoré majú priamy vplyv na objemovú účinnosť valčekového hydrogenerátora. Simulačný model bol úspešne použitý pre optimalizáciu rozvodových dosiek valčekového hydrogenerátora a vhodnosť simulačného modelu potvrdili následné merania. Práca obsahuje aj analýzu síl pôsobiacich na vodiaci prstenec, ktorej výsledky boli taktiež potvrdené meraním. Analýza týchto síl môže vylepšiť v konečnom dôsledku parametre budúcich tlakových regulácií. Práca ďalej obsahuje základné porovnanie použitých tlakových regulácií. Všetky uskutočnené merania potvrdili, že valčekový hydrogenerátor s premenlivým geometrickým objemom s testovanými tlakovými reguláciami je schopný úspešne pracovať v hydrostatickej prevodovke.

Druhá časť práce analyzuje potenciál výkonových úspor valčekového hydrogenerátora s premenlivým geometrickým objemom pre dve mobilné aplikácie - teleskopický nakladač s hmotnosťou 9 ton a kombajn s hmotnosťou 20 ton. Analýza vyžaduje jednorozmerný simulačný model hydrostatického pohonu s teplotnou predikciou hydrostatickej prevodovky. Dva rozdielne koncepty variabilného doplňovacieho systému hydrostatickej prevodovky sú porovnané so štandardným doplňovacím systémom pre pracovný a transportný režim oboch vybraných typov vozidiel. Simulácia pohonu vozidla s valčekom hydrogenerátorom s premenlivým geometrickým objemom vo funkcii doplňovacieho hydrogenerátora a obtokovou clonou potvrdili vyššie úspory iba v prípadoch, kedy rýchlosť doplňovacieho hydrogenerátora bola výrazne vyššia a prietok cez obtokovú clonu do skrine hlavného hydrogenerátora zabezpečil dostatočné chladenie. Najvyššie výkonové úspory boli dosiahnuté s premenlivým preplachovacím systémom, ktorého prietok sa menil podľa požiadaviek hydrostatickej prevodovky. Záver druhej časti práce sa zaoberá metodikou dimenzovania veľkosti doplňovacieho hydrogenerátora.

Kľúčové slová: variabilný valčekový doplňovací hydrogenerátor, optimalizácia rozvodovej dosky, jedno rozmerný simulačný model, pohon s hydrostatickou prevodovkou, preplachovací systém, potenciál výkonových úspor, tlaková regulácia, teleskopický nakladač, kombajn.

TABLE OF CONTENTS

NOMENCLATURE AND ABBREVIATIONS.....	13
1 INTRODUCTION	21
1.1 Motivation	22
1.2 Goals	23
2 STATE OF THE ART.....	25
2.1 Roller Pump	25
2.2 Variable Charging System.....	31
3 THEORETICAL BACKGROUND OF ROLLER PUMPS.....	35
3.1 Basic Equations.....	36
3.2 Fluid Equations.....	39
3.3 Roller Equations	43
3.4 Derivation of Cam Ring Forces	44
3.5 Roller Sealing Contact	47
4 ROLLER PUMP CONTROL.....	49
4.1 Pressure Compensator (PC) Controls	51
4.2 Control Dynamics	54
4.2.1 Simple PC Control.....	54
4.2.2 Spool PC Control.....	57
4.3 Performance Measurements.....	60
4.3.1 Pressure Ramps.....	60
4.3.2 Speed Ramps	63
4.3.3 Response and Recovery.....	66
5 PORT PLATE OPTIMIZATION	69
5.1 Simulation Method	71
5.2 Optimization Method	73
5.3 Simulation and Optimization Results	75

5.4	Verification Method	81
5.4.1	Volumetric Efficiency	81
5.4.2	Control Spring Force	85
5.5	Verification of Simulation Results	87
6	MODELLING OF HYDROSTATIC DRIVETRAIN FOR POWER SAVING EVALUATION	93
6.1	Variable Roller Charge Pump in HST	97
6.2	Simulation Model of the Drivetrains	100
6.2.1	Hydro-Mechanical Drivetrain Model	101
6.2.2	HST Thermal Model	102
6.2.3	Drivetrain Model Implementation	106
6.3	Verification of Simulation Model	107
7	POWER SAVING POTENTIAL	113
7.1	Analyze vehicles and their operating conditions	113
7.1.1	Telehandler Results for Loading	115
7.1.2	Telehandler Results for Transport	121
7.1.3	Combine Harvester Results for Transport	121
7.1.4	Combine Harvester Results for Harvesting	123
7.2	Recommendations for Sizing of a Variable Charge Pump in HST	124
8	CONCLUSION	129
8.1	Contribution of Doctoral Thesis	130
	REFERENCES	131
	AUTHOR'S PUBLICATIONS	136
	ATTACHMENTS	139

NOMENCLATURE AND ABBREVIATIONS

Symbol	Unit	Description
A	(m^2)	Orifice cross section area
A_f	(m^2)	Surface area used for forced convection
A_n	(m^2)	Surface area used for natural convection
A_{ser}	(m^2)	Servo area
A_{spo}	(m^2)	PC spool area
B_{cam}	$(\text{N}\cdot\text{m}\cdot\text{s})$	Cam ring damping
C_c	$(\text{m}^3\cdot\text{Pa}^{-1})$	Oil compliance
c	$(\text{J}\cdot\text{kg}^{-1}\cdot\text{K}^{-1})$	Specific heat coefficient
c_c	$(\text{J}\cdot\text{kg}^{-1}\cdot\text{K}^{-1})$	Component specific heat coefficient
c_n	(-)	Target value vector
c_{oil}	$(\text{J}\cdot\text{kg}^{-1}\cdot\text{K}^{-1})$	Oil specific heat coefficient
D_{rol}	(m)	Roller diameter
D_{rot}	(m)	Rotor diameter
d_{cam}	(m)	Cam ring inner diameter
E	(J)	Control volume energy
e_{rot}	(m)	Rotor eccentricity
e_{rotMax}	(m)	Maximal rotor eccentricity
F_c	(N)	Centrifugal force
F_{cor}	(N)	Coriolis force
F_{cham}	(N)	Chamber pressure force
F_{fcam}	(N)	Cam ring friction force
F_{frot}	(N)	Rotor friction force
F_{ncam}	(N)	Cam ring normal force
F_{nrot}	(N)	Rotor normal force
F_{spr}	(N)	Cam ring spring force
F_{spr0}	(N)	Cam ring spring preload

F_{whe}	(N)	Traction force
f_{rol}	(-)	Wheel rolling resistance coefficient
G_n	(-)	Quality criteria vector
G_{VCPf}	(-)	VCP transfer function (with flow input)
G_{VCPp}	(-)	VCP transfer function (with pressure input)
g	($m \cdot s^{-2}$)	Gravitation acceleration constant
h_f	($W \cdot m^{-1} \cdot K^{-1}$)	Forced convection heat transfer coefficient
h_{in}	(J)	Input enthalpy
h_{moon}	(m)	Half-moon height
h_n	($W \cdot m^{-1} \cdot K^{-1}$)	Natural convection heat transfer coefficient
h_{out}	(J)	Output enthalpy
I_{eng}	($kg \cdot m^{-2}$)	Engine rotational inertia
I_{cam}	($kg \cdot m^{-2}$)	Cam ring rotational inertia
I_{pum}	($kg \cdot m^{-2}$)	Pump rotational inertia
I_{rol}	($kg \cdot m^{-2}$)	Roller rotational inertia
i_{mec}	(-)	Mechanical transmission ratio
K	(Pa)	Fluid Bulks modulus
K_A	(Pa)	Adiabatic Bulks modulus
K_{cam}	($N \cdot m$)	Cam ring spring rate
K_f	($N \cdot m^{-1}$)	Flow force gain
K_{lea}	($m^3 \cdot s^{-1} \cdot Pa^{-1}$)	Leakage coefficient
K_{pre}	(m^3)	Pressure torque gain
K_q	($m^2 \cdot s^{-1}$)	Spool flow gain
K_{VCP}	(m^3)	Pump flow gain
k_{spo}	($N \cdot m^{-1}$)	PC spool spring rate
L_G	(-)	Quality criteria vector length
m_c	(kg)	Component mass
\dot{m}_{in}	($kg \cdot s^{-1}$)	Input oil mass flow
\dot{m}_{out}	($kg \cdot s^{-1}$)	Output oil mass flow

m_{rol}	(kg)	Roller mass
m_{veh}	(kg)	Vehicle mass
n_{mot}	(s ⁻¹)	Motor speed
n_{pum}	(s ⁻¹)	Pump speed
n_{rot}	(s ⁻¹)	Rotor speed
O_{pinX}	(m)	Pivot horizontal offset
O_{pinY}	(m)	Pivot vertical offset
P_{cool}	(W)	Cooling power
P_{fue}	(W)	Fuel power
$P_{lossConM}$	(W)	Motor power control losses
$P_{lossConP}$	(W)	Pump power control losses
P_{loss}	(W)	Power losses in the circuit
$P_{lossCheck}$	(W)	Check valves power losses
P_{lossCP}	(W)	Charge pump power losses
$P_{lossCPRV}$	(W)	CPRV power losses
$P_{lossHose}$	(W)	Power losses in hoses (pressure drops)
$P_{lossHPRV}$	(W)	HPRV power losses
P_{lossLF}	(W)	LF power losses
P_{lossM}	(W)	Motor power losses (kit losses and pressure drops)
P_{lossP}	(W)	Pump power losses (kit losses and pressure drops)
$P_{lossMTotal}$	(W)	Overall power motor losses
$P_{lossPTotal}$	(W)	Overall power pump losses
P_{whe}	(W)	Wheel power
p	(Pa)	Pressure
p_{atm}	(Pa)	Atmospheric pressure
p_{ch}	(Pa)	Charge pressure
p_{dis}	(Pa)	Discharge pressure
p_{HP}	(Pa)	High pressure
p_{inn}	(Pa)	Inner chamber pressure

p_{LP}	(Pa)	Low pressure
p_{out}	(Pa)	Outer chamber pressure
p_{set}	(Pa)	Control setting pressure
p_{sys}	(Pa)	System (drivetrain) pressure
Q	($m^3 \cdot s^{-1}$)	Flow rate
Q_{CF}	($m^3 \cdot s^{-1}$)	Cooling flow rate
Q_{caseM}	($m^3 \cdot s^{-1}$)	Motor case flow rate
Q_{caseP}	($m^3 \cdot s^{-1}$)	Pump case flow rate
Q_{caseCP}	($m^3 \cdot s^{-1}$)	Charge pump leakage flow rate
Q_{contM}	($m^3 \cdot s^{-1}$)	Motor control flow rate
Q_{contP}	($m^3 \cdot s^{-1}$)	Pump control flow rate
Q_{ch}	($m^3 \cdot s^{-1}$)	Charge pump flow rate
Q_{check}	($m^3 \cdot s^{-1}$)	Check valves flow rate
Q_{CPRV}	($m^3 \cdot s^{-1}$)	CPRV (or bypass) flow rate
Q_e	($m^3 \cdot s^{-1}$)	Effective output flow rate
Q_e	($m^3 \cdot s^{-1}$)	Effective output flow rate
Q_{gL}	($m^3 \cdot s^{-1}$)	Gap flow rate – left roller side
Q_{gR}	($m^3 \cdot s^{-1}$)	Gap flow rate – right roller side
Q_{HP}	($m^3 \cdot s^{-1}$)	High pressure flow rate
Q_{HPout}	($m^3 \cdot s^{-1}$)	Flow rate from HP to outer chamber
Q_{HPinn}	($m^3 \cdot s^{-1}$)	Flow rate from HP to inner chamber
Q_{HPRV}	($m^3 \cdot s^{-1}$)	HPRV valves flow rate
Q_{in}	($m^3 \cdot s^{-1}$)	Control volume input flow rate
Q_{leakM}	($m^3 \cdot s^{-1}$)	Motor leakage flow rate
Q_{leakP}	($m^3 \cdot s^{-1}$)	Pump leakage flow rate
Q_{LF}	($m^3 \cdot s^{-1}$)	Loop flushing flow rate
Q_{LP}	($m^3 \cdot s^{-1}$)	Low pressure flow rate
Q_{LPout}	($m^3 \cdot s^{-1}$)	Flow rate from LP to outer chamber
Q_{LPinn}	($m^3 \cdot s^{-1}$)	Flow rate from LP to inner chamber

Q_{Loa}	$(m^3 \cdot s^{-1})$	Load flow rate
Q_{out}	$(m^3 \cdot s^{-1})$	Control volume output flow rate
Q_{pum}	$(m^3 \cdot s^{-1})$	Pump flow rate
Q_{se}	$(m^3 \cdot s^{-1})$	External flow losses rate
Q_{sf}	$(m^3 \cdot s^{-1})$	Filling flow losses rate
Q_{si}	$(m^3 \cdot s^{-1})$	Internal flow losses rate
Q_{sk}	$(m^3 \cdot s^{-1})$	Compression flow losses rate
Q_{sucCP}	$(m^3 \cdot s^{-1})$	Charge pump suction flow from tank
\dot{q}	$(J \cdot s^{-1})$	Heat rejection rate
\dot{q}_{CA}	$(J \cdot s^{-1})$	Convective-radiative heat transfer rate
\dot{q}_{FC}	$(J \cdot s^{-1})$	Forced convection heat transfer rate
r_{whe}	(m)	Wheel radius
T	(K)	Temperature
T_A	(K)	Ambient temperature
T_c	(K)	Component mass temperature
T_F	(K)	Fluid temperature
T_{dam}	$(N \cdot m)$	Damping torque
T_e	$(N \cdot m)$	Effective torque
T_{eng}	$(N \cdot m)$	Engine torque
T_f	(K)	Fluid temperature
T_{loop}	(K)	Loop oil temperature
T_{mot}	$(N \cdot m)$	Motor torque
T_{pum}	$(N \cdot m)$	Pump torque
T_s	$(N \cdot m)$	Torque losses
T_{Tank}	(K)	Tank oil temperature
T_{the}	$(N \cdot m)$	Theoretical torque
t	(s)	Time
u_{cam}	(m)	Cam ring radius (from rotor center)
V	(m^3)	Control fluid volume

V_{dea}	(m^3)	Dead volume
V_F	(m^3)	Fluid volume
V_g	(m^3)	Pump displacement
V_{gMax}	(m^3)	Maximal pump displacement
V_L	(m^3)	Air volume
V_{imm}	(m^3)	Inner chamber volume
V_{max}	(m^3)	Maximal volume
V_{out}	(m^3)	Outer chamber volume
v_{veh}	$(m \cdot s^{-1})$	Vehicle speed
v_{whe}	$(m \cdot s^{-1})$	Wheel speed
\dot{W}	$(J \cdot s^{-1})$	Work rate
w_{rol}	(m)	Roller width
x_{Rrol}	(m)	Roller radial stroke
x_{Trol}	(m)	Roller tangential stroke
z_{rol}	$(-)$	Number of rollers

Greek Letters

α_D	$(-)$	Orifice discharge coefficient
β_{dev}	$(-)$	Deviation angle caused by a rotor eccentricity
γ	(K^{-1})	Thermal volumetric expansion coefficient
ε	$(-)$	Emissivity of the black body
η_{chp}	$(-)$	Charge pump efficiency
η_{eng}	$(-)$	Engine efficiency
η_{hm}	$(-)$	Hydro-mechanical efficiency
η_{mec}	$(-)$	Mechanical transmission efficiency
η_{mot}	$(-)$	Motor efficiency
η_{pum}	$(-)$	Pump efficiency
η_t	$(-)$	Overall efficiency
η_v	$(-)$	Volumetric efficiency

κ	(-)	Polytropic exponent
λ	(-)	Parameterizing function
ρ_{oil}	($\text{kg}\cdot\text{m}^3$)	Oil density
σ	(-)	Optimization coefficient
σ_{SB}	($\text{W}\cdot\text{m}^{-2}\cdot\text{K}^{-4}$)	Stefan-Boltzmann constant
ν	($\text{m}\cdot\text{s}^{-2}$)	Kinematic viscosity
φ	(-)	Angular position (angle)
φ_0	(-)	Angular offset from analyzed chamber to the origin
φ_{cam}	(-)	Cam ring angle
φ_{cham}	(-)	Chamber angular position (angle)
$\ddot{\varphi}_{rol}$	(s^{-2})	Roller angular acceleration
φ_{rot}	(-)	Rotor angle
ψ_{dev}	(-)	Chamber deviation angle
ω_{pum}	(s^{-1})	Pump shaft speed
ϑ	(-)	Slope (hill) angle
ϑ_{moon}	(-)	Half-moon angle
ϑ_{cham}	(-)	Chamber pressure force angle
ϑ_{rol}	(-)	Roller force angle

Abbreviations

1-D	One dimensional
BIBO	Bounded input bounded output
CFD	Computational fluid dynamics
CP	Charge pump
CPL	Cross port leakage
CPRV	Charge pump relief valve
CVT	Continuously variable transmission
FCP	Fixed charge pump
Fr.	Front

HP	High pressure
HPRV	High pressure relief valve
HST	Hydrostatic transmission
IPC	International patent classification
ISO	International organization for standardization
LP	Low pressure
LF	Loop flushing
LPG	Liquid petroleum gas
MBS	Multi body simulations
No	Number
PC	Pressure compensator
SAE	Society of automotive engineers
TMP	Transit mixer pump
VCP	Variable charge pump

1 INTRODUCTION

Hydrostatic drivetrains are used in many areas of mobile applications where high power density, dynamic performance and flexible installation are required [1]. Especially the CVT (Continuously Variable Transmission) ability and high power density are important for mobile working machines, where hydrostatic transmissions (HST) together with other hydrostatic drivetrain components fulfill hard requirements of mobile machine producers. An easy overload protection, low inertia and dynamic braking capability are next advantages of the HST. The key disadvantage of the HST is lower efficiency in comparison with discrete gear transmission [2].

The basic HST is a hydraulic system. It contains: pump, motor, hoses, required control systems, required valves and charge pump (CP). The example of the simple hydrostatic drivetrain is shown in *Fig. 1.1*.

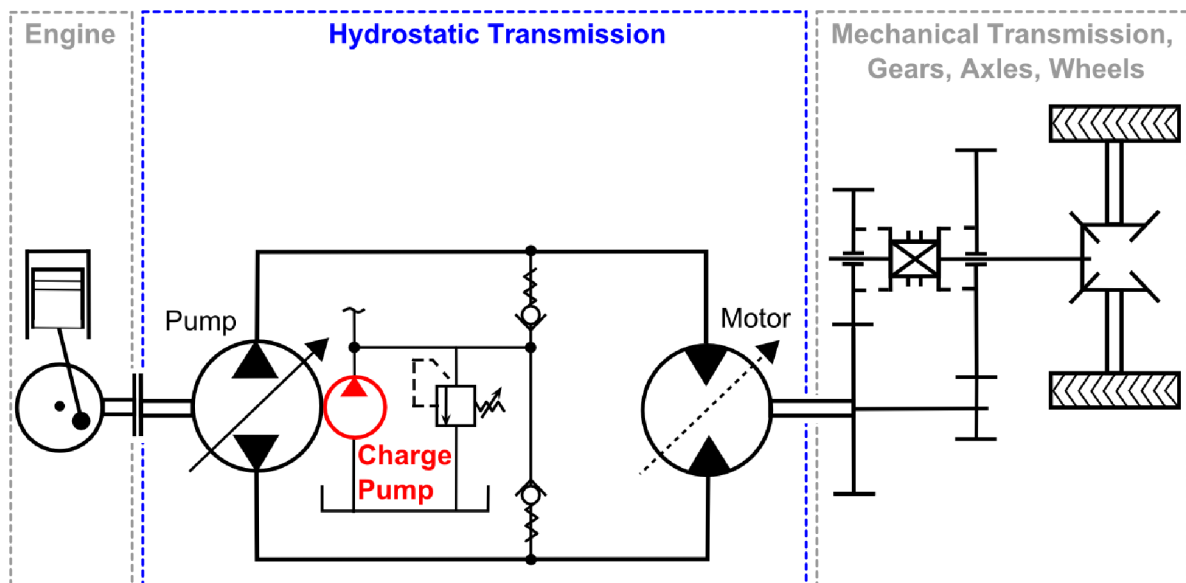


Fig. 1.1: The example of the simple hydrostatic drivetrain.

In this figure the charge pump is represented by red color. It can be seen that the charge pump is (usually) mounted on the main pump shaft. In the most cases, the charge pump is implemented into main pump end cap due to design space limitation in the HST.

The CP doesn't participate on the energy transfer from the engine to wheels but it has to ensure a correct HST functionality and performance. The charge pump has to provide enough flow for all demanded functions (displacement controls, flushing...) and ensure enough flow for maintaining sufficient pressure in the low pressure line to prevent cavitation. Based on the previous text it becomes clear, that the charge pump is one of the key components in the hydrostatic drivetrain system. The failure of the CP results in a failure of the whole hydrostatic drivetrain.

The CP is not only the key component with high demands on the durability, but it is also the component with power demands. Due to the fact that the CP doesn't participate on the energy transfer from the engine to wheels, it is clear, that the input CP power is considered as a power loss from the drivetrain point of view. Based on this, each decrease of the CP input power demand means the drivetrain power loss decrease with the same value.

1.1 Motivation

The actual mobile machinery market indicates a lot of global trends but one trend is stable, the trend of focusing on ownership costs minimization. It is caused by many factors, from which two are the most important. The first one is simply fuel cost. The behavior of fuel costs on the world market shows a still increasing trend, which is driven by stable increase of world oil consumption and decrease of world oil supplies. Due to these facts fuel costs forecast has an increasing trend. The second factor is the exhaust regulations driven by government regulations. The European EURO IIIb and US TIER 4 regulations are already valid [3], [4]. These regulations progressively decrease exhaust emissions for combustion engines, and again the exhaust regulation forecast has an increasing trend. Fuel costs and exhaust regulations act on the mobile machinery industry in the same direction and result in the requirement for high efficiency of drivetrains.

Many works focused on the main drives of mobile machines, can be found (for example [5], [6]) but auxiliary drives could also contribute to higher efficiency of mobile machines, for example fan drive, steering and charge systems are powered by the combustion engine too. A focus on the charge pump in the hydrostatic transmission can show that the fixed pumps don't act in all operating conditions very well. The charge pump delivers in some conditions higher flow than is required. An application of a variable charge pump into hydrostatic transmissions, which can act according to the system needs, could save additional energy and therefore increase efficiency.

The variable charge pump in the HST has to fulfill following requirements: displacement variability, compact design, durability, pressure compensator control availability and low cost. Based on this, variable gear pump, variable vane pump and variable roller pump were considered for the variable charge pump application. The roller pump and the vane pump are very similar. Manufacturing costs and the durability of the roller pump prefers the variable roller charge pump instead of the variable vane pump.

The power saving potential of variable charge pump is depending on the ratio of pump displacement variability, the bigger the ratio, the higher the potential of power savings. Due to the high variability of the displacement of a variable roller charge pump, which is for example higher than the standard variability of a variable gear pump [7], it was chosen for efficiency analyses in this work.

Different power savings, filling and cooling demands could be expected for different working cycles and various drivetrain structures (vehicles). The variable roller charge pump has to ensure power savings with an adequate filling and cooling function for various working conditions and vehicle types. Due to this, suitability and power saving potential of a variable roller charge pump in the hydrostatic drivetrain have to be evaluated. The power saving potential is not only depending on the displacement variability but also on the pump efficiency. Thus the full power saving potential of a variable roller pump could be achieved with an optimization of the port plates design because the efficiency of a roller pump is determined by port plate design similar to the valve plate design in axial piston pump.

The presented work should be focused on the energy saving potential of a variable roller charge pump used in mobile machines. Finally it means the potential for fuel savings and emissions. These savings should be achieved by the displacement variability of the charge pump. Previous implementation efforts of a variable charge pump were not successful because a lot of theoretical knowledge was not available and the power saving potential was

not interesting for mobile machines producers in the past due to relatively low mobile machine ownership costs. The supposition is that with implementation of variable roller charge pump with maximal displacement 20 cm^3 into hydrostatic drivetrain could be saved about 3-5% of engine power when it is not necessary to ensure high charging flow. Of course better results could be achieved with bigger charge pumps. The durability of the pump, cooling demands decrease and possible drive simplification via system components changes in existing circuits are next possible benefits for mobile machinery.

1.2 Goals

This work deals with a variable roller pump theoretical analysis, an optimization and its application into existing systems, especially into hydrostatic transmissions. Generally, the goals and the whole work can be divided into two parts.

The first part is more focused on the component analysis. The theory for roller pump is not generally published and this theory has to be derived in comprehensive form. This theory enables the simulation model building which allows, together with suitable optimization methods, efficiency optimization focused on the volumetric efficiency. The key elements which determine pump efficiency are the kidneys on the port plates. Due to this, whole optimization is realized through the port plate design changes. Proposed port plate designs have to be tested and measurements compared with simulations for the confirmation of the theory.

The second part of this work is focused on the system analysis based on a 1-D (one dimensional) drivetrain simulation. This simulation model has to include a thermal hydrostatic transmission sub-model as well. The power saving potential of the variable charge pump is analyzed for two different mobile working machines (vehicles). These analyses require a proposal of a variable charge pump implementation into hydrostatic transmission. The gained experiences are formed into sizing methodology for variable charge pumps. The work has to extend the actual state of the art in variable roller pump control and its application into hydrostatic transmission. Based on the previous lines and state of the art, the following goals can be defined:

- Derivation of theory (kinematics, dynamics, hydromechanics) of a variable roller pump (necessary for building a 1-D simulation model).
- Optimization of a variable roller pump with focus on the (volumetric) efficiency.
- Port plate design as one of the main variable roller pump parts responsible for efficiency value. This design has to use 1-D simulation model developed according to derived theory.
- Testing of designed port plates.
- Analysis of power saving potential for two selected mobile working machines.
- Proposal of a modification of a variable roller charge pump system in existing hydrostatic transmission systems.
- Creation of sizing methodology for variable roller charge pump in hydrostatic transmission.
- Extension of the state of the art in the field of the variable roller charge pump control and its use in hydrostatic systems.

2 STATE OF THE ART

State of the Art is defined, in one of many definitions, as "the incorporation of new ideas and the most up to date knowledge in order to make advancements in the already existing knowledge" [8]. According to this definition, "state of the art" is the process with which a new unique idea is incorporated in any field of technology, literature and architecture. In general language is State of the Art defined as the development of new techniques and procedures by expert people in a particular field [8]. As an example of Roller pump State of Art is selected and shortly described a few well known patents and non-patent literature information.

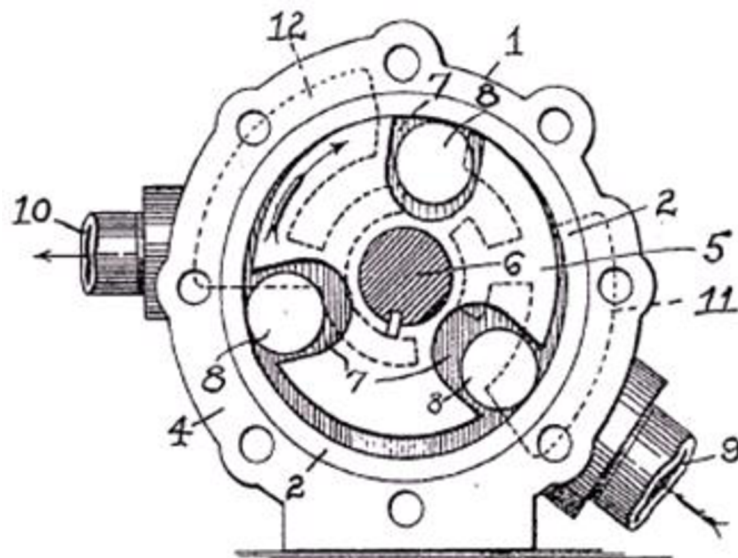


Fig. 2.1: Selected invention part from GB306031A.

2.1 Roller Pump

With roller vane pump in the title or abstract and F04C as the European Classification, can be found 143 results in the worldwide databases. The effort to commercialize roller pumps in hydraulic area is known since 1928, when L. P. Barlow filed of the first patent applications GB306031A related to rotary pumps in which roller pistons are impelled around the inside of a chamber through the -medium of a slotted rotor (*Fig. 2.1*). Since that time roller pump has been started to be employed in a wide variety of applications for many years. See as well for example patents GB450595A (1934), GB489955A (1937), US2460018A (1945), GB591143A (1947), GB654808A (1948), GB856687A (1957), GB1171907A (1969), US3938918A (1974), JP59196986A (1983) and many others. For our needs most of all interesting inventions are published in last two decades.

Patent publication US6312243B1 (1997) relates to a roller vane pump (*Fig. 2.2*) used for operating an automatic transmission for motor vehicles and in particular for pumping automatic transmission fluid in a continuously variable transmission. In this patent publication is stated that the pump is provided with pump housing, a rotor located in the pump housing and rotatable by means of a drive shaft, a cam ring located around rotor and roller elements slideably accommodated with some tolerance in slots on the periphery of the rotor. During rotation of the rotor, the roller elements interact in a sealing manner with the surface

of the cam ring. The cam ring, the rotor, the roller elements and the pump housing define a number of pump chambers, which may arrive interact with hydraulic channels in the pump housing for allowing flow of fluid to and from the pump chambers. Fluid is communicated between a hydraulic channel and a pump chamber either through one or more suction ports for allowing a predominantly axial flow of fluid to a pump chamber, or through one or more discharge ports for allowing a predominantly axial flow of fluid out of a pump chamber.

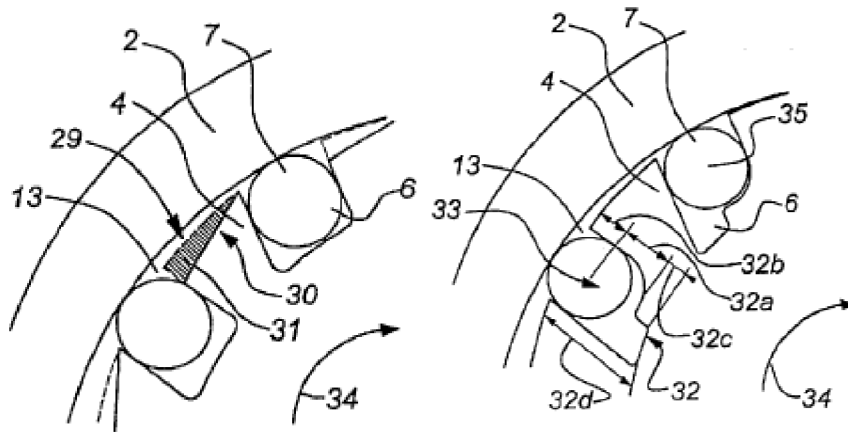


Fig. 2.2: Selected invention part from US6312243B1.

Such a roller vane pump is known also from the European patent EP0555909B1 (1992). This patent states that roller vane pump is in particular adapted for pumping of large volumes of fluid particularly automatic transmission fluid, while maintaining a high pressure in a hydraulically controlled and operated continuously variable transmission used for motor vehicles.

An invention presented in patent publication US6447277B1 (2000) relates to a mechanically driven roller vane pump (*Fig. 2.3*) used for operating an automatic transmission for motor vehicles, in particular a continuously variable transmission (CVT). In this patent is stated that the aim of the invention is to reduce the noise generated by the pump, to reduce the wear of pump parts, and to obtain higher pump efficiency. This aim is, according to the insight underlying the present invention, achieved in enlarging the surface area of the apertures through which fluid is allowed to flow to and from the pump chambers. In particular, this aim is achieved in providing for a modified shape of the ridge, wherein at least one of an inner surface and an outer surface of the ridge extends substantially parallel to the cam ring surface over a substantial part of the tangential dimension of said ridge. At the same pump yield, a larger surface area of the apertures means a less extreme under pressure, i.e. a higher feed pressure in a pump chamber when in communication with the feed channels, which results in a reduction of noise generated by the pump and in a reduction of wear of pump parts. The surface area of the apertures in the known roller vane pump is smaller than said surface area in the pump according to the present invention, because in the known pump the ridge surfaces have the shape of a segment of a circle and extend substantially parallel to the circular periphery of the carrier. With this known shape of the ridge, the distribution of the flows of fluid among the inner aperture and the outer aperture is not well-balanced and not optimal for most tangential positions of the carrier. In a preferred embodiment of the pump according to the invention, the surface area of the apertures is at a maximum, because the ridges are located such that the radial distance between the center lines of the ridges and the cam ring surface is substantially equal to the radius of the roller elements.

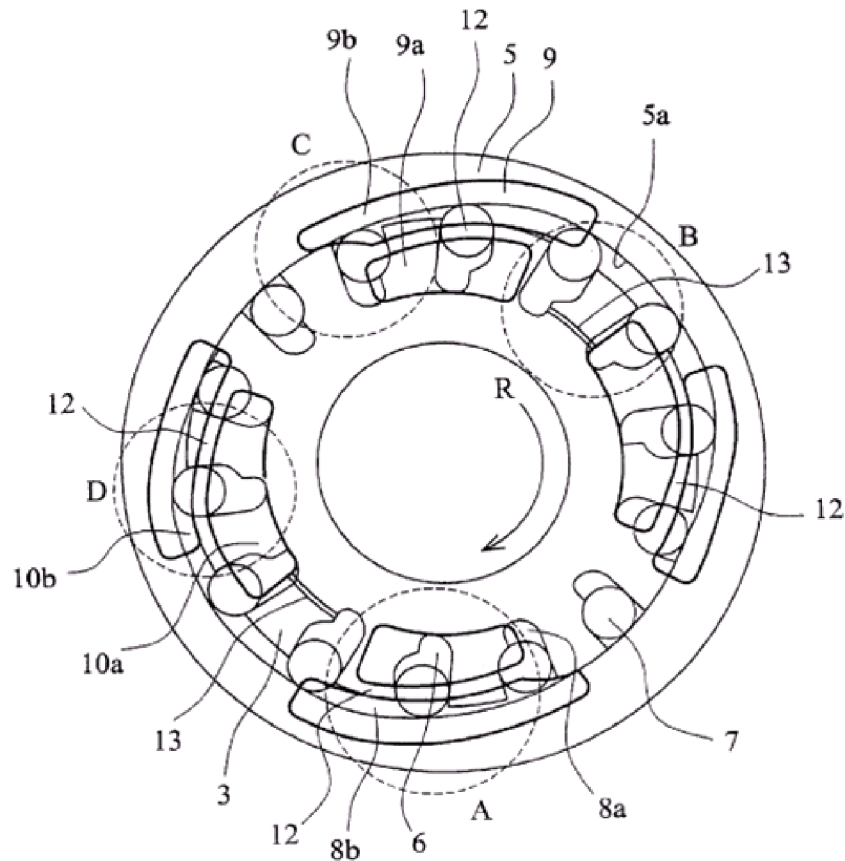


Fig. 2.3: Selected invention part from US6447277B1.

This configuration also provides an optimal axial support of the roller elements by supporting the roller elements centrally and over a maximum possible surface area of the roller elements for a given radial width of the ridges. Another drawback of the known roller vane pump is that the roller elements are known to intermittently loose contact with the cam ring surface, which is particularly undesirable at the instance the fluid pressure in a pump chamber associated with a roller element changes from the feed pressure to the discharge pressure and vice versa. This undesired loss of contact amounts to wear of pump parts, noise generated by the pump and a decrease in pump efficiency. The roller element loses contact with the cam ring surface when a force generated by a pressure difference between the carrier chamber and the corresponding cam chambers is directed radially inward and has a higher value than the centrifugal force, which is directed radially outward. The roller element then moves in radial inward direction under influence of a resultant force, which is directed radially inward, and loses contact with the cam ring surface. Such an undesired movement occurs when the fluid pressure in the carrier chamber is lower than the mean fluid pressure of the corresponding cam chambers.

With this construction, a less abrupt pressure increase in the carrier chamber is obtained than with the known construction wherein the carrier chamber arrives directly into communication with a discharge aperture having a relatively large radial dimension. With respect to the known constructions incorporating an end-part having a radial width which increases in the direction of rotation of the carrier, the pump performance is improved in that for a substantial part of the range of rotational speeds of the carrier gradual pressure changes in the pump chamber are obtained.

It was found that a groove having a rectangular cross section is particularly suitable for a CVT like application of the roller vane pump, wherein the pump must be able to cope with high pressures and a widely variable rotational speed of the carrier. Such a groove preferably has a depth in axial direction that increases in the direction of rotation of the carrier. Due to the gradual pressure changes that will be achieved with the measure according to the invention, the noise generated by the pump is reduced as is the wear of pump parts. In a preferred embodiment of the pump according to the present invention, the pump is provided with a gap between the roller elements and the carrier in tangential direction. In a preferred embodiment of the invention the width of the gap in tangential direction is dimensioned such that the rate at which the fluid pressure changes in the cam chamber during operation substantially corresponds to that in the carrier chamber. According to the invention the width of the gap in tangential direction may also be dimensioned such, that it corresponds to a minimum width in tangential direction required for allowing said pressure difference to become approximately zero. It is remarked, that taking a minimum width of the gap for achieving the above-mentioned requirements is highly advantageous, because then the amount of tangential movement and the tangential speed of the roller elements is limited, thereby limiting pump noise and wear. A width in tangential direction having a value in the range from 0.03 mm to 0.18 mm was found to be particularly suitable. In a presently favored design of the roller vane pump such range corresponds to about 0.5 to 2.5 percent of a diameter of the roller element.

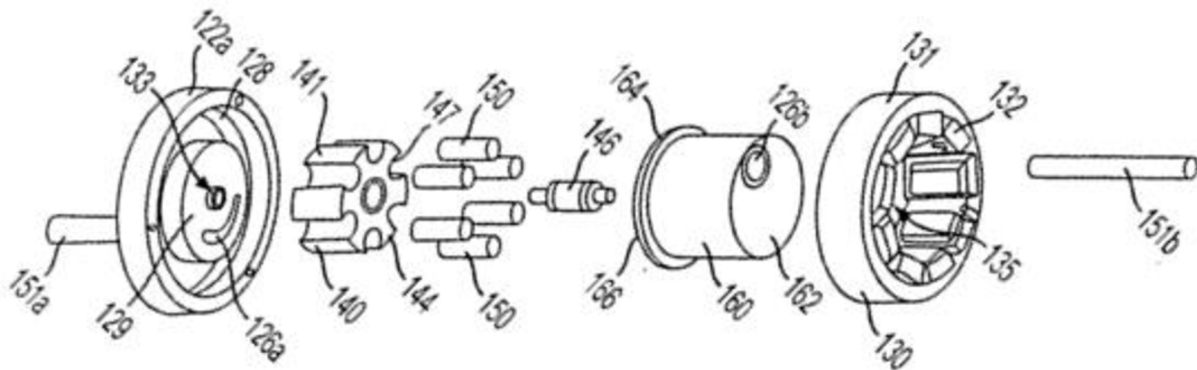


Fig. 2.4: Selected invention part from US2010047097A1.

The subject (Fig. 2.4) of patent application US2010047097A1 (2008) or US2010047088A1 (2008) are directed to a roller vane pump driven by an electric motor, wherein the rotor assembly of the electric motor also serves to pressurize the working fluid. In an effort to simplify pump design US6109887A (1997), the disclosure of which is herein incorporated by reference in its entirety, has added a blade to a rotor to push the working fluid. The patent US6109887A says that the overall pump is still relatively large as a blade was simply added onto a traditional rotor. In view of the above, there is a need for an improved pump that has parts which serve multiple functions to simplify design and decrease the overall profile. Pumps in accordance with the subject disclosure have numerous applications such as fuel cells or as a cooling pump for a spacecraft, avionics equipment or for computers and high-power electronics. Such pumps are miniature and can pump fluids in pumped two-phase electronics cooling loops and be used for any applications requiring a small pump. The subject disclosure is also directed to a vane pump assembly including a cylindrical pumping wall having an inner circumferential surface defining a pumping chamber. A rotor assembly is eccentrically mounted with respect to the cylindrical pumping wall for axial rotation, the rotor assembly having a rotor body defining a plurality

of circumferentially spaced apart radially extending vane pockets intermediate projections, each projection being magnetic. A cylindrical roller is supported in each radially extending vane pocket and a stator assembly surrounds the cylindrical pumping wall. The stator assembly has windings for generating a magnetic field to act upon the projections. Housing surrounds the stator assembly and defines inlet and outlet ports for ingress and egress of fluid. Preferably, the rotor body has six projections and six vane pockets and the stator assembly has nine windings. The cylindrical pumping wall may include a closed end and an open end, which has been sealed to the housing to form a pressure boundary around the rotor assembly and within the stator assembly, wherein the open end of the cylindrical pumping chamber has a flange that is hermetically sealed to an annular groove formed in an inner face of the housing.

Literature search presented in this thesis shows some works dealing with roller pumps as well. Danardono and coauthors deal with fixed LPG roller vane pump in [9]. They focused on the roller pump which is used for LPG fuel pumping from the tank. The purpose of this work was to optimize the design of the roller vane pump in order to suppress cavitation and increase fuel flow rate with computational fluid dynamics (CFD) simulations. Simulations were performed at pump speed 2600 min^{-1} and delta pressure 5 bar. Increase of the inlet port cross section area, modification of the rotor size and increase of chamber volume gave the best results in increasing the flow rate of the pump with acceptable risk of the cavitation. Change of the kidney timing didn't have a significant influence.

Kinematic and force analysis were done by Zhurba and Cleghorn in [10]. The authors deal with a fixed balanced (double acting pump) roller pump, which is used as a pressure source for transmission, accessory drive and other applications. Obtained equations include inputs such as geometry, shaft speed, inlet pressure and outlet pressure. The outputs are shaft torque, dynamic and kinematic parameters of the roller. The model includes dissipative forces to account for hydraulic effects. A comparison between measurements and simulations shows a very good agreement, but in low delta pressures up to 5 bar only. This work provides a good base for kinematic and dynamic analysis of a double action (balanced) roller pump, which could be adapted for single action (unbalanced) roller pump.

Jiadi and coauthors analyzed a roller slot design for a fixed balanced (double acting pump) roller pump in [11]. The target of this work was to decrease the contact force between roller and cam ring. The optimal slot angle is 42.5° according to the calculation performed in this article. The similar works from the same research group can be found in [12], [13]. Both articles deal with a roller pump for spraying applications. These pumps operate in low pressures.

The roller pump control is not the main focus of this work. Actually no article about roller pump controls are available but articles which deal with a vane pump control could be used due to the identical principle of the displacement change. Very good papers were written by Karmel in [14], [15], [16]. These works analyze forces acting on the vane pump cam ring and describe the dynamics of the control in linearized way.

Another literature source is a thesis written by Tyler Bo Li in [17]. This thesis describes the design, modeling, control and efficiency of a hydraulic actuation system for a variable displacement vane pump, which is motivated by the need for enhanced efficiency and compactness in mobile hydraulic systems. Another good research was done by Patrick Dean in [18]. Dean's research is focused more on the control approach, but described also the pump dynamics at the beginning of the thesis.

Energy savings of the variable vane pump used for engine lubricating are investigated by Meira and co-authors in [19]. The variable vane pump achieved average power saving about 56% in comparison with the standard fixed gear (g-rotor) pump. The total fuel savings are approaching up to 3 %. Variable vane pumps are widely used for the engine oil lubrication.

The state of the art in this work doesn't focus primary on the alternative pump types such as variable vane pumps and variable gear pumps. Variable vane pumps are widely produced and implemented in many applications and theoretically they can be used for the charging system also. Work on the assumption, that roller pumps have higher durability and lower manufacturing costs prefer the application of a variable roller pump.

The variable gear pump could be a very good alternative to the roller and vane pumps in the future. Especially interesting and intensive work of Andrea Vacca on the gear variable gear pump could bring real application [7]. Actually it looks that the main disadvantage of the variable gear pump is limited displacement variability up to 40% of the maximal displacement (100%...60%).

It becomes clear the holistic theory of roller pumps is not published in available literature yet. The base for the theory derivation is a book written by Jaroslav Ivantysyn and Monika Ivantysynova [20]. This book deals with vane pumps among other things such as one dimensional simulation approach and axial piston pumps. The knowledge from this book can be used for the initial theory derivation based on the equation derived for a vane pumps. Fitch and Hong describe the vane pump principle in [21] and the general hydraulic simulation approach in [22]. The book from John Cundiff gives a base overview about vane pumps in [2]. The general one dimension hydraulic simulation approach can be found in books from Manring [23], Noskiewicz [24], Turza [25] and Nevrlý with co-authors [26].

Search for actual applications of roller pump in the industry shows only two applications. The first application is an automotive industry, where this pump type is used for fuel pumping [27]. The second is a sprayer application [28], where roller pumps are used for chemicals pumping. The example of spraying pump is shown in *Fig. 2.5*.



Fig. 2.5: Fixed roller pumps produced by company Hypro [28].

Both applications have a different focus than pump. Especially delta pressure level is significantly lower (<10 bar) than delta pressure demanded in our applications (20-40 bar) and both applications use fixed displacement pumps. Base on this search it is clear that actual market doesn't offer variable roller pump with parameters similar to our demands.

2.2 Variable Charging System

As mentioned, no actual application of fixed or variable roller pumps is available in hydrostatic transmissions on the market. An internal variable charge pump is also not available on the market. Some dozers use an external variable charging system which functionality is much more complex. The charge pump is realized with variable axial piston pump, which is used for additional functions as well. Variable charge pump in open hydraulic circuit was analyzed in [29]. Globally the solution with Variable Charge Pump of the open tractor hydraulic circuit presents power saving of about 28% considering the entire duty cycle.

Hydraulic systems can be found in the worldwide patent database under European Classification F15 or F16. Mostly, results are related to charge pumps used in hydrostatic systems as transmissions or steering (WO2008121203A1, US2008/0238187 A1, US7007468 B1, US6176085B1, DE102009056624A1) or variable pumps as an auxiliary part of a pump unit (WO2008138711A1, WO2008138712A1).

Variable charge pump systems in patents literature occur mainly in patents coming from companies like John Deere, Bosch Rexroth, Hitachi, Caterpillar and HydroGear. The search of the key word "variable charge pump" in categories B60K, F16H, F04B, F15B or F01B according to the classification IPC found several documents dealing with a variable charge pump in systems. No document dealing with a variable roller charge pump in a system was found. It can be concluded that variable roller charge pumps are not used in actual applications.

In the patent US8567544B is stated that a hybrid hydraulic power transmission system for all terrestrial's vehicles comprises a prime mover and an accumulator which could also be used as the main load bearing full or partial frame for all those vehicles. A hydraulic power integrator is operatively connected to the prime mover and the accumulator and selectively able to draw power for the vehicle from the prime mover, the accumulator, or a combination thereof. The hybrid hydraulic system may have a secondary unidirectional variable charge pump on the same shaft as that of the power integrator. This secondary unidirectional variable charge pump recharges the accumulator if the prime mover has extra torque and/or the accumulator have extra oil pressure.

In US7954317B2 a hydraulic system for an agricultural vehicle is proposed. This patent stated that the hydraulic system comprises a main hydraulic circuit, which is fed with hydraulic fluid by a main hydraulic pump, a variable displacement charge pump which supplies charge pressure to the main hydraulic pump, and lubricating hydraulic circuits. In order to keep efficiency losses on the vehicle to a minimum, particularly at high engine speeds, part of the hydraulic fluid delivered by the charge pump can be diverted to the lubricating hydraulic circuit. The variable or adjustable charge pump is set such that, in the charge pressure hydraulic circuit, a certain charge pressure is always reached, which is maintained by the charge pump by alteration of the delivery volume.

A Caterpillar hydraulic system, described in US2008/0238187A1, has a reservoir configured to hold a supply of fluid. In the patent is stated that the hydraulic system also has a variable displacement pump (Fig. 2.6) configured to supply charge fluid and pilot control fluid to the hydraulic system.

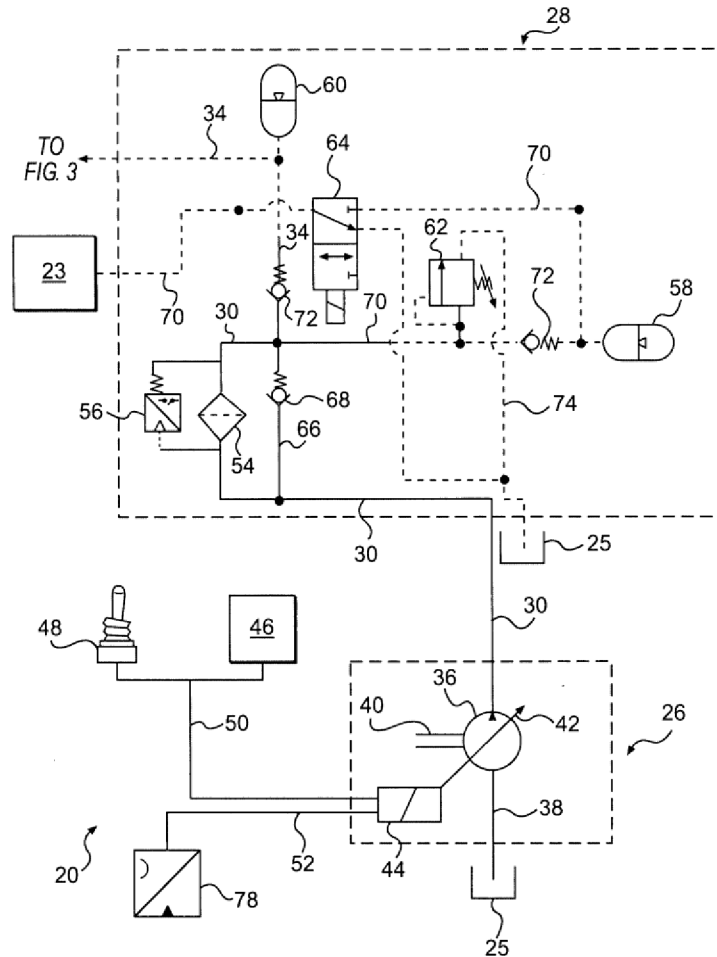


Fig. 2.6: Selected invention part from US2008/0238187A1.

Invention US2010/0119383A1 relates to a pump unit comprising a main pump and a charge pump having a variable pump capacity. This invention says that the pump unit comprises a main pump and a charge pump having a variable pump capacity. An adjusting means is provided for adjusting the pump capacity of the charge pump; the adjusting means is acted upon with an adjusting force that is dependent on an inlet pressure of the main pump. By generating an adjusting force that is dependent on the pressure present at the inlet side of the main pump, it is ensured that there is an immediate reaction to the adjustment of the pump capacity of the charge pump if the inlet pressure of the main pump changes. In this manner it is possible to prevent pressure spikes, and it is ensured that an undersupply of the main pump and, therefore, an occurrence of cavitation are reliably prevented. This has a positive effect on the service life of the main pump. The decisive factor is that the pump capacity is adjusted as a function of the pressure on the inlet side. Pressure fluctuations that are due, e.g., to a filter located between the main pump and the charge pump, have no effect.

A pressurized hydraulic (hydrostatic) fluid system in US2005/0132701A1 accordance with the preferred embodiment of the present invention includes a charge pump, a hydraulic

motor drivingly coupled to the charge pump, and a main hydraulic unit adapted to function as a hydraulic pump. In this patent is stated that the main hydraulic unit is provided to drive the hydraulic motor when functioning as the hydraulic pump. The charge pump of the present invention is in fluid communication with the main hydraulic unit when the main hydraulic unit functions as the hydraulic pump for maintaining a sufficient inlet pressure in the main hydraulic unit functioning as the pump. Moreover, the charge pump flow is proportional to the main hydraulic unit flow and so the hydraulic fluid system of the present invention is prone to waste less power.

Purpose of JPS58102806A is to prevent an occurrence of energy loss and cavitation of the oil pressure closed circuit for driving actuator by a method wherein a charge pump comprises a capacity variable oil pressure pump which is controlled in accordance with the pressure of a main circuit on a low pressure side. This patent says that the charge pump comprises a capacity variable oil pressure pump. A displacement volume variable mechanism of the capacity variable charge pump is controlled by a control cylinder. The control cylinder includes a pilot pipe to connect a pressure chamber and the discharge side of the capacity variable charge pump. With such a construction, when the pressure of the main circuits on the low pressure side is larger than a preset pressure, the push away volume variable mechanism is maintained at a neutral position. To the contrary, when the pressure is smaller than the pre-set value, the mechanism is moved to a pressurized oil discharge position so that the occurrence of energy loss and cavitation in the actuator driving oil pressure circuit can be prevented effectively.

Probably the most related patent to the variable charging system is the patent number US8833069B2. The invention deals with a variable charge pump connected with a variable flushing system. The flushing system is controlled electronically. The system overview can be seen from Fig. 2.7.

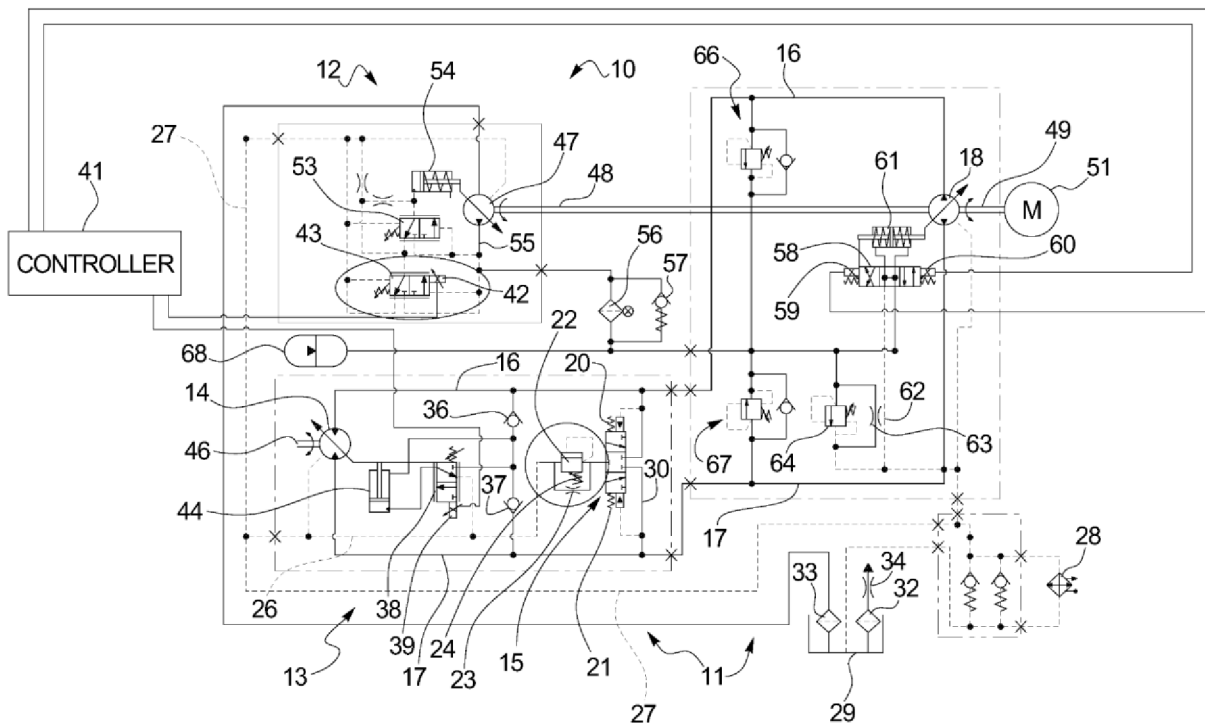


Fig. 2.7: Selected invention part from US8833069B2.

Till now no (for the purposes of present work) literature (article, book, report) was found focused on the variable charge pump system development or evaluation of its power saving potential in hydrostatic transmission. The general approach to a system could be found in many books, which deal with hydrostatic transmissions, for example [20], [21], [2], [24], [26], [30], and [31], [32]. Next possible sources are dissertation theses as [6], [5] and articles such as [33]. In the [2] could be founded more information about charge pump sizing.

The previous state of the art investigation is focused on the charge pump displacement variability but it is necessary to mention that there is another possibility how to decrease charge pump power demands. It is clear, that the demand for the charge pressure level is depending on the HST working conditions. This alternative approach is based on the charge pressure regulation according to the HST demands. For example the charge pressure is reduced in idle mode with a separate electric actuated pressure relief valve. This is not a very sophisticated approach, but applied in some of today's mobile applications. There are certain limits of this method and power savings are lower than savings achieved with a variable charge pump. The disadvantage of the charge pressure regulation is the pump performance dependency on the charge pump pressure level. The most interesting combination and the most expensive could be a variable charge pump with electronically adjusted pressure control.

Based on the literature search it could be concluded that this doctoral thesis could fill a missing place in the actual State of the Art. Especially in the area of the roller pump dynamics, kinematics and system implementation. The main contribution of doctoral work to the actual State of Art will be complexity of the phenomena accounted for the variable roller charge pump investigation.

3 THEORETICAL BACKGROUND OF ROLLER PUMPS

Starting line for the roller pump research is the theory of vane pumps which is already very well published and confirmed by a lot of real applications. The examples of the vane pumps theory are presented in [21] and [20].

The variable roller pump is one alternative way how to realize a variable pump for low pressure applications which is the main added value of this pump. The roller pump could be used as an auxiliary pump or as a charge pump.

Roller pumps are not very common in hydraulic systems. Generally, the roller pump is a special modification of a vane pump where vanes are replaced by rollers. So, a lot of vane pump knowledge can be applied on roller pumps. The typical configuration of a roller pump with fixed geometric volume is shown in *Fig. 3.1*. The basic parts of roller pumps are rotor (carrier) with roller slots, rollers, cam ring (stator) and port plates. Inlet (low pressure - LP) and outlet (high pressure - HP) kidneys of the port plates can be split to outer and inner kidneys according to displacement chamber location.

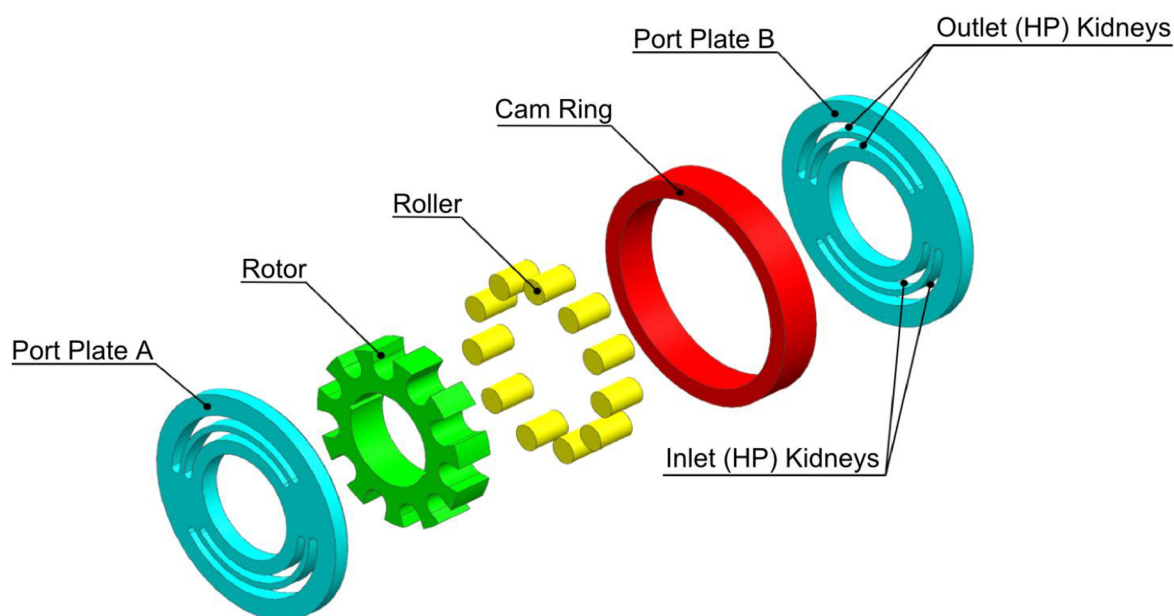


Fig. 3.1: Roller pump parts – exploded view.

The outer displacement chambers are located between rotor and cam ring and are limited in the circumferential direction by the rollers. The inner displacement chambers are located between rotor and rollers in roller slots. The *Fig. 3.1* and *Fig. 3.2* help to explain the pump function. The rotor is placed eccentrically; it means there is a distance between rotor center and cam ring center. This distance is called rotor eccentricity. The rollers can move radially in the slots and they are pressed against the cam ring by the centrifugal force. The rollers are loaded by the pressure in inner and outer chambers. For a correct pump function, it is necessary to ensure the sealing effect with the contact between rollers and cam ring. Due to the eccentricity of the rotor, the displacement of outer and inner chambers increase during half a rotor revolution, it means that the fluid is sucked and during second part of the revolution, the displacement decrease and the fluid is delivered to the pump outlet [20].

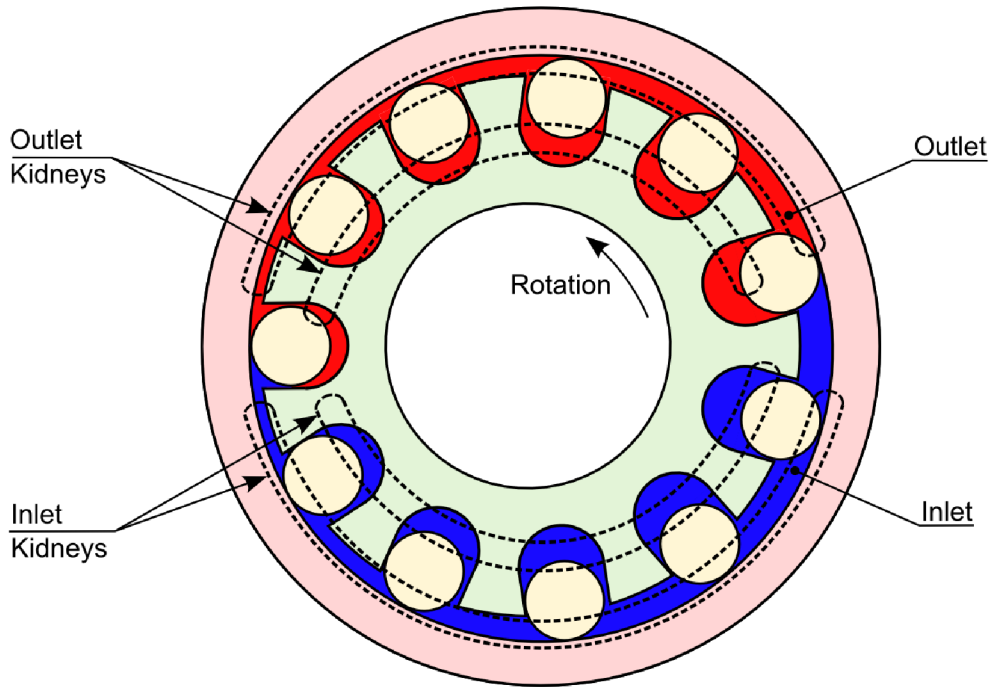


Fig. 3.2: Roller pump schematic view.

The kinematic equations for chamber displacements and fluid equations have to be derived according to the simulation method based on one-dimensional modeling with pressure build up equations. The next important step is the calculation of the cross section areas which are connecting the chambers to kidneys.

3.1 Basic Equations

The equation given in [20] for calculation of a vane pump displacement can be used for the roller pump. The geometrical pump displacement is determined as:

$$V_g = 2 \cdot w_{rol} \cdot e_{rot} \cdot z_{rol} \cdot d_{cam} \cdot \sin \frac{\pi}{z_{rol}} \quad (3.1)$$

where w_{rol} is the roller width, e_{rot} is rotor eccentricity, z_{rol} is number of rollers and d_{cam} is inner diameter of cam ring. A cut view and basic geometry of the roller pump are shown in Fig. 3.3.

The effective output flow rate Q_e for constant pump Δp can be written as a difference between theoretical flow Q_{teo} and volumetric losses Q_s :

$$Q_e = Q_{teo} - Q_s \quad (3.2)$$

$$Q_e = n_{rot} \cdot V_g - (Q_{si} + Q_{se} + Q_{sk} + Q_{sf}) \quad (3.3)$$

where n_{rot} is rotor speed, Q_{si} are internal flow losses, Q_{se} are external flow losses, Q_{sk} are compression flow losses and Q_{sf} are filling flow losses.

The filling losses Q_{sf} will be neglected because this work starts with lower speeds where a chamber filling was assumed as a relatively sufficient.

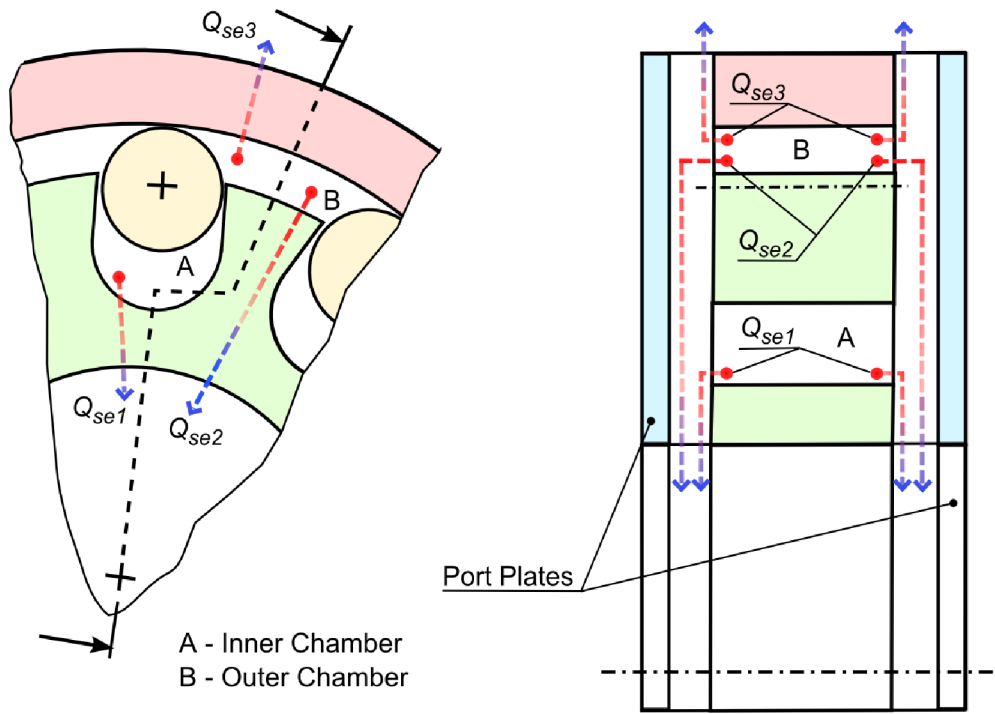


Fig. 3.4: External leakage in roller pump, A – Inner Chamber, B – Outer Chamber.

These gap leakages flow from inner/outer chambers to the case of displacement machine through a gap between rotor, cam ring and port plates:

$$Q_{se} = \sum_{i=1}^{z_{rol}} (Q_{se1} + Q_{se2} + Q_{se3} + Q_{se4}) \quad (3.7)$$

External losses are not focus of this work and for this reason they are not used in the simulation model due to the assumption that external leakages are not significantly affected by port plate design.

For calculation of the total amount of internal cross port leakage (CPL), the following equation is used:

$$Q_{si} = \sum_{i=1}^{z_{rol}} (Q_{si1} + Q_{si2} + Q_{si3} + Q_{si4}) \quad (3.8)$$

Partial internal leakages (CPL) Q_{si1} , Q_{si2} , Q_{si3} can be calculated with using the orifice equation [21] where α_D is discharge coefficient, A is orifice cross section area, p_{out} , p_{inn} are pressures, i outer and inner chambers, ρ_{oil} is fluid density. Flows Q_{si1} , Q_{si4} have to be calculated with orifice equations and the pressures build up equations:

$$Q_{si,i} = \alpha_D \cdot A \cdot \sqrt{\frac{2 \cdot (p_{out} - p_{inn})}{\rho_{oil}}} \cdot \text{sign}(p_{out} - p_{inn}) \quad (3.9)$$

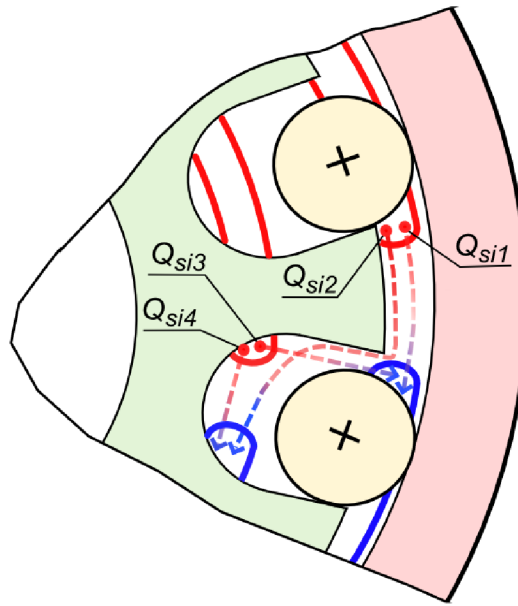


Fig. 3.5: Internal leakage in a roller pump – cross ports.

Following equations for the torque and efficiency requires real derived pump displacement, but for simplifications reasons V_g is taken into account. The effective input torque T_e of a real roller pump is the sum of the theoretical torque T_{the} and total torque losses T_s :

$$T_e = T_{the} + T_s = \frac{\Delta p \cdot V_g}{2\pi} + T_s \quad (3.10)$$

For the pump overall efficiency η_t , the well-known basic equations could be derived:

$$\eta_t = \eta_{vol} \cdot \eta_{hm} \quad (3.11)$$

where the volumetric efficiency η_v and the η_{hm} hydro-mechanical efficiency can be written as:

$$\eta_{vol} = \frac{Q_e}{V_g \cdot n_{rot}} \quad (3.12)$$

$$\eta_{hm} = \frac{V_g \cdot \Delta p}{2\pi \cdot T_e} \quad (3.13)$$

3.2 Fluid Equations

The one dimensional simulation approach requires using the pressure build up equations for the calculation of the pressure in the outer and inner chambers. The following general equation [20] describes the change of chamber pressure p with volume V :

$$\frac{dp}{dt} = \frac{K_A}{V(t)} \cdot \left(\sum Q - \frac{dV(t)}{dt} \right) \quad (3.14)$$

The previous equation could be applied on the inner p_{inn} and outer p_{out} chamber pressure calculation of the roller pump:

$$\frac{dp_{inn}}{dt} = \frac{K_A}{V_{inn,i}(t)} \cdot \left(Q_{LP_{inn}} - Q_{HP_{inn}} + Q_{gL} + Q_{gR} - \frac{dV_{inn,i}(t)}{dt} \right) \quad (3.15)$$

$$\frac{dp_{out}}{dt} = \frac{K_A}{V_{out,i}(t)} \cdot \left(Q_{LP_{out}} - Q_{HP_{out}} - Q_{gL} - Q_{gR} - \frac{dV_{out,i}(t)}{dt} \right) \quad (3.16)$$

The inner chamber displacement is V_{inn} and outer chamber displacement is V_{out} . The variables $Q_{HP_{inn}}$, $Q_{HP_{out}}$ in equations (3.15) are (3.16) are flows from the outlet (HP) to the inner/outer chamber. $Q_{LP_{inn}}$ and $Q_{LP_{out}}$ are flows from the inlet (LP) to the inner/outer chamber, Q_{gL} representing flow from inner chamber number i to outer chamber number i through the gap between the roller and the roller slot. Q_{gR} represents the flow from the inner chamber number i to the outer chamber number $i-1$ through the gap between the roller and the roller slot. The numbering (i) of chambers and flows is shown in *Fig. 3.3*. The graphic explanation of model building is shown in the next section 5.1, *Fig. 5.4*.

The flows Q_{HP} , Q_{LP} , Q_{gL} and Q_{gR} in equations (3.15), (3.16) can be calculated from the general orifice equation (3.9) with respect of the flow direction. The inlet and outlet orifice areas for these flows Q_{HP} , Q_{LP} were calculated with a special inlet outlet orifice area tool which was developed for this purpose.

This tool is based on a digital analysis and the output of this tool is the area of the covering between the chamber cross section and the kidney cross section in relation to (rotor) rotation angle. The calculation algorithm of this tool consists of four steps. The first step is a cross section plot of the demanded chamber in the required position with kidneys (all in black color and fixed scale) and counting the number of black pixels within the figure via an optical analysis algorithm. The second step is plotting the same picture without kidney and counting of black pixels again. The next step is building the difference of the sum with kidney and without the kidney. At the last step, this difference is converted to a cross section of kidney of the analyzed chamber, position and kidney with usage of a scale factor (area/one pixel). These steps were implemented into an algorithm in Matlab, so that the cross section areas of all chambers and all demanded discrete positions are calculated according to the user parametric input. A simplified view on the tool's principle is shown in *Fig. 3.6*.

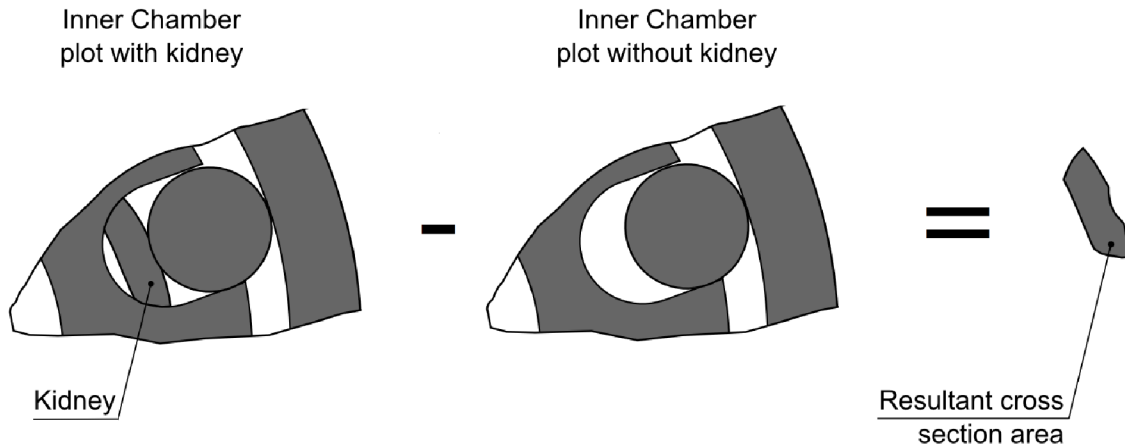


Fig. 3.6: Principle of the cross section calculation tool.

The cross section areas of gap flows (roller slot flows shown in Fig. 3.7) Q_{gR} , Q_{gL} are depending on the pressure difference around the roller. These areas were calculated analytically.

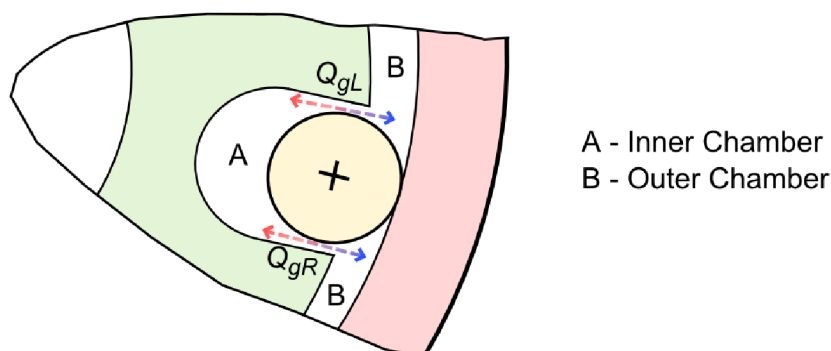


Fig. 3.7: Possible gap flows (roller slot flows).

The volumes V_{out} and V_{inn} in pressure build up equations (3.15), (3.16) represent the outer chamber volume and the inner chamber volumes, presented in Fig. 3.8.

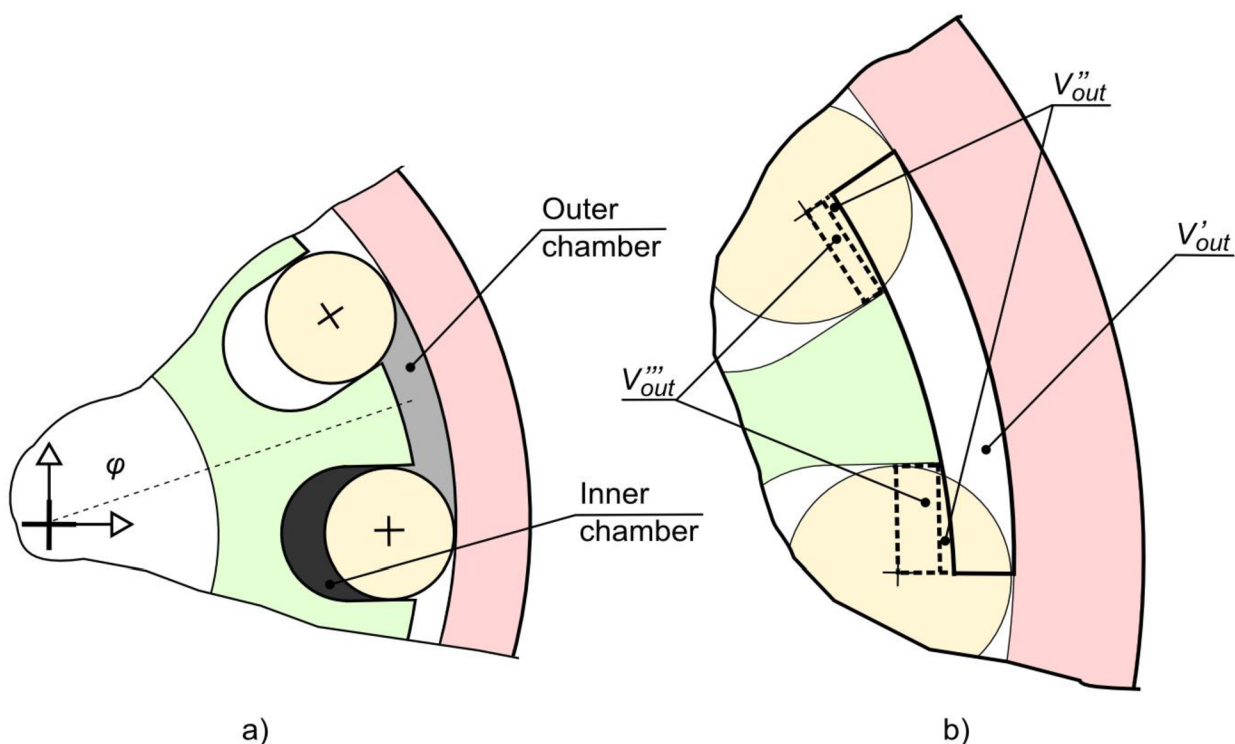


Fig. 3.8: Partial chamber volumes and schematic view on separation of outer chamber.

According to the equations (3.15), (3.16), it is necessary to determine the volumes V_{out} and V_{inn} of the chambers and the time derivation of these volumes. The cam ring radius u_{cam} (shown in Fig. 3.3) could be written with radius angle φ as [20]:

$$u_{cam}(\varphi) = e_{rot} \cdot \left(\cos \varphi + \frac{e_{rot}}{2 \cdot d_{cam}} \cdot \cos(2 \cdot \varphi) + \frac{d_{cam}}{2 \cdot e_{rot}} - \frac{e_{rot}}{2 \cdot d_{cam}} \right) \quad (3.17)$$

The roller pump has two types of chambers (*Fig. 3.8a*). The first, the outer volume V_{out} (volume between rollers) has to be divided to four parts for a simple calculation as shown in *Fig. 3.8b*.

Outer chamber volume can be calculated as a sum of a partial volumes V and minus half of roller (with diameter D_{rol}):

$$V_{out}(\varphi) = V'_{out} + V''_{out} + V'''_{out} - w_{rol} \cdot \frac{\pi \cdot D_{rol}^2}{8} \quad (3.18)$$

The first part of the outer volume V'_{out} represents according to *Fig. 3.8b* the volume between the cam ring, rotor and rollers center. The second part and third part were created by a separation of the outer volume. The width of the roller is corresponding to the variable w_{rol} and rotor diameter to the variable D_{rot} . The first part V'_{out} is equal to the integral:

$$V'_{out} = w_{rol} \cdot \int_{\varphi - \frac{\pi}{z_{rol}}}^{\varphi + \frac{\pi}{z_{rol}}} \left[\frac{(u_{cam}(\varphi))^2 - \left(\frac{D_{rot}}{2}\right)^2}{2} \right] d\varphi \quad (3.19)$$

and the second part (half-moon) as:

$$V''_{out} = w_{rol} \cdot \left[\frac{h^2}{2} \cdot (\vartheta - \sin \vartheta) \right] \quad (3.20)$$

where half-moon angle ϑ_{moon} and half-moon height h_{moon} :

$$\vartheta_{moon} = 2 \cdot \arcsin \cdot \frac{w_{slo}}{2 \cdot h} \quad (3.21)$$

$$h_{moon} = \frac{D_{rot}}{2} - \frac{\sqrt{D_{rot}^2 - w_{slo}^2}}{2} \quad (3.22)$$

The third part can be written as:

$$V'''_{out} = w_{rol} \cdot \left(2 \cdot \left(\frac{D_{rot}}{2} - h + \frac{D_{rol}}{2} \right) - u_{cam} \cdot \left(\varphi - \frac{\pi}{z_{rol}} \right) - u_{cam} \cdot \left(\varphi + \frac{\pi}{z_{rol}} \right) \right) \quad (3.23)$$

The inner chamber volume is equal to:

$$V_{inn}(\varphi) = w_{rol} \cdot \left(w_{slo} \cdot \left(u_{cam}(\varphi) - \frac{D_{rol}}{2} - u_{min} \right) + \frac{\pi \cdot w_{slo}^2 - \pi \cdot D_{rol}^2}{8} \right) \quad (3.24)$$

In both expressions for the outer volume V_{out} in (18) and the inner volume V_{inn} in (21), the angle φ can be substituted by following equation:

$$\varphi = 2 \cdot \pi \cdot n_{rot} \cdot t + \varphi_0 \quad (3.25)$$

where φ_0 is initial angular offset from analyzed chamber to the origin. The volumes $V_{inn}(t)$ and $V_{out}(t)$ are functions of time and they could be derived in time after a substitution. These time derivations of the volumes are used in equation (3.15) and equation (3.16). Derivations of chamber volumes in time are not shown in this work due to their long expression.

3.3 Roller Equations

The determination of roller forces is depending on the coordinate system which was chosen for final force determination.

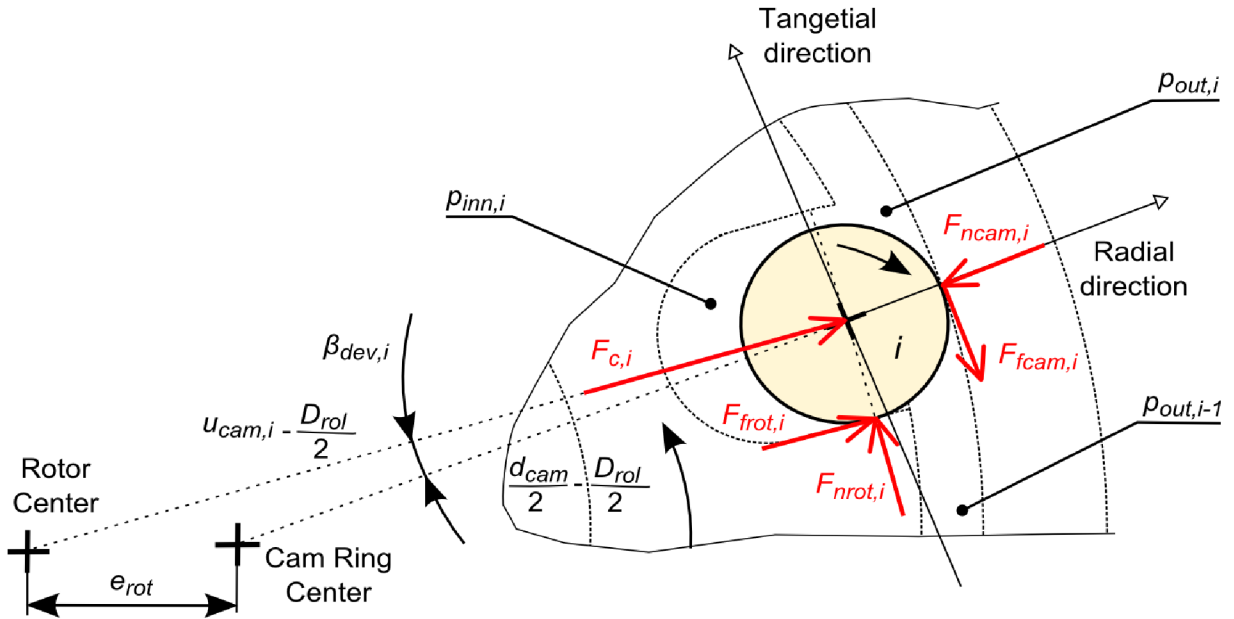


Fig. 3.9: Roller force analysis.

In this case, the coordinate system center in Fig. 3.9 is placed into roller center. The radial direction x_{Rrol} (axis) for coordinating system was chosen on the connection line from roller center to the cam ring center with positive orientation heading out from the rotor center. The tangential direction x_{Trol} is perpendicular to the radial direction and positive axis orientation is corresponding to the rotor rotation.

The roller rotation acceleration around own roller centerline is defined by the variable $\ddot{\varphi}_{rol}$. The roller mass is m_{rol} and the roller inertia is I_{rol} . Fig. 3.9 shows: normal roller forces F_{ncam} and F_{nrot} , friction roller forces F_{fcam} and F_{frot} and centrifugal roller force F_c . According to Fig. 3.9 and previous text, the following equations of motion (radial equation: (3.26), tangential equation (3.27) and rotation equation (3.28) are written:

$$\begin{aligned}
 m_{rol} \cdot \ddot{x}_{Rrol,i} = & \left[F_{c,i} + F_{frot,i} + \left(p_{inn,i} - \frac{p_{out,i} + p_{out,i-1}}{2} \right) \cdot w_{rol} \cdot D_{rol} \right] \cdot \\
 & \cdot \cos(\beta_{dev,i}) + \left[F_{nrot,i} - \left(\frac{p_{out,i} - p_{out,i-1}}{2} \right) \cdot w_{rol} \cdot D_{rol} \right] \cdot \\
 & \cdot \sin(\beta_{dev,i}) - F_{ncam,i}
 \end{aligned} \quad (3.26)$$

$$\begin{aligned}
m_{rol} \cdot \ddot{x}_{Trol,i} = & \left[-F_{c,i} - F_{frot,i} - \left(p_{inn,i} - \frac{p_{out,i} + p_{out,i-1}}{2} \right) \cdot w_{rol} \cdot \right. \\
& \cdot D_{rol} \left. \right] \cdot \sin(\beta_{dev,i}) - F_{fcam,i} - F_{cor,i} + \\
& + \left[F_{nrot,i} - \left(\frac{p_{out,i} - p_{out,i-1}}{2} \right) \cdot w_{rol} \cdot D_{rol} \right] \cdot \cos(\beta_{dev,i})
\end{aligned} \quad (3.27)$$

$$I_{rol} \cdot \ddot{\varphi}_{rol,i} = (F_{frot,i} - F_{fcam,i}) \cdot \frac{D_{rol}}{2} \quad (3.28)$$

The Coriolis force can be calculated with rotor acceleration $\ddot{\varphi}_{rot}$ as:

$$F_{cor,i} = 2 \cdot m_{rol} \cdot \dot{\varphi}_{rot} \cdot \dot{x}_{rol,i} + m_{rol} \cdot \ddot{\varphi}_{rot} \cdot \left(u_{cam} - \frac{D_{rol}}{2} \right) \quad (3.29)$$

and the deviation angle β_{dev} , caused by rotor eccentricity, could be determined from the cosine theorem in the following way:

$$\beta_{dev,i} = \cos^{-1} \left[\frac{- \left((e_{rot})^2 - \left(\frac{d_{cam} - D_{rol}}{2} \right)^2 - \left(u_{cam,i} - \frac{D_{rol}}{2} \right)^2 \right)}{2 \cdot \left(\frac{d_{cam} - D_{rol}}{2} \right) \cdot \left(u_{cam,i} - \frac{D_{rol}}{2} \right)} \right] \quad (3.30)$$

These equations are valid when the roller is in contact of the trailing edge of the rotor. When the roller is in contact of the leading edge of the rotor the direction of the normal contact force between rotor-roller has to be changed.

The following simplifications of the roller force calculations have to be implemented in the simulation model used in the optimization tool due to the high complexity of the model. The friction and Coriolis forces are neglected, rotor eccentricity is equal to zero and the radial and tangential forces acting on the rollers in steady state are:

$$F_{ncam,i} = \left(p_{inn,i} - \frac{p_{out,i} + p_{out,i-1}}{2} \right) \cdot D_{rol} \cdot w_{rol} + m_{rol} \cdot \frac{(2 \cdot \pi \cdot n_{rot})^2}{u_{cam}(\varphi) - \frac{D_{rol}}{2}} \quad (3.31)$$

$$F_{nrot,i} = \left(\frac{p_{out,i} - p_{out,i-1}}{2} \right) \cdot D_{rol} \cdot w_{rol} \quad (3.32)$$

3.4 Derivation of Cam Ring Forces

The derivation of the cam ring forces is important for a suitable control system design. Each sophisticated control or port plate design requires a cam ring force calculation. The main forces acting on the cam ring can be identified according to the variable roller pump design (Fig. 4.3). They are: roller forces, pressure forces and spring force. The pivot friction was neglected. The most important force from the design point of view is the force which is acting on the cam ring spring. This force will be derived based on the pressure force calculation.

The pressure force acting on the cam ring is the biggest part of the total spring force calculation and it is depending on the pressure profile in the outer chamber, which calculation was presented in previous chapters. The calculation of the chamber area which is loaded with chamber pressure is shown in Fig. 3.10.

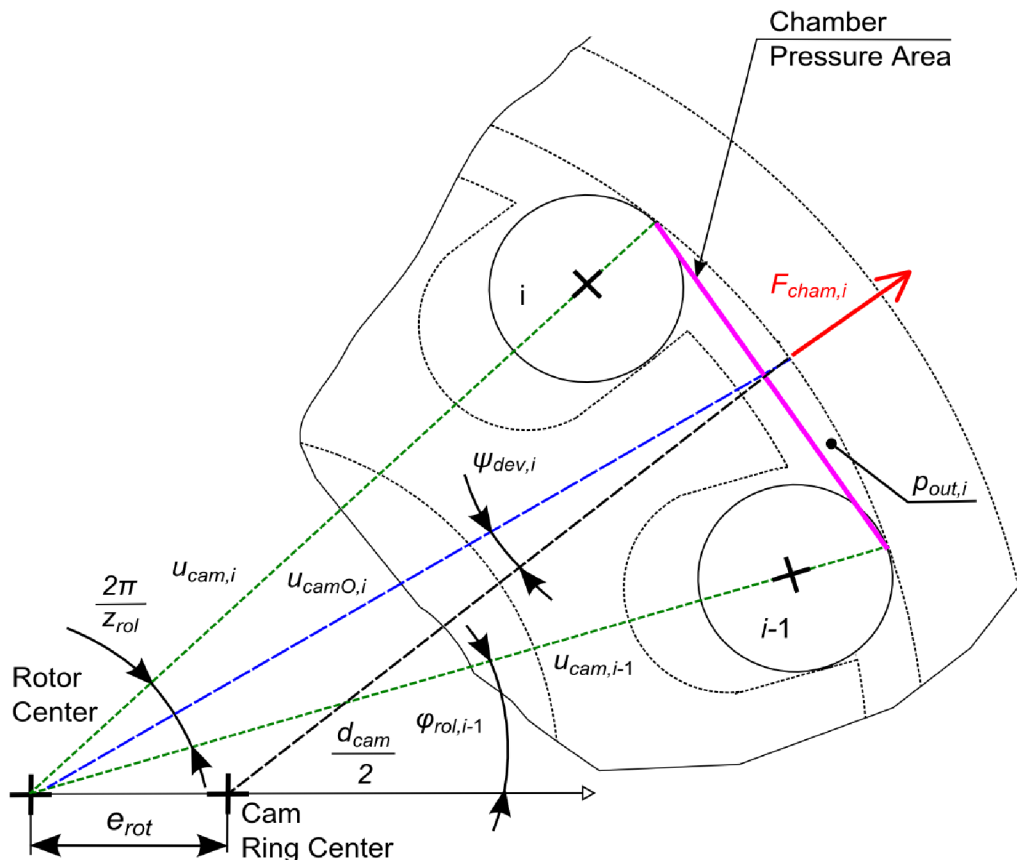


Fig. 3.10: Pressure force of outer i -chamber.

The resultant outer pressure force acting on the cam ring area (magenta color) can be calculated also with the Cosine theorem, according to equation (3.33) [34]:

$$F_{cham,i} = p_{out,i} \cdot w_{rot} \cdot \sqrt{(u_{cam,i})^2 + (u_{cam,i-1})^2 - 2 \cdot u_{cam,i} \cdot u_{cam,i-1} \cdot \cos\left(\frac{2 \cdot \pi}{Z_{rol}}\right)} \quad (3.33)$$

The particular forces acting on the cam ring are presented in Fig. 3.9 where the direction and origin of each force is defined. Due to the rotor eccentricity it is necessary to determine the angles of the roller and chamber forces. The angles of the roller and chamber forces are known only for the coordinate system with the center in the rotor center, but for the resultant cam ring force calculation, the origin in the cam ring center can significantly simplify the whole calculation. The angle transformation equations are shown in equations (3.34) and (3.35), where ϑ_{rol} presents the angle of the roller force and ϑ_{cham} presents the angle of chamber pressure forces. The roller deviation angle β_{dev} can be obtained from roller force calculation presented in the previous chapter. In a similar way as β_{dev} , the chamber deviation angle ψ_{dev} can be also derived:

$$\vartheta_{rol,i} = \varphi_{rol,i} + \beta_{dev,i} \quad (3.34)$$

$$\vartheta_{cham,i} = \varphi_{cham,i} + \psi_{dev,i} \quad (3.35)$$

The spring force – the force acting against the compression spring - can be calculated as a sum of all forces acting on the cam ring.

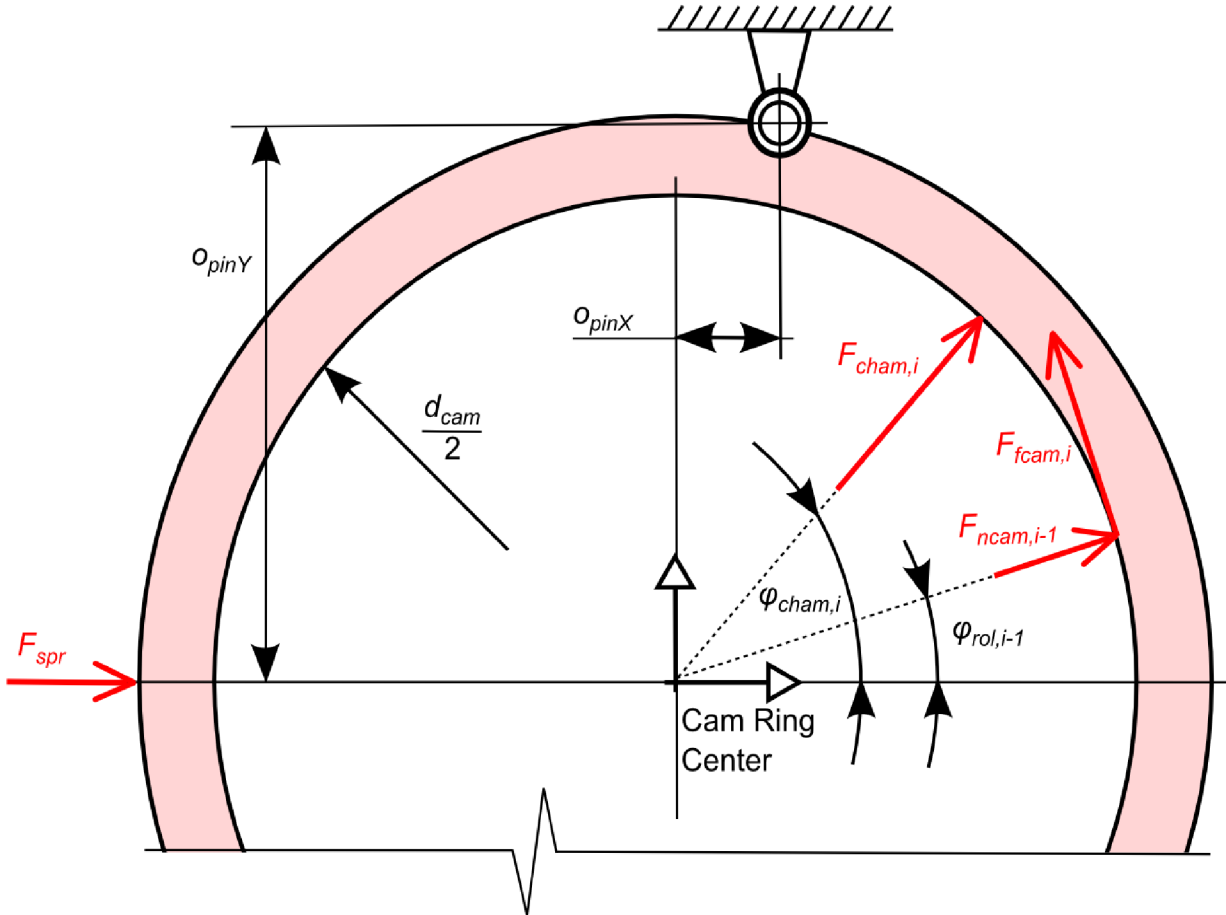


Fig. 3.11: Forces acting on the cam ring.

In the case of steady state and with neglecting the pivot and cam ring friction, the final equation (3.36) for the spring force calculation is derived:

$$F_{spr} = -\frac{1}{o_{pinY}} \cdot \sum_{i=1}^{z_{rol}} o_{pinY} \cdot (F_{cham,i} \cdot \cos \vartheta_{cham,i} + F_{rol,i} \cdot \cos \vartheta_{rol,i}) + o_{pinX} \cdot (F_{cham,i} \cdot \sin \vartheta_{cham,i} + F_{rol,i} \cdot \sin \vartheta_{rol,i}) + F_{cam,i} \cdot \frac{d_{cam}}{2} \quad (3.36)$$

The pivot horizontal offset o_{pinX} and vertical offset o_{pinY} are defined according to Fig. 3.11. Both distances are referred to the cam ring center.

3.5 Roller Sealing Contact

As mentioned before, for the correct pump function it is necessary to ensure a stable sealing contact between rollers and cam ring. At the ideal operation conditions, the resultant force of the roller is equal to centrifugal force and this force is acting against the cam ring. But this effect is caused by the pressure balance between pressures acting on rollers in radial direction. This condition could not be ensured in transition areas when the chamber connection to kidneys is starting or finishing. Transition areas cause not ideal behavior of the radial and tangential roller force balance by non-ideal pressure profiles in the chambers. At the end, the non-stable contact between roller and cam ring contributes to a reduced volumetric efficiency. The non-stable contact could decrease the sealing effect between roller and cam ring and connect two outer chambers, which could increase cross port flow in the transition area and decrease pressure peaks in the chambers. The cut down of volumetric efficiency decrease total efficiency of the pump and it results in lower energy savings.

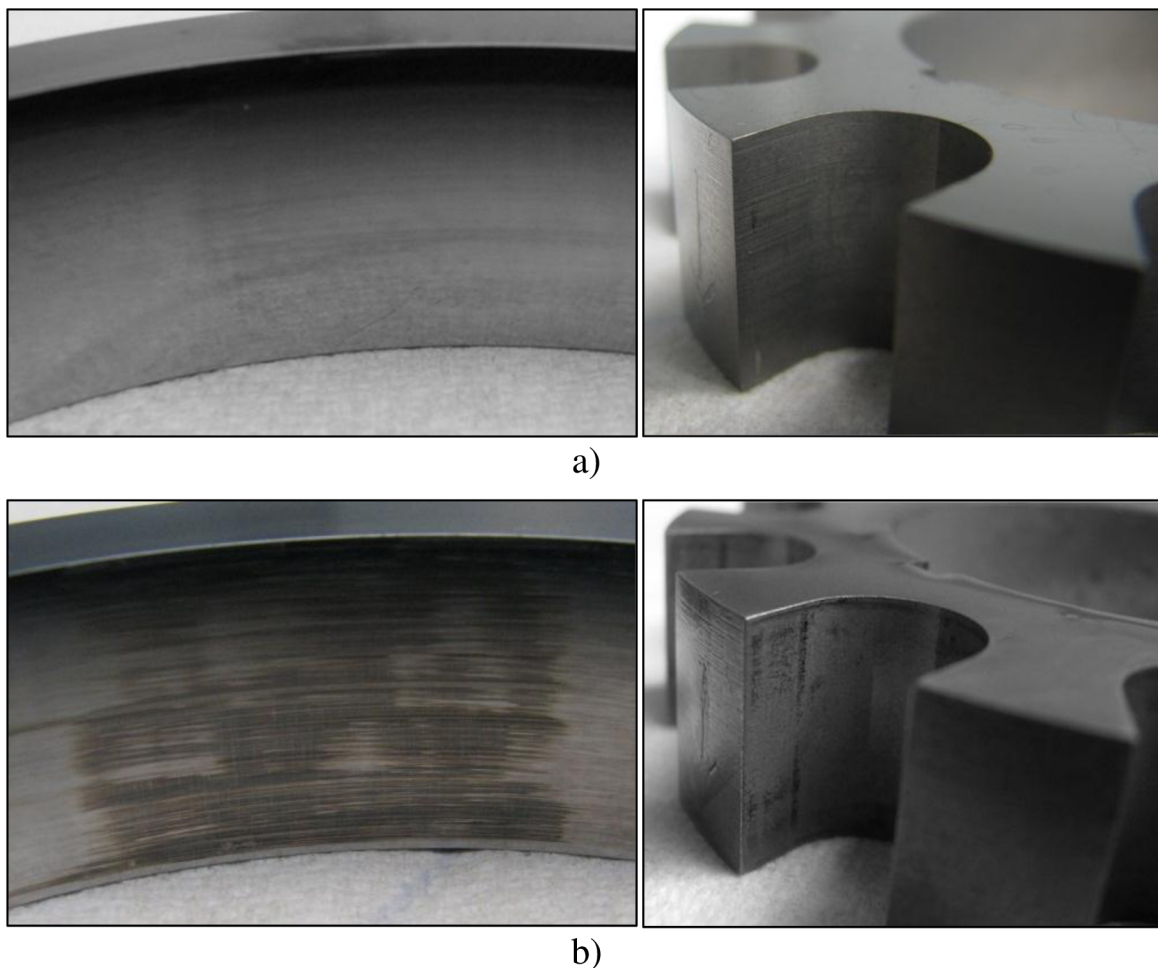


Fig. 3.12: Results of sliding contact between cam ring ,rollers and rotor during durability test of non-optimized hardware under Δp 40 bar, inlet oil temperature 80 °C and speed 2500 min⁻¹ , a) after 10 hour, b) after 80 hours.

It means that the roller pressure balance is very important for the pump performance and durability. Based on the previous lines it becomes clear that a pump simulation based optimization will be very helpful in this area.

Generally, the application of any cross port flows (*Fig. 3.5*) in the pump design has a disadvantage resulting in a cut down of volumetric efficiency but it has an advantage in the cutting down pressure peaks in the chambers, which has a positive effect on the pump durability. The pressure peak decrease has a direct impact on the wear of the components which has to be scoped during the design and optimization process. The rollers, rotor and cam ring are parts which primary suffer from pressure peaks in chambers: The pressure peaks can result in wear marks at these parts. The explanation of the wear mark creation is that the pressure peaks in the chambers increase contact pressure. The increase of the contact pressure could result in a short stop of the roller rotation on cam ring and short sliding contact between roller and cam ring. It can be visually observed after a durability test of the roller pump, where marks on the cam ring, rollers or rotor were made. One example of non-optimized hardware with marks is shown in *Fig. 3.12*.

Thus a tool which has to be developed should simulate the pump behavior with the focus on cross port leakage and pressure profile in the pump chambers. The tool should provide a port plates design with lower pressure peaks and acceptable cross port flow. The core part of this numerical tool is a simulation model especially designed for cross port leakage and chamber pressure evaluation. This focus has the advantage of giving an indication to total pump efficiency via cross port leakage which is a measurable output for the important tool validation. For this reason, the tool is focused on kidney design.

4 ROLLER PUMP CONTROL

All pump control principles used for variable roller pumps are based on the displacement change. Generally, the purpose of the displacement control is to control pump performance or/and decrease pump power demands when it is not necessary.

The principle of the roller pump displacement change could be explained with basic equation (3.1) used for displacement calculation. This equation shows that the volume (displacement) of the roller pump is depending on the cam ring inner diameter, the number of rollers, the width of rollers and the rotor eccentricity. The change of the pump displacement is realized by the rotor eccentricity variability in this case. For example, a similar principle could be seen at variable vane pumps applied in the automotive or in the general hydraulic industry [35], [36], [37], [38]. Theoretically, the variable roller pump could be equipped with a lot of control variants such as the displacement control, the torque control, the pressure compensated control, the load sensing (flow compensator) control or another control type. Many applications use small pumps as a pressure sources and due to this, these pumps use a mechanical pressure compensated control which is used in the application investigated in this work also. Due to this, this work deals mainly with the pressure compensator control only.

Generally, each pressure compensator control tries to keep the outlet pressure constant if it is possible. The better overview about the pressure compensator control function gives *Fig. 4.1*. This figure shows idealized flow-pressure characteristic.

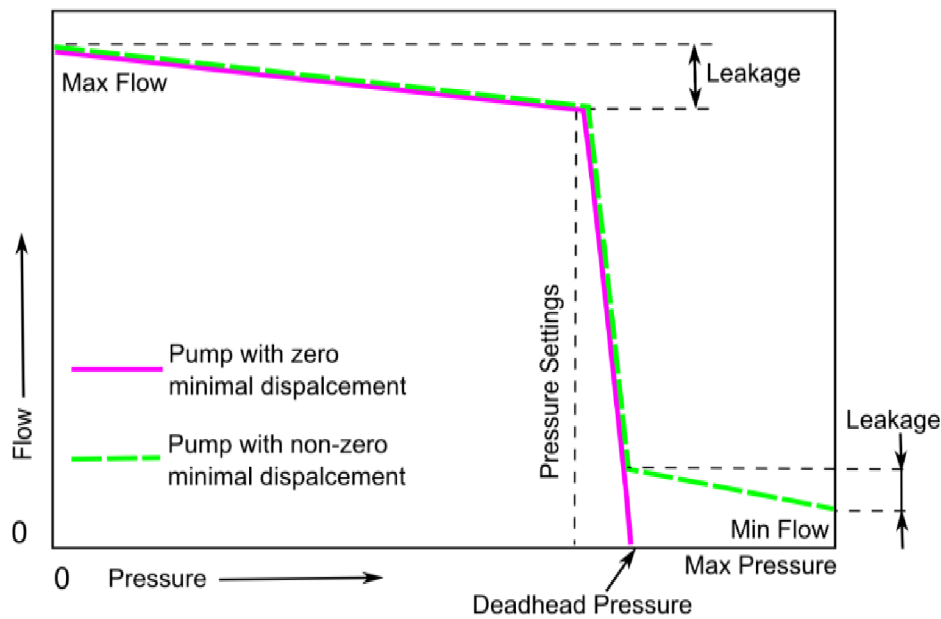


Fig. 4.1: Idealized pressure-flow ($p-Q$) characteristic of the pressure compensated pump with pump configuration.

This curve is obtained by loading the ideal pressure compensated pump with relief valve (or variable orifice). The pump runs at constant speed. The slight flow decrease between minimal pressure and pressure setting is depending on the pump volumetric efficiency or with other words on the pump leakage [2]. When the outlet pressure reaches the pressure setting (of pressure compensator), the pump displacement begins to decrease and the pump flow decreases up to zero or to minimal flow corresponding to the minimal displacement.

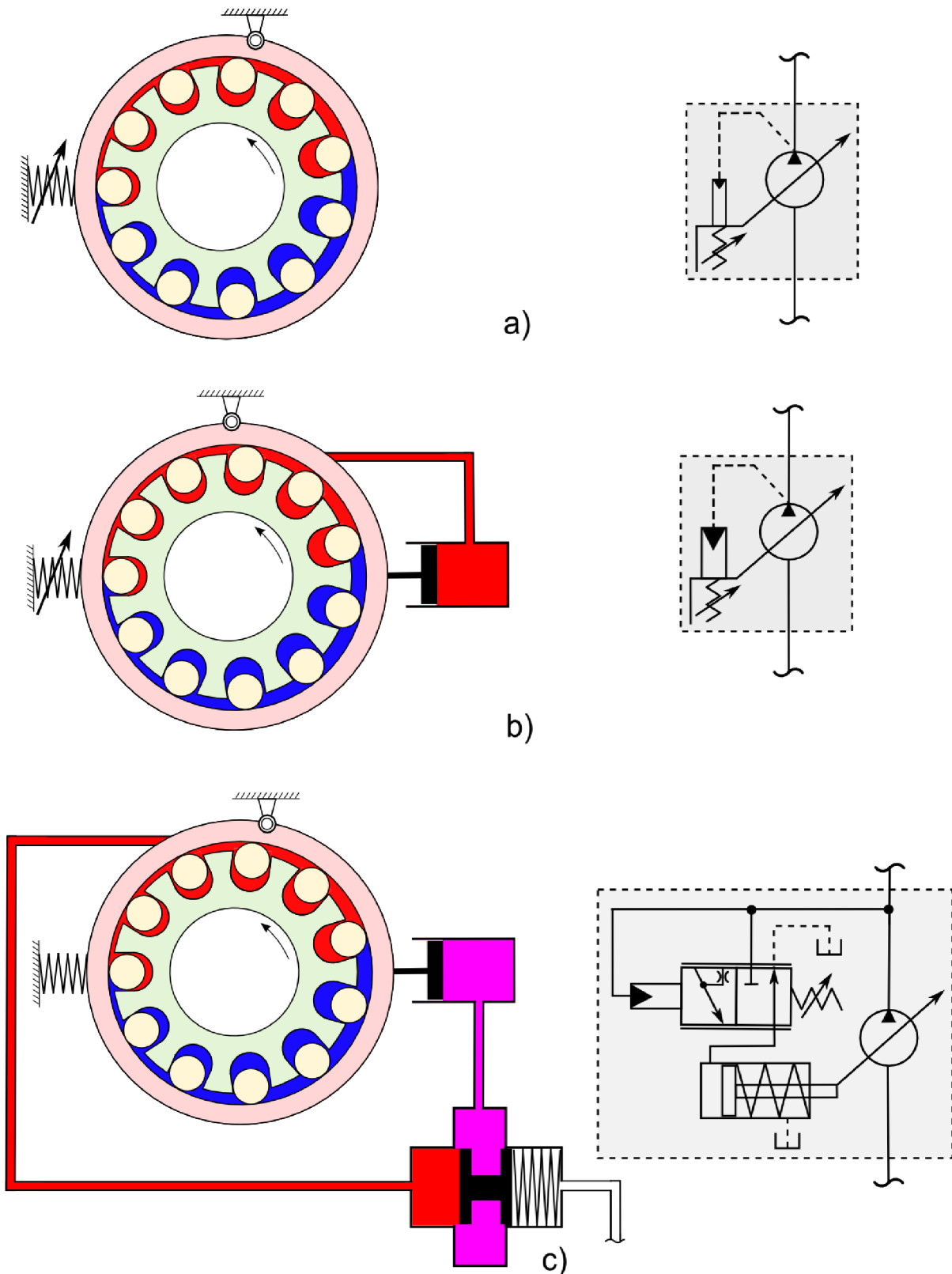


Fig. 4.2: Proposed control variants for variable roller pump.
 a) Variable roller pump with simple pressure compensator control.
 b) Variable roller pump with simple servo pressure compensator control.
 c) Variable roller pump with spool pressure compensator control.

The pump with minimal non-zero displacement is not able to achieve deadhead pressure with zero outlet flow which is also shown in this figure. The rate of the flow (displacement) decrease corresponds to the rate of the pressure compensator spring or with other words it corresponds to the overall proportional control gain at pumps with more complicated and sophisticated control system. Pumps with a non-zero minimal displacement show slight flow decrease at the end of the p - Q due to the volumetric efficiency too.

The advantage of the pressure compensated control (with a pump, when the minimal displacement is zero) is that the pressure compensated pump is able to keep deadhead pressure with minimal pump flow when the load flow demand in a circuit is minimal.

This feature decreases the input pump power and the pump saves energy what is the main advantage in comparison with a fixed pump. The pump is in minimal displacement with the outlet pressure equal to the deadhead pressure, this operation condition is called a standby mode. The power consumption in this case is minimal. The power consumption covers only friction losses at the pump and pump leakage [2]. Our application and other applications where zero flow is not demanded can be equipped with a pressure compensated pump with non-zero minimal displacement.

Three types of the pressure compensator control were selected for our application based on the requirements. All types are shown in *Fig. 4.2* - the simple pressure compensator (PC) control, the servo pressure compensator (PC) control and the spool pressure compensator (PC) control.

4.1 Pressure Compensator (PC) Controls

The principle of the simple pressure compensator (PC) control used in this work can be described with following sentences: The pump displacement is proportionally depending on the rotor-cam ring eccentricity, which changes with the cam ring motion around the pivot. At low outlet (discharge) pressure (HP) the pump displacement is in maximum (maximum rotor eccentricity) due to higher spring force (spring preload) and the lower outlet pressure force acting on the cam ring. The resultant force pushes on the cam ring and holds the cam ring at the maximal rotor eccentricity, it means at the maximal displacement. A growth of the outlet pressure increases the outlet pressure force on the cam ring, which acts against the spring force which becomes smaller than the outlet pressure force.

The resultant force on the cam ring changes direction and moves (rotates) the cam ring to the lower eccentricity (displacement). The reduction of the pump displacement results into a decrease of the outlet flow which reduces the pump outlet pressure. It means that a suitable spring design (spring preload, spring rate) can ensure a constant outlet pressure, which is demanded in charge pump application.

During the pump operation, high pressure (HP) forces act on the cam ring and try to rotate cam ring against the spring force around the cam ring pivot (*Fig. 4.3*). Theoretically, it means that the increase of the outlet pressure (HP) reduces the pump displacement. An adjustment of the control spring preload allows a change of the outlet pressure when the control starts to be active. The spring rate has direct impact on the pressure vs. displacement sensitivity. The achievement of the same displacement with a stiffer spring requires a higher outlet pressure than the control with a more soft spring. So, pump needs a higher outlet pressure for achievement of the minimal displacement with a higher spring rate than with a lower spring rate.

The control mechanism is clear to understand, but the theoretical description is much more complicated. The cam ring forces calculation is very important for the spring force selection and suitable control design of the pump. The behavior of cam ring forces is similar to the behavior of swash plate forces acting on the swash plate at an axial piston unit which causes the cam ring force non-linearity.

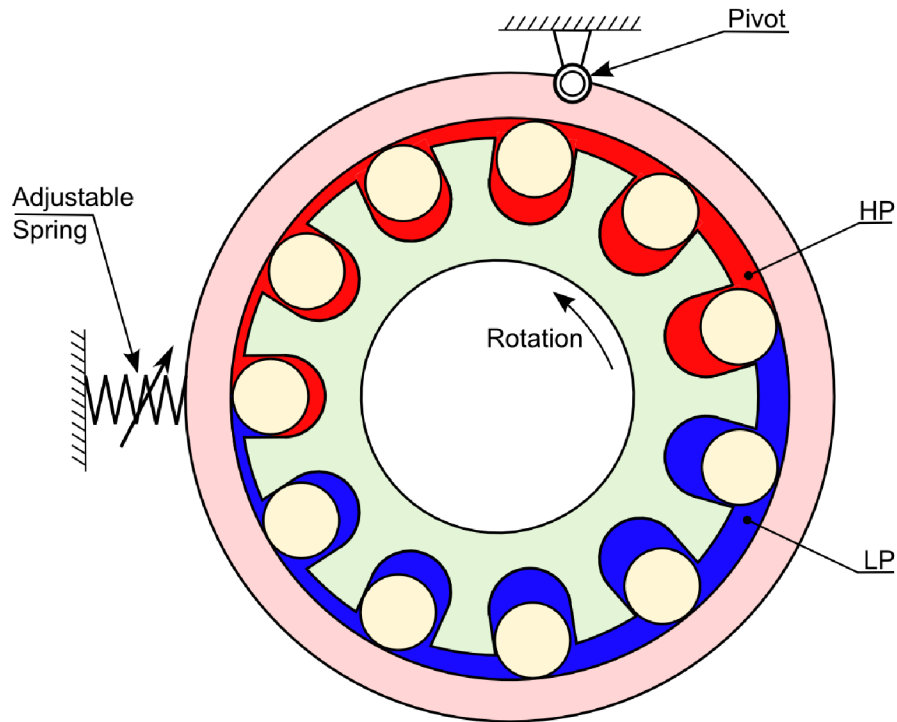


Fig. 4.3: Principle of variable roller pump simple pressure compensator (PC) control.

Used simple pressure compensator control is sensitive to the cam ring forces which have a negative impact on the control performance but on the other hand the whole pump design is very simple and robust. The biggest advantages of this design are: minimal design space requirements and very low costs. The performance measurement of this control is elaborately described in section 4.2. During the pump measurements it was confirmed that the presented simple PC control is suitable for charge pump applications and for other application with lower focus on the control performance. One example of the system test can be seen in *Fig. 6.6*. The measurements of the simple PC control resulted in applications of more sophisticated control design which is described in following sections. The more sophisticated control was applied due to validation of the idea that the variable roller pump is able to operate with better performance if it is required.

The servo pressure compensator control is similar to the simple PC control, but it may solve the weakness of the simple pressure control – significant sensitivity to the cam ring forces, what means sensitivity to the operation conditions. The first design change is the zero pivot pin offset, which minimizes the cam ring forces, which normally pushes cam ring in the direction of the maximal displacement. This function in this control is ensured with a more powerful control spring. The force acting against the cam ring is ensured by servo piston, which cylinder is connected to the pump outlet. It means that the pump displacement is depending on the outlet pressure and spring force. Theoretically it can result into a better

pressure control characteristics than a simple PC control. The costs of this control will be higher than simple PC control but lower than the spool PC control. This control wasn't realized and due to this, previous assumptions were not confirmed by measurements.

Applications with a demand for better control performance, especially with very low hysteresis, have to be equipped for example with a spool PC control. The schematic view on a variable roller pump with a PC control with a servo cylinder and a spool valve is shown in *Fig. 4.4*. The main design difference in the comparison with the simple PC control is in the hydraulic cylinder actuation and the PC spool valve implementation. The piston force acting on the cam ring tends to de-stroke (decrease displacement) and is proportional to the hydraulic pressure in the cylinder. The pressure in hydraulic cylinder (servo) is maintained by the PC spool stroke. The stroke is depending on the force balance between the outlet pump pressure and the spring force. The pressure setting of the spool PC control is adjusted by the PC spool spring. The spool PC control tries similar to the simple PC control (or servo pressure compensator control) to maintain the outlet pressure at the demanded value.

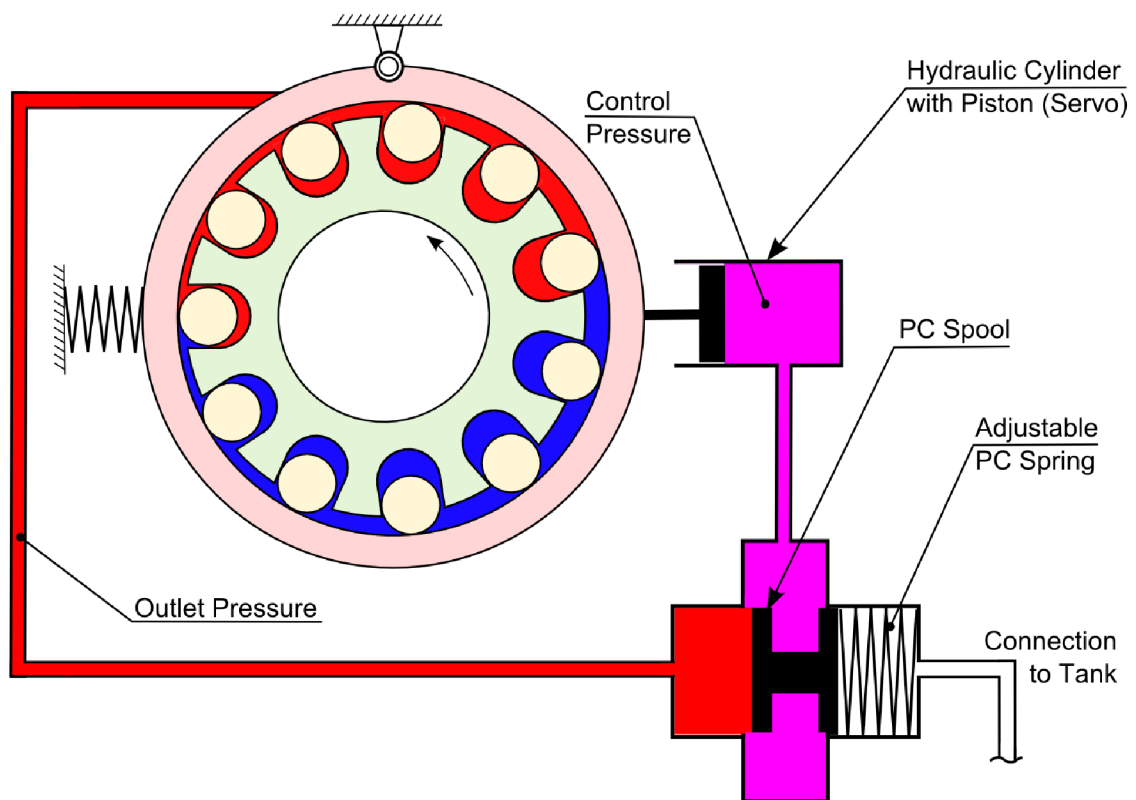


Fig. 4.4: Variable roller pump with spool PC control.

All measurements confirmed that the spool PC control rapidly decreases the hysteresis and decrease overshoots which is caused by a lower dependency on the cam ring forces and higher control forces which overcome the friction forces easily. With other words, a whole control has a higher overall proportional gain. The tested pump with a spool PC control, servo cylinder and spool valve used the same pivot offset as the pump with a simple spring control.

This control type is the most expensive control type but on the other hand it provides significant better performance than the simple pressure control, confirmed by measurements in section 4.2. The cost difference between a spool PC control and a servo PC with servo

cylinder is caused by an additional PC spool, PC spool bore, guide, PC spool spring and adjustable screw, which enables a simple pressure adjustments of the spool PC control pressure.

4.2 Control Dynamics

The purpose of this chapter is to provide basic information about VCP dynamics with a simple pressure compensator control (regulation) and spool compensator control. The servo pressure compensator control wasn't realized, but the mathematical description of this control type is similar to the simple PC control. The basic investigation requires a lot of simplifications which are mentioned later. Available literature provides a good basement for a control/system model development, for example: Karmel [15], [23], Noskievic [24], Turza [25], Perry [39], Merrit [40], Manring [41], Koreis [42]. The general control theory can be found for example in [43], [44]. The presented approach is suitable for a first investigation in this area. For further analyses and control development, the 1-D nonlinear pump and control model is a mandatory. This deep control and system analysis is not focus of this work.

4.2.1 Simple PC Control

The simplified cam ring dynamics of the VCP with simple PC control (*Fig. 4.3*) is described by following equation:

$$I_{cam} \cdot \ddot{\varphi}_{cam} + B_{cam} \cdot \dot{\varphi}_{cam} + K_{cam} \cdot \varphi_{cam} = p_{dis} \cdot (d_{cam} \cdot w_{rol}) \cdot (e_{rotMax} + o_{pinX}) - F_{spr0} \cdot o_{pinY} \quad (4.1)$$

where I_{cam} is the cam ring rotational inertia, φ_{cam} is the cam ring angle (the rotor eccentricity e_{rot} can be easily calculated from known φ_{cam}), B_{cam} is the cam ring damping, K_{cam} is the spring rate, p_{dis} is the discharge (outlet pressure), d_{cam} , w_{rol} are cam ring (roller) dimensions (*Fig. 3.3*), e_{rotMax} is the maximal rotor eccentricity, o_{pinX} , o_{pinY} are distances between cam ring center and pivot center and F_{spr0} is the spring preload. The spring preload torque ($F_{spr0} \cdot o_{pinY}$) can be rewritten and the resultant equation is:

$$I_{cam} \cdot \ddot{\varphi}_{cam} + B_{cam} \cdot \dot{\varphi}_{cam} + K_{cam} \cdot \varphi_{cam} = (p_{set} - p_{dis}) \cdot (d_{cam} \cdot w_{rol}) \cdot (e_{rotMax} + o_{pinX}) \quad (4.2)$$

This equation can be simply rewritten with Laplace transform. The output of this equation is the cam ring angle φ_{cam} which is the input of a pump flow equation and the pump flow Q_{VCP} is input of the pressure build up equations [39]. The linear system model build on this approach can be seen in *Fig. 4.5*. Used variables are listed in *Tab. 4.1*.

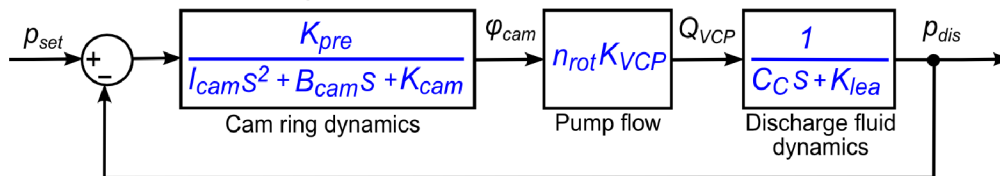


Fig. 4.5: Linearized block diagram of the pump and simple pressure compensator control with pressure input.

Tab. 4.1: VCP parameters and simple PC control parameters.

VCP with Simple PC Control				
Description	Variable	Calculation	Value	Unit
Cam ring inner diameter	d_{cam}	Drawing	$80.77 \cdot 10^{-3}$	m
Cam ring width	w_{rol}	Drawing	$16 \cdot 10^{-3}$	m
Max rotor eccentricity	e_{rotMax}	Drawing	$2.08 \cdot 10^{-3}$	m
Pin offset - Y direction	o_{pinY}	Drawing	$47 \cdot 10^{-3}$	m
Pin offset - X direction	o_{pinX}	Drawing	$3.8 \cdot 10^{-3}$	m
Maximal pump displacement	V_{gMax}	Estimated	$17 \cdot 10^{-6}$	m ³
Cam ring inertia	I_{cam}	Calculated (Steiner theorem)	0.00005	kg·m ²
Cam ring damping	B_{cam}	Estimated	30	N·m·s
Spring rate	K_{cam}	$k_{spr} \cdot (o_{pinY})^2$	233.3146	N·m
Pressure torque gain	K_{pre}	$\frac{d_{cam} \cdot w_{cam} \cdot (e_{rotMax} + o_{pinX})}{\tan^{-1} \frac{e_{rotMax}}{o_{pinY}}}$	$2.1969 \cdot 10^{-6}$	m ³
Pump flow gain	K_{VCP}	$\frac{V_{gMax}}{\tan^{-1} \frac{e_{rotMax}}{o_{pinY}}}$	$3.8439 \cdot 10^{-4}$	m ³
Pump speed	n_{rot}	Defined	30	s ⁻¹
Oil compliance	C_c	$\frac{V_{dis}}{K_A}$	$1.493 \cdot 10^{-13}$	m ³ ·Pa ⁻¹
Leakage coefficient	K_{lea}	Estimated	$1.1 \cdot 10^{-11}$	m ³ ·s ⁻¹ ·Pa ⁻¹

The pump pressure transfer function $G_{VCPp}(s)$ can be derived from the previous block diagram shown in Fig. 4.5. The derived equation is:

$$G_{VCPp}(s) = \frac{K_{pre} \cdot n_{rot} \cdot K_{VCP}}{(I_{cam}s^2 + B_{cam}s + K_{cam}) \cdot (C_c s + K_{lea}) + K_{pre} \cdot n_{rot} \cdot K_{VCP}} \quad (4.3)$$

In the standard form this transfer can be written as:

$$G_{VCPp}(s) = \frac{K_{pre} \cdot n_{rot} \cdot K_{VCP}}{K_{pre} \cdot n_{rot} \cdot K_{VCP} + K_{cam} \cdot K_{lea}} \cdot \frac{1}{\left[\frac{I_{cam} \cdot C_c}{K_{pre} \cdot n_{rot} \cdot K_{VCP} + K_{cam} \cdot K_{lea}} \right] s^3 + \left[\frac{B_{cam} \cdot C_c + I_{cam} \cdot K_{lea}}{K_{pre} \cdot n_{rot} \cdot K_{VCP} + K_{cam} \cdot K_{lea}} \right] s^2 + \left[\frac{B_{cam} \cdot K_{lea} + K_{cam} \cdot C_c}{K_{pre} \cdot n_{rot} \cdot K_{VCP} + K_{cam} \cdot K_{lea}} \right] s^2 + 1} \quad (4.4)$$

The Bounded Input Bounded Output (BIBO) definition of stability says; that the system is stable if the output is bounded for all bounded inputs [44]. The rule necessary for stability is: If all poles of the transfer function have negative parts, then the system is stable. If any pole is positive (or positive part of the pole), then the system is unstable [43].

In the investigated case of the simple PC control, poles are negative ($-7.999 \cdot 10^5$, $-10.2842 + 53.9894i$, $-10.2842 - 53.9894i$). Thus this system is stable. The bode plot of this linearized system is shown in Fig. 4.6. The bandwidth frequency is about 13 Hz according to this graph. The step response is shown in Fig. 4.7.

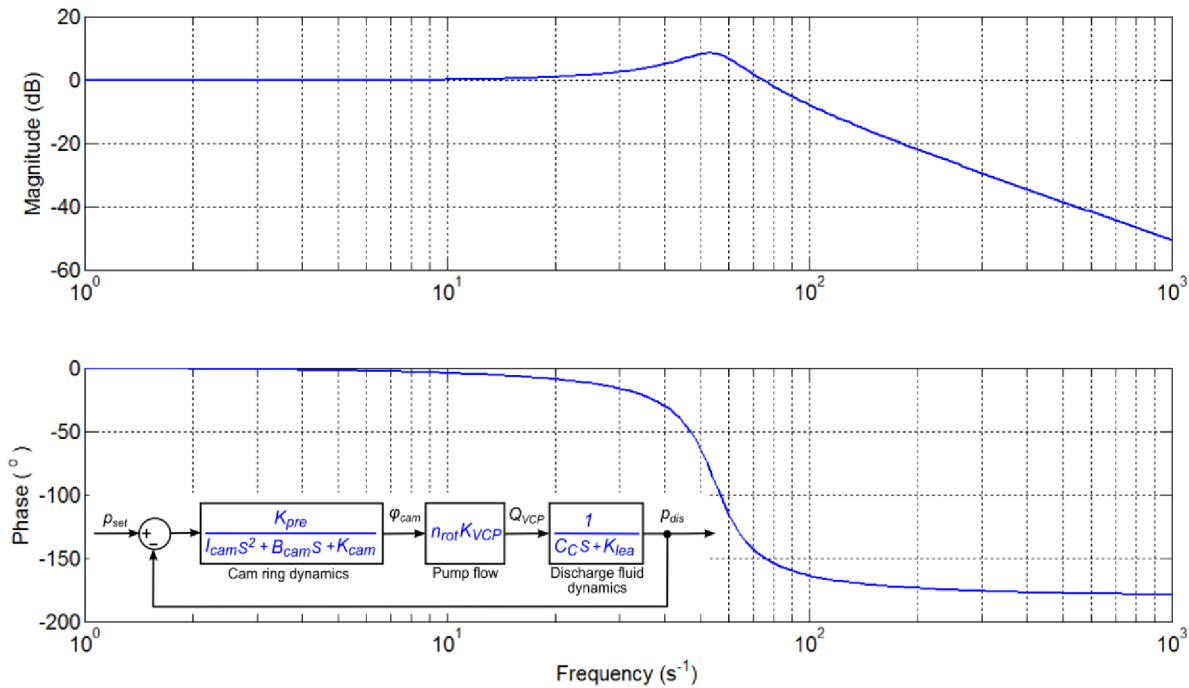


Fig. 4.6: Bode diagram of the linearized VCP pump with the simple PC control (Frequency in $\text{rad} \cdot \text{s}^{-1}$).

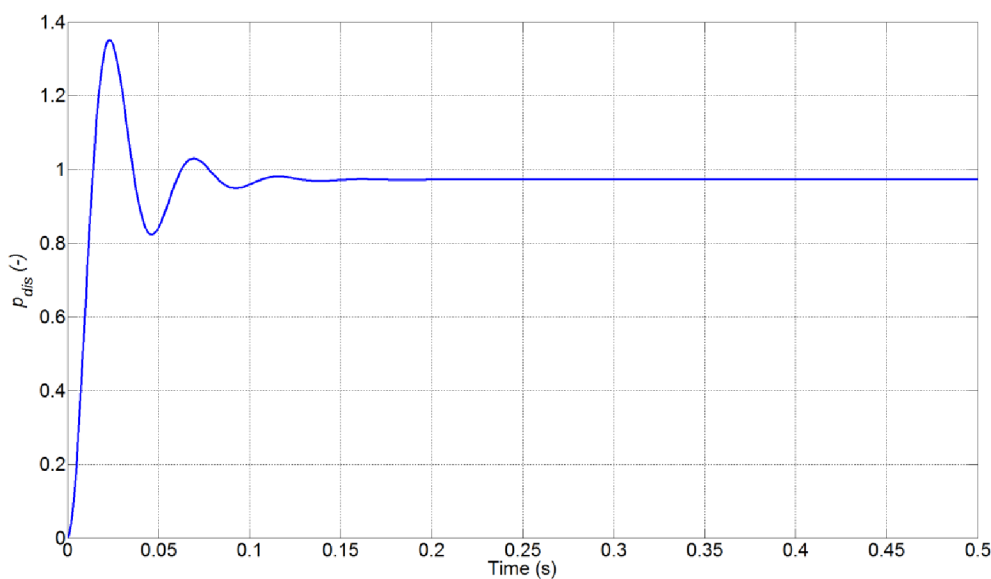


Fig. 4.7: Step response of the linearized VCP pump with simple PC control.

The previous calculations and plots are based on the linearized system model. This model neglects: nonlinearities of the cam ring forces and friction forces. The pump leakage is depending only on the discharge pressure p_{dis} and other effects such as filling losses, flow and pressure pulsation are not considered. The cam ring damping is parameter which was only estimated and the real value can be significantly depending on a lot parameters and operating conditions. All these facts have to be taken into account during results evaluation.

The first information about the system stability and bandwidth frequency is important but more precise information can be obtained only from measurements or 1-D nonlinear simulations. The step response simulation shows fast response with permanent offset from demanding value 1. It is probably caused by a relatively low proportional gain of the simple PC control (regulation). It can negative influence VCP performance parameters.

Normally the pressure setting of the control is constant and input to the system is a flow demand Q_{Loa} which is changing during pump operation. *Fig. 4.8* follows this architecture.

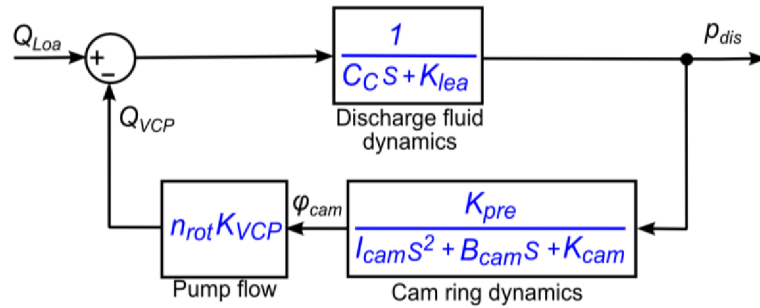


Fig. 4.8: Linearized block diagram of the pump and simple pressure compensator control with flow input.

The transfer function of this system is written as:

$$G_{VCPf}(s) = \frac{-(I_{cam}s^2 + B_{cam}s + K_{cam})}{(I_{cam}s^2 + B_{cam}s + K_{cam}) \cdot (C_C s + K_{lea}) + K_{pre} \cdot n_{rot} \cdot K_{VCP}} \quad (4.5)$$

4.2.2 Spool PC Control

The precise dynamic description of the spool PC control (*Fig. 4.4*) is more complicated [14], [15], [16]. The very good base for the model build can be found in Manring's works, mainly in [41] and Perry's work [39]. The major part of this work can be applied for the investigated pump. According to Manring the dynamic equation of the variable roller pump with spool PC control can be written as:

$$\dot{\varphi}_{cam} = \frac{2 \cdot K_q}{A_{ser} \cdot o_{pinY}} \cdot \left(\frac{A_{spo}}{k_{spl} + 2 \cdot K_{fq}} \right) \cdot (p_{set} - p_{dis}) \quad (4.6)$$

Then the block diagram of the spool PC controlled pump is shown in *Fig. 4.9* and the corresponding transfer function is shown in equation (4.7). This model can be used in PC controlled pumps where the servo pressure is corresponding approximately to the half of the discharge pressure [41]. This ratio is corresponding to the VCP with the spool PC control at common operation conditions. The approach neglects cam ring friction and damping forces. The primary focus of this model is the spool and servo dynamic properties such as the spool and servo proportional gain.

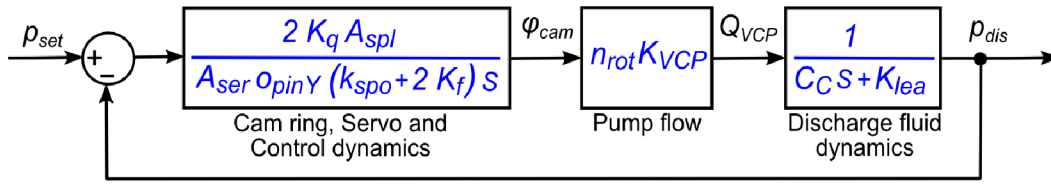


Fig. 4.9: Linearized block diagram of the pump and spool pressure compensator control with pressure input.

$$G_{VCPp}(s) = \frac{\frac{2 \cdot K_q}{A_{ser} \cdot o_{pinY}} \cdot \left(\frac{A_{spo}}{k_{spo} + 2 \cdot K_f} \right) \cdot n_{rot} \cdot K_{VCP}}{C_c s^2 + K_{lea} s + \frac{2 \cdot K_q}{A_{ser} \cdot o_{pinY}} \cdot \left(\frac{A_{spo}}{k_{spo} + 2 \cdot K_f} \right) \cdot n_{rot} \cdot K_{VCP}} \quad (4.7)$$

The pump flow and leakage model was considered the same as for simple PC control. Newly introduced variables are listed in Tab. 4.2. The spool flow gain and flow force gain are calculated based on the spool valve geometry [41].

Tab. 4.2: VCP parameters and spool PC control parameters.

VCP with Spool PC Control				
Description	Variable	Calculation	Value	Unit
Max rotor eccentricity	e_{rotMax}	Drawing	$2.08 \cdot 10^{-3}$	m
Pin offset - Y direction	o_{pinY}	Drawing	$47 \cdot 10^{-3}$	m
Maximal pump displacement	V_{gMax}	Estimated	$17 \cdot 10^{-6}$	m^3
Pump flow gain	K_{VCP}	$\frac{V_{gMax}}{\tan^{-1} \frac{e_{rotMax}}{o_{pinY}}}$	$3.8439 \cdot 10^{-4}$	m^3
Pump speed	n_{rot}	Defined	30	s^{-1}
Oil compliance	C_c	$\frac{V_{dis}}{K_A}$	$1.493 \cdot 10^{-13}$	$m^3 \cdot Pa^{-1}$
Leakage coefficient	K_{lea}	Estimated	$2.3 \cdot 10^{-11}$	$m^3 \cdot s^{-1} \cdot Pa^{-1}$
Servo piston area	A_{ser}	Drawing	$5.7256 \cdot 10^{-4}$	m^2
PC Spool area	A_{spo}	Drawing	$1.9635 \cdot 10^{-5}$	m^2
Spool spring rate	k_{spo}	Drawing	37140	$N \cdot m^{-1}$
Spool flow gain	K_q	Calculated according to [41]	0.257	$m^2 \cdot s^{-1}$
Flow force gain	K_f	Calculated according to [41]	11560	$N \cdot m^{-1}$

The stability analysis with table parameters shows that all poles are negative (-77.027+54.068i, -77.027-54.068i) and the system can be considered as a stable. The bandwidth frequency (-3 dB) can be taken from bode graph in Fig. 4.10. The bandwidth frequency of the VCP with spool PC control is about 133 Hz. This value is relatively high;

normally PC control pumps have lower bandwidth frequencies. The step response is shown in Fig. 4.11. Simulation results have to be considering with respect to simplifications in the linearized model. The figure shows that the response of the pump is faster than the simple PC control. The offset of the discharge pressure is minimal. Base on this, it can be concluded that the overall proportional gain is higher than the proportional gain of the simple PC control. The gain is probably higher than in the reality. This can be caused by simplifications. A high proportional gain could have a positive influence on the system performance such as hysteresis decrease or fast system response and minimal system dependency on the disturbing signals. On other hand it can have a negative influence on the control (system) stability.

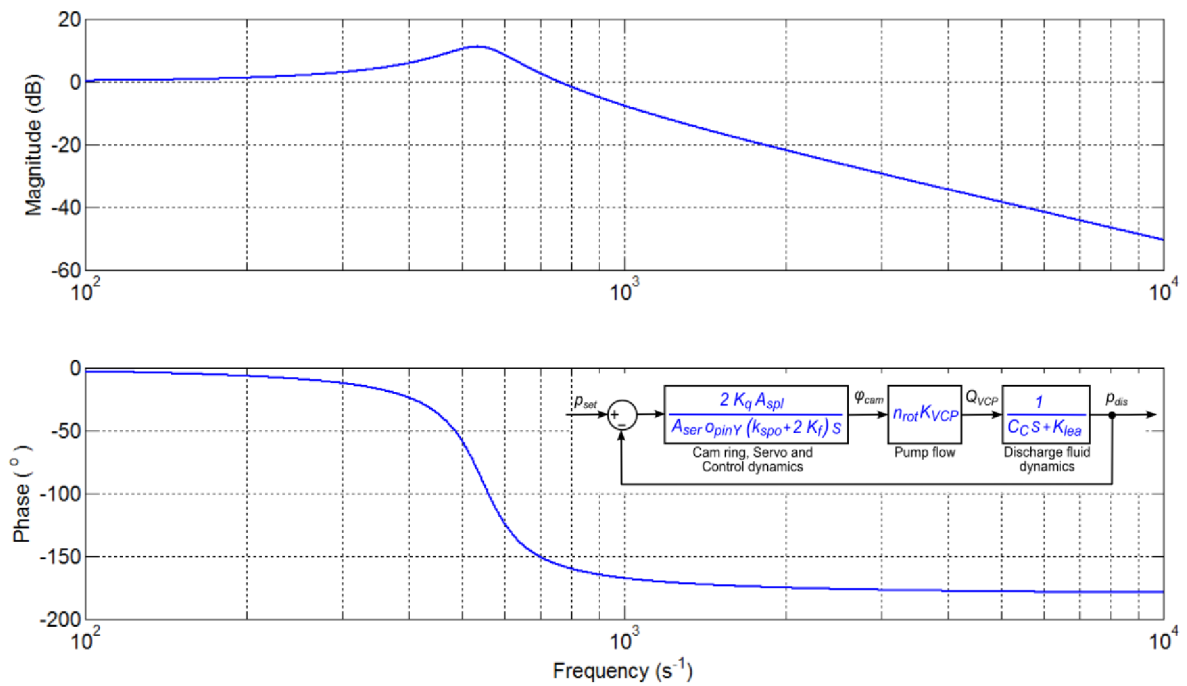


Fig. 4.10: Bode diagram of the linearized VCP pump with the spool PC control (Frequency in $\text{rad}\cdot\text{s}^{-1}$).

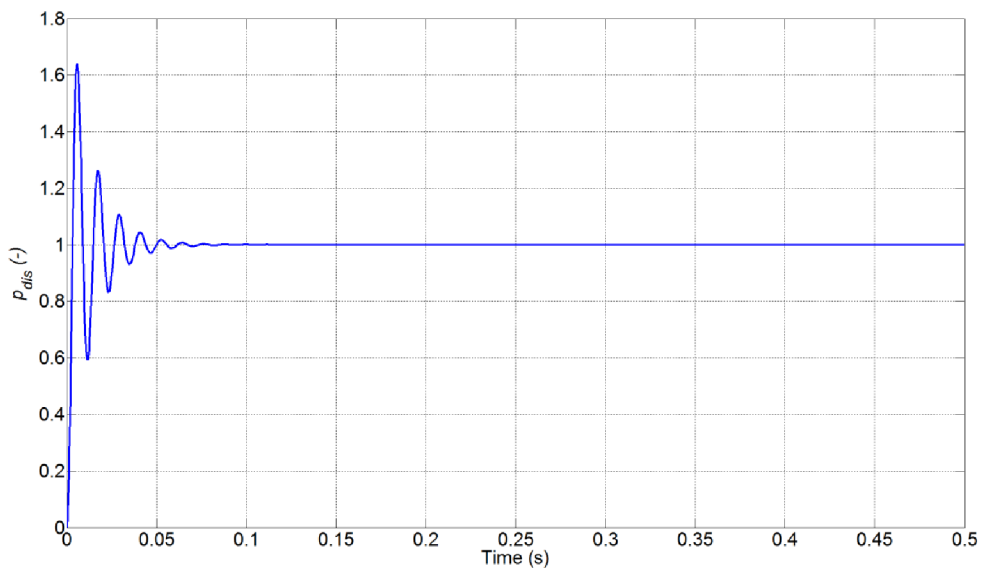


Fig. 4.11: Step response of the linearized VCP pump with spool PC control.

4.3 Performance Measurements

The primary function of the performance measurements was the validation of the pump pressure compensator (PC) control. Normally, the performance measurements for open circuit pumps equipped with PC controls consist of three main test types: the pressure ramp, the speed ramp and the response-recovery test. Tested pumps were equipped with the simple PC control and the spool PC control. Measured results presented in this section provide only examples for better overview about the pump control performance and used tests.

4.3.1 Pressure Ramps

The pressure ramp measurement of the pump with the simple PC control is shown in *Fig. 4.12*. The circuit diagram in this figure shows the simplified hydraulic circuit used for measurements. Generally, the used circuit configuration was identical with configuration from the efficiency measurement in *Fig. 5.13*. The difference is only in the active pump displacement control, which was used for performance tests. The pump speed was 3000 min^{-1} and the inlet oil temperature 50°C was constant during the test. The VCP loading was realized with a relief valve loading ramp. Duration of the loading ramp was 90 s. The outlet pressure was increased for 30 s, for 30 s the outlet pressure was constant and for 30 s the outlet pressure was decreased. The starting relief valve setting of the loading ramp was 10 bar and the maximal value was 30 bar what can be seen in *Fig. 4.12*.

The first graph in this figure presents the outlet (charge, HP) pressure p_{ch} and the pump flow Q_e in dependence on the time. At the low outlet pressure, the pump runs at the maximal displacement, which can be seen from the non-reduced flow until 15 s. At 15 s, the outlet pressure achieves 18 bar (PC settings) which results in a displacement reduction and therefore the pump flow drops down. The minimal displacement was achieved with the outlet (charge) pressure 23 bar. This displacement change from maximal to minimal displacement is connected with the charge pressure increase about 5 bar. The pump displacement in the active control range is depending on the outlet pressure or with other words pump control is not able to maintain the constant outlet pressure in the active range. In the ideal case, the PC control is able to maintain constant outlet pressure. This effect is caused by the control spring rate and the cam ring forces behavior. Theoretically, the lower spring rate will make this change more ideal. The behavior of the simple pressure control is not ideal, but suitable for a charge pump application. Decreasing of the relief valve setting from 30 bar to 10 bar (60 s – 90 s) shows hysteresis in bottom (p - Q) graph. In this case the hysteresis is caused by friction, cam ring pivot offset and a relatively low control proportional gain. This can be seen also from basic simulation in *Fig. 4.7*.

The measurement of the spool PC control is shown in *Fig. 4.13*. The loading circuit configuration is identical with previous test. The pump speed was constant 3000 min^{-1} and the inlet oil temperature was constantly 50°C . The pump outlet was connected to the relief valve with variable setting. The VCP was loaded with the pressure ramp. Duration of the loading ramp was 90 s, consisting of an outlet pressure increase for 30 s, a constant pressure for 30 s and a pressure decrease for 30 s. The initial relief valve setting ramp was 15 bar and maximal value was 40 bar what can be seen in *Fig. 4.13*. The control setting was about 22 bar.

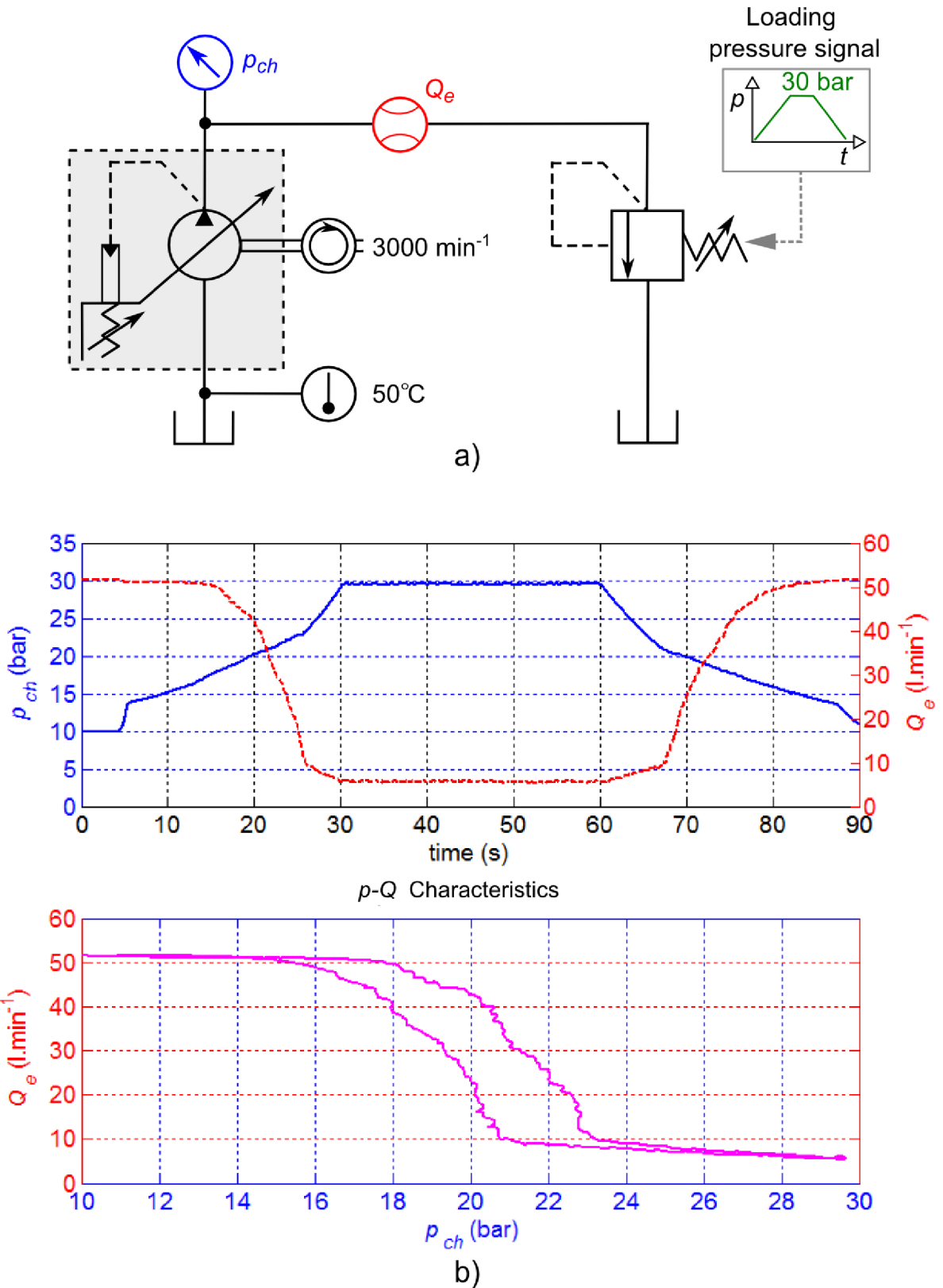


Fig. 4.12: Measurement of VCP pressure ramp with simple pressure control.
 a) Simplified hydraulic circuit diagram used for measurements.
 b) Measured charge pressure, pump flow and p - Q characteristic.

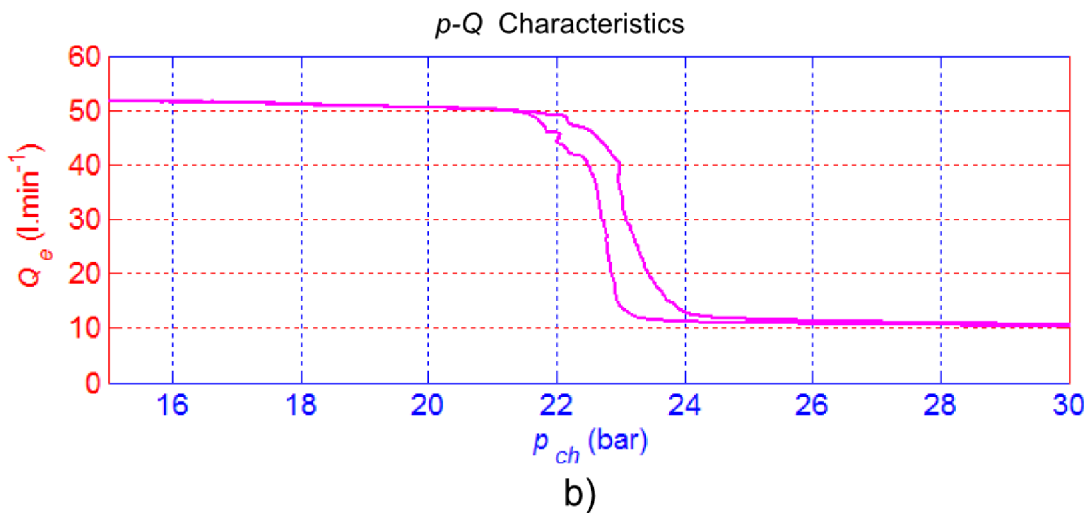
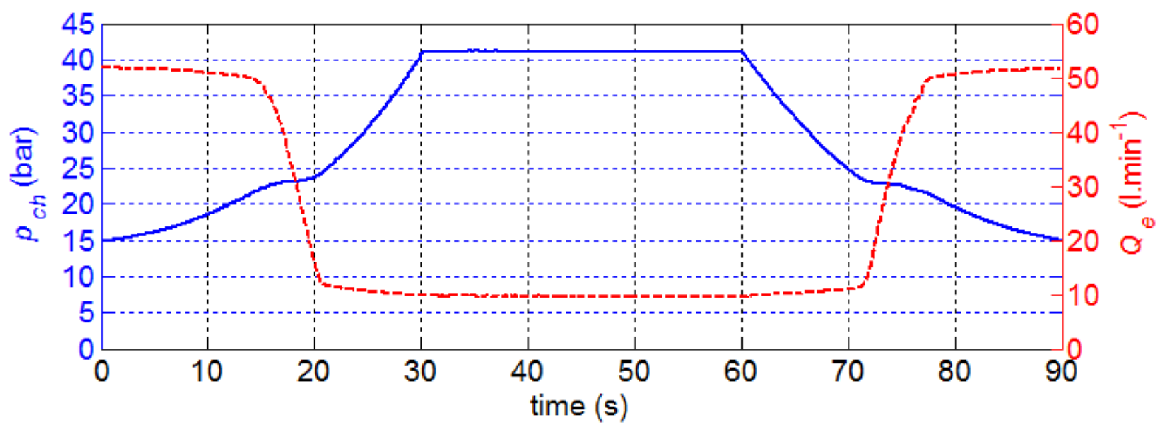
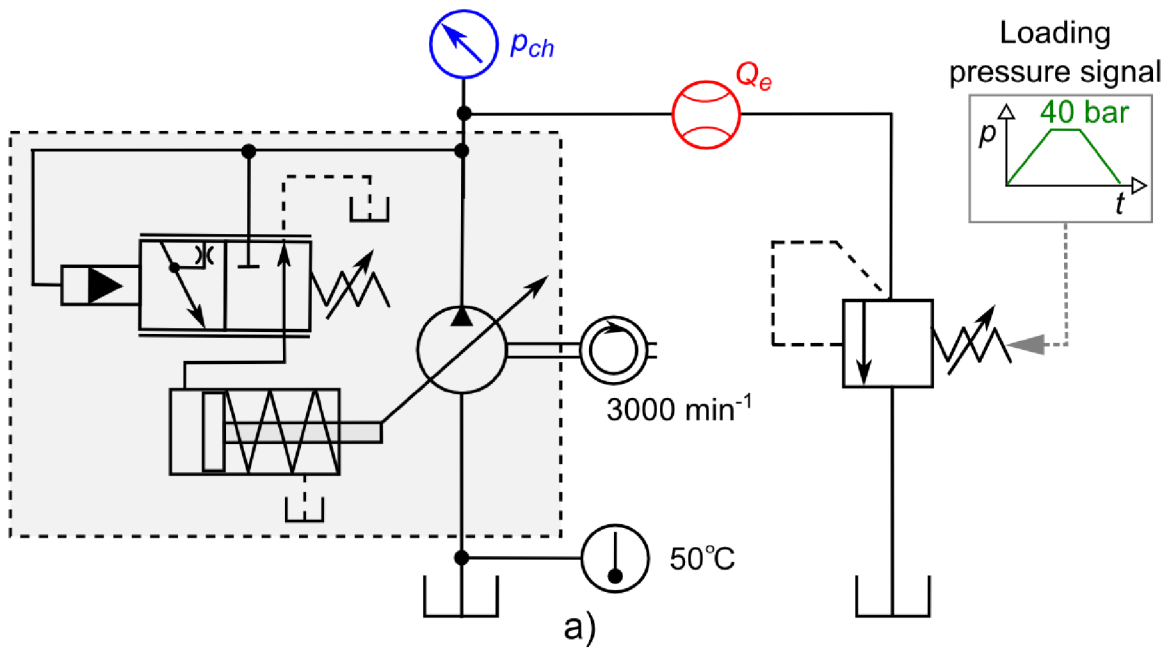


Fig. 4.13: Measurement of VCP pressure ramp with PC control.
 a) Simplified hydraulic circuit diagram used for measurements.
 b) Measured charge pressure, pump flow and p - Q characteristic.

It can be seen that the pump displacement in the active control range is again depending on the charge pressure or with other words pump control is not able to maintain the constant outlet pressure in active range. The spool PC control has more ideal behavior than a simple PC control due to a higher proportional gain (*Fig. 4.11*). The simple pressure control requires about 5 bar of pressure change (it can be adjusted by spring with lower rate) for complete displacement change that is more than a PC control, which requires only 2 bar.

4.3.2 Speed Ramps

The speed ramp measurement of the simple pressure control is shown in *Fig. 4.14* at the next page. The upper part of the figure (*Fig. 4.14a*) presents simplified hydraulic circuit diagram for speed ramp measurements. The sensors were used from efficiency measurements. The main difference of the circuit configuration between the pressure ramp measurements and the presented speed ramp measurements is the loading device. The speed ramp measurements are normally performed with a constant orifice at the pump output instead of the relief valve for pressure ramps.

The pump speed is ramped from 500 min^{-1} at the beginning up to 4000 min^{-1} at 60 s. The maximal pump speed of 4000 min^{-1} is constant from 60 s until 90 s. The next 60 s, the pump speed decreases from 4000 min^{-1} to the idle speed 500 min^{-1} . The inlet oil temperature was 50°C during the whole cycle. The pump shaft speed, the outlet (charge) pressure and the pump flow is shown in *Fig. 4.14b*. During speed ramping, the outlet pressure and the pump flow show overshoots at 40 s, which is corresponding to the time, when the simple pressure control starts to operate. At this moment, the charge pressure ensures sufficient force acting on the cam ring against the compression control spring. The outlet pressure force is higher than the compression spring preload and the pump displacement is reducing, ensuring constant flow and charge pressure until 110 s. The similar overshoot occurs at 110 s when the control ends operation. In this case, the charge pressure force acting on the cam ring is lower than the compression spring preload and the cam ring reaches maximal displacement. Clear speed-pressure characteristic is shown at the bottom part of the *Fig. 4.14b*. This graph directly shows a pump hysteresis and a relatively constant outlet (charge) pressure except for pressure overshoots at 2700 min^{-1} (40 s and 110 s). The whole hysteresis for pump with simple PC control is up to 2 bar and at overshoots up to 4 bar.

The spool PC control speed measurement is shown in *Fig. 4.15*. The simplified hydraulic circuit is again shown in the upper part (*Fig. 4.15a*). All measurement devices and loading conditions are identical with previous simple pressure measurements.

Measured charge pressure and flow are shown in *Fig. 4.15b*. The outlet pressure increases with the pump speed. At 38 s, charge pressure and flow are saturated because of PC control which starts to operate at the outlet pressure level corresponding to the PC spool spring preload. At 110 s full pump displacement is achieved again. The pressure and flow characteristics of the PC control show ideal behavior without overshoot. The speed-pressure characteristic shows minimal hysteresis in *Fig. 4.15b*.

The speed ramp measurements confirm similar to the pressure ramp measurements that the spool PC control shows better performance with minimal pressure overshoots and minimal hysteresis. This behavior is caused again with the different control approach and different control proportional gains. The spool of the PC control is able to control the outlet pressure more precisely than the standard simple PC control due to higher gain.

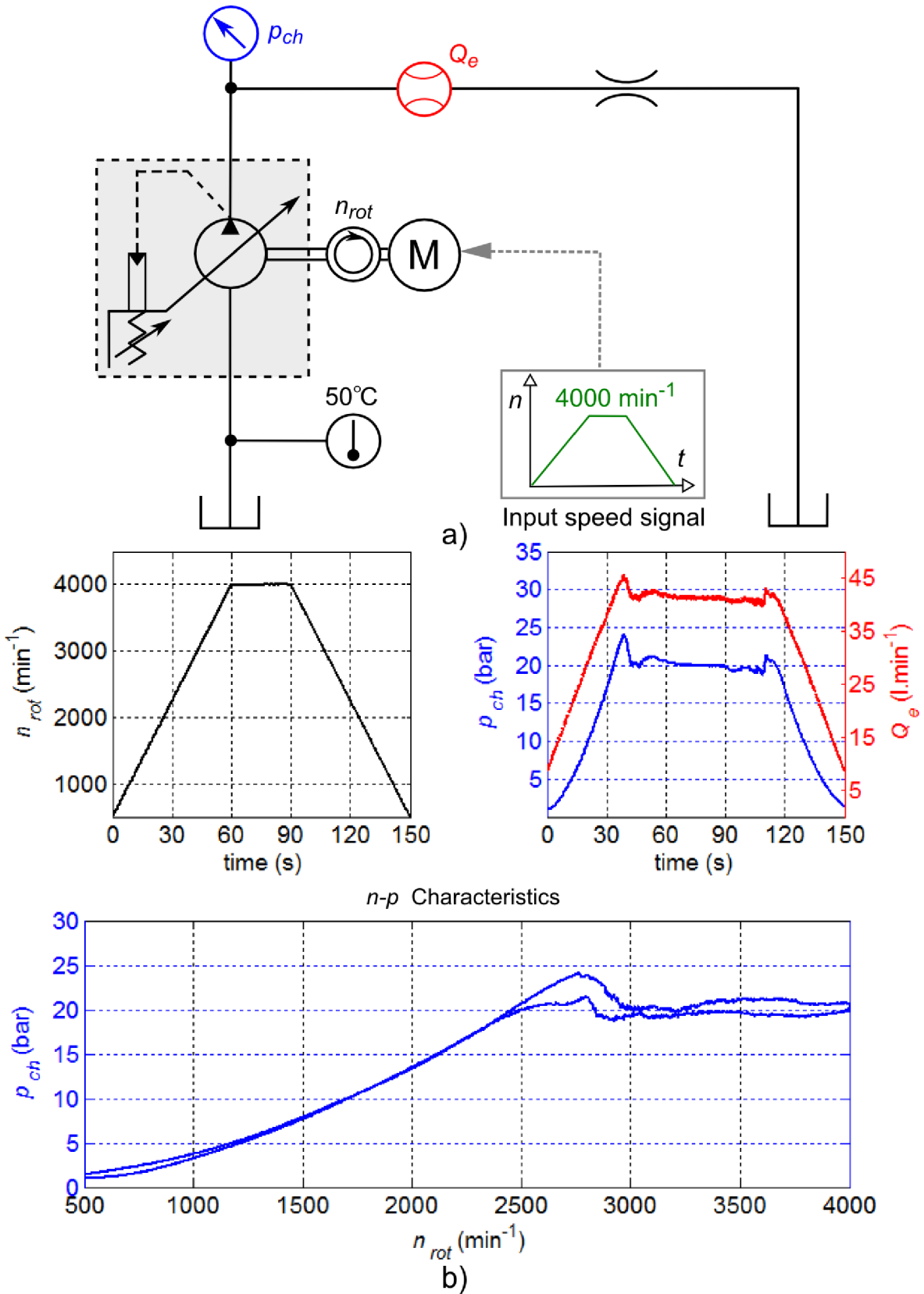


Fig. 4.14: Measurement of VCP speed ramp with simple pressure control.
 a) Simplified hydraulic circuit diagram used for measurements.
 b) Measured speed, charge pressure, pump flow and n-p characteristic.

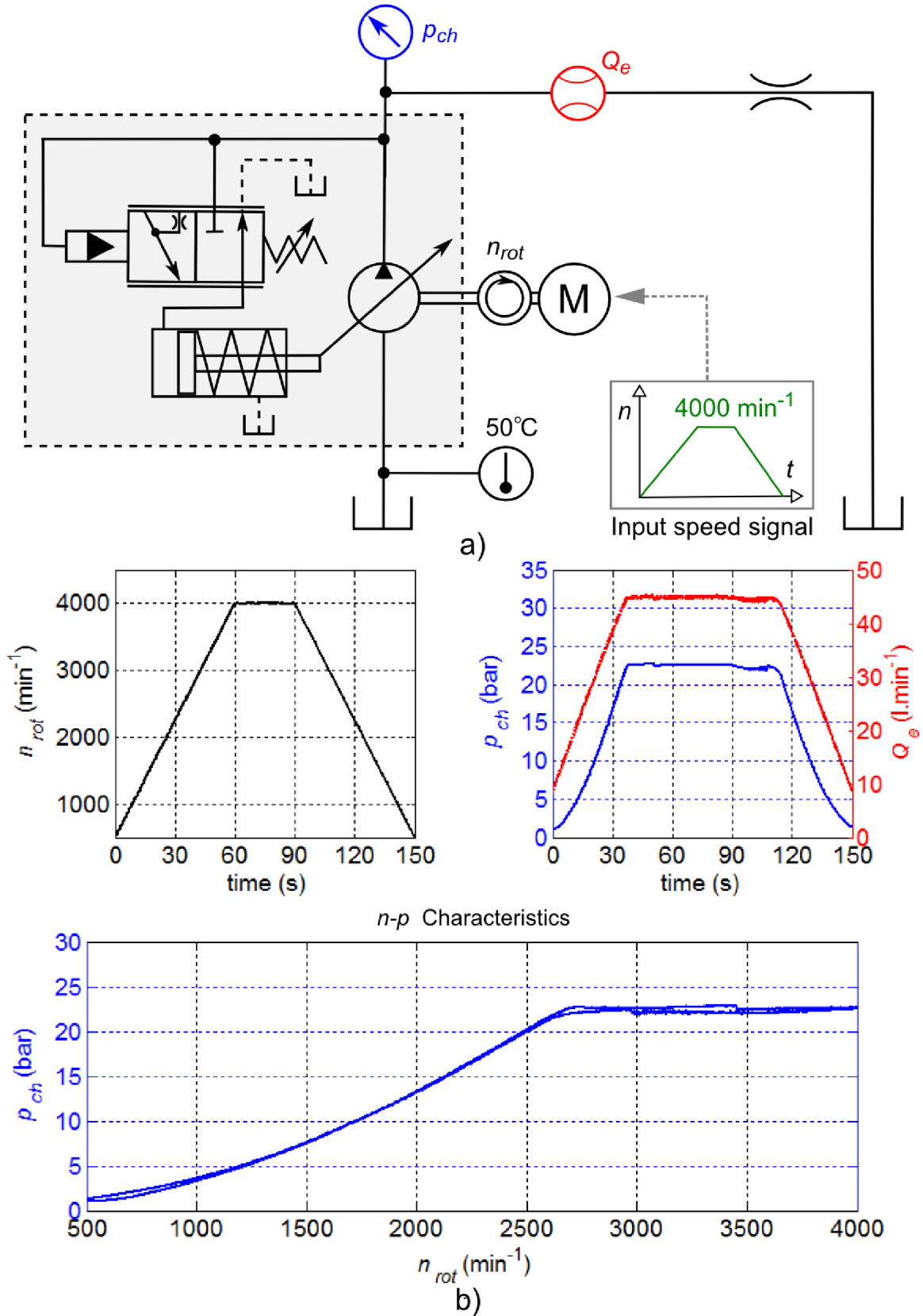


Fig. 4.15: Measurement of VCP speed ramp with PC control.
 a) Simplified hydraulic circuit diagram used for measurements.
 b) Measured speed, charge pressure, pump flow and n - p characteristic.

4.3.3 Response and Recovery

The last important measurement is a response and recovery test for pressure compensator control types. The testing procedure is described in standard SAEJ745 [45]. The response and recovery times definition is presented in *Fig. 4.16*.

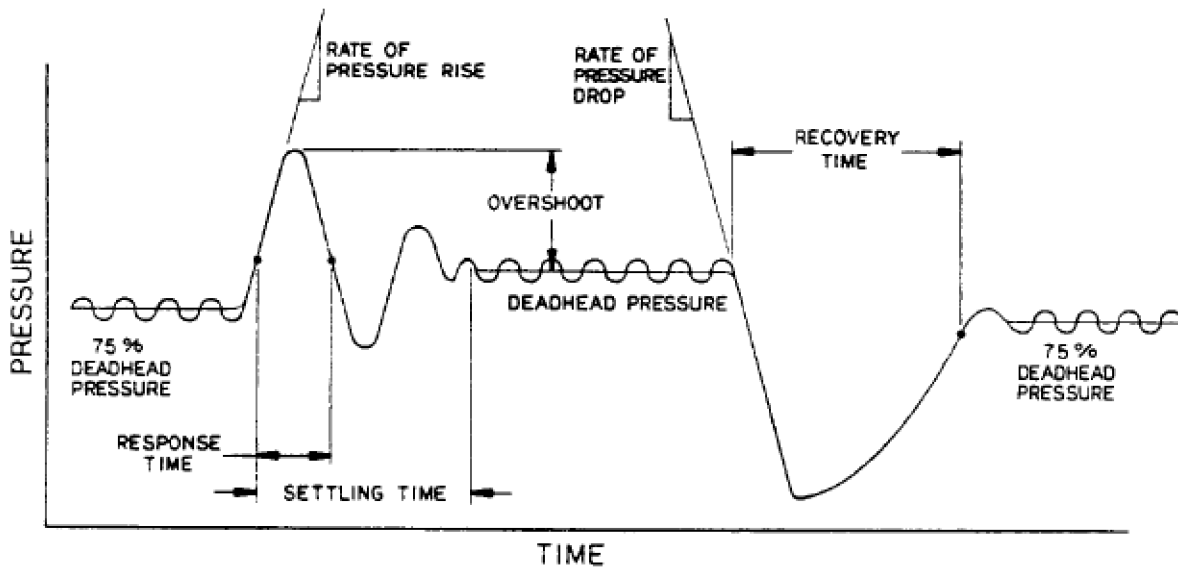


Fig. 4.16: Response and recovery time definition [45].

The simplified circuit diagram of the response and recovery measurement based on SAEJ745 for the simple pressure control is shown in *Fig. 4.17a*.

The pump runs at full displacement with constant speed against two orifices, the first one is part of the shutoff valve and the second orifice is mounted in the line connected to the tank. The outlet (charge) pump pressure $p_{ch} = 11$ bar is constant and the simple pressure control is not active. The shutoff valve is quickly energized and the shutoff valve (orifice) is closed. The solenoid current to the shutoff valve is shown in *Fig. 4.17b*. The rapid close of the shutoff valve at 3 s (and at 11 s) results in a rapid outlet (charge) pressure increase up to 33 bar which is the setting of the simple PC control. The constant pressure was ensured by a displacement reduction, visible in *Fig. 4.17b*. The pump reacts on the shutoff valve closure with a fast displacement reduction which ensured the outlet pressure at the level of the simple pressure control setting. At 6 s (and 16 s) the shutoff valve is rapidly opened. The pump displacement is increased up to the maximal displacement, but it is not enough to keep the pressure control setting which the pump tries to hold. The outlet pressure settles at initial outlet pressure level ($p_{ch} = 11$ bar).

It can be seen that the VCP pump with the simple PC control provides sufficient dynamics for charge pump applications. The pump displacement decrease and increase is very fast and the pump doesn't produce any significant outlet (charge) pressure overshoots, undershoots or any significant lag. In the case of the demand for more ideal response-recovery behavior, the charge pump system can be equipped with a hydraulic accumulator. The target of this work isn't a detail investigation of the pump control. The response and recovery wasn't measured for the spool PC control. But experiences from open circuit pumps with spool PC controls together with performed basic simulations give realistic assumption that the PC control dynamics will be sufficient too.

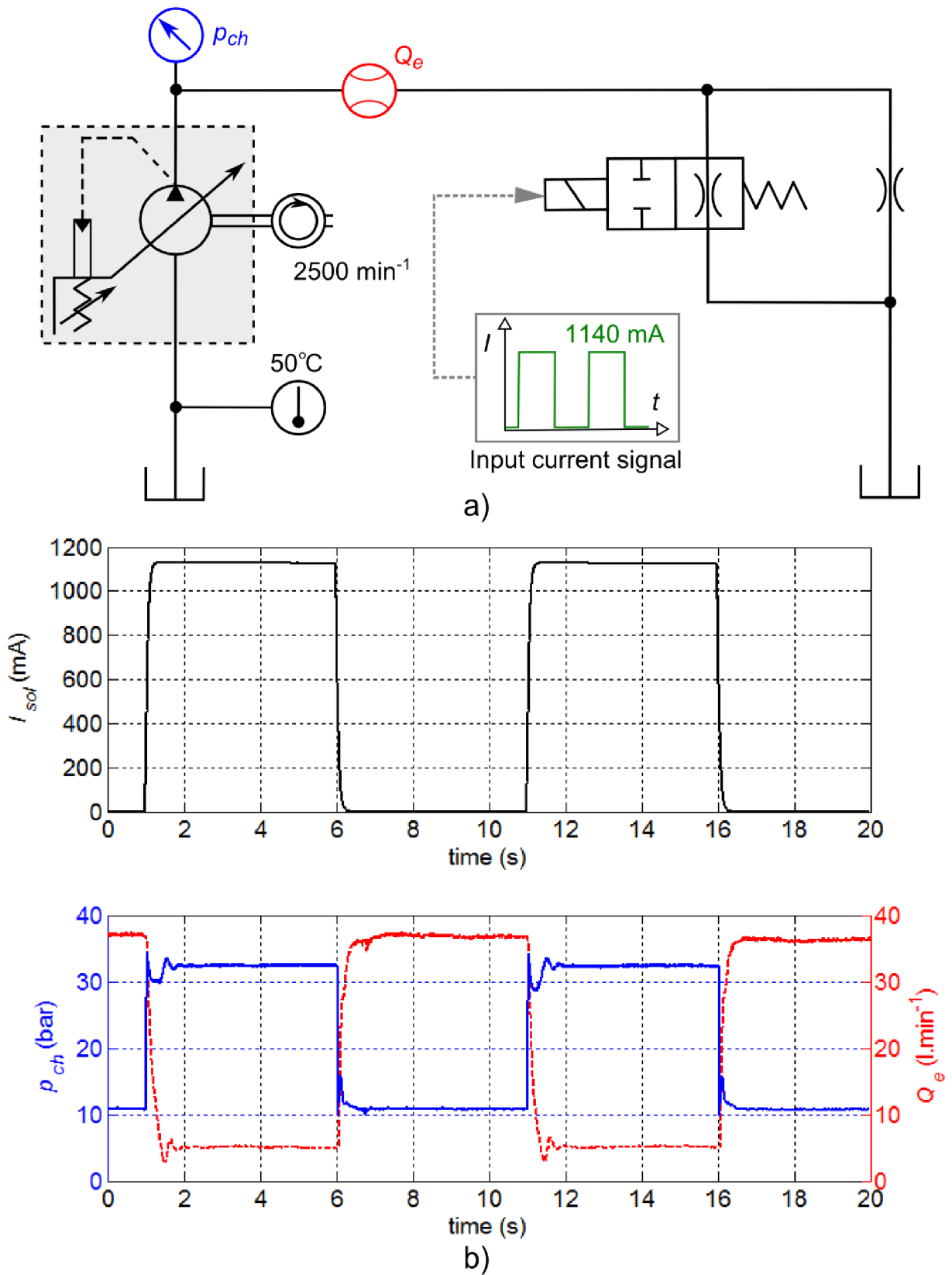


Fig. 4.17: Measurement of VCP response-recovery with simple pressure control.

a) Simplified hydraulic circuit diagram used for measurements.

b) Measured shutoff valve current, charge pressure, pump flow.

5 PORT PLATE OPTIMIZATION

The port plate optimization is focused primary on the volumetric efficiency at the maximal pump displacement in this work. Generally, there is a lot of options for optimization and increase of the overall pump efficiency. The hydro-mechanical efficiency (mainly friction losses) can be optimized by material selection, component design etc. but volumetric efficiency contributes to also the overall efficiency. Especially the kidney design of the port plates has a huge impact on the pump volumetric efficiency and pressure profile in the chambers, which is related with component wear and noise. Due to this, the volumetric efficiency was selected for optimization, similar to an axial piston pump, where valve plate design plays a very important role too. The sophisticated way to make an optimization is a simulation based optimization. The core of each simulation based optimization is a mathematical simulation model together, with an optimization algorithm [46]. Generally, three options of simulation model were considered.

The first one is a simulation model based on the one dimensional approach (1-D). The 1-D modelling theory for the roller pump was described in Chapter 3. The one dimensional (1-D) approach allows a relatively short simulation time which is ideal for the port plate simulation based optimization like a standard piston pump valve plate optimization. This approach includes the hydraulic and mechanic equations. The modelling approach of the 1-D hydraulic/mechanic model realized in Matlab-Simulink is shown in Fig. 5.1.

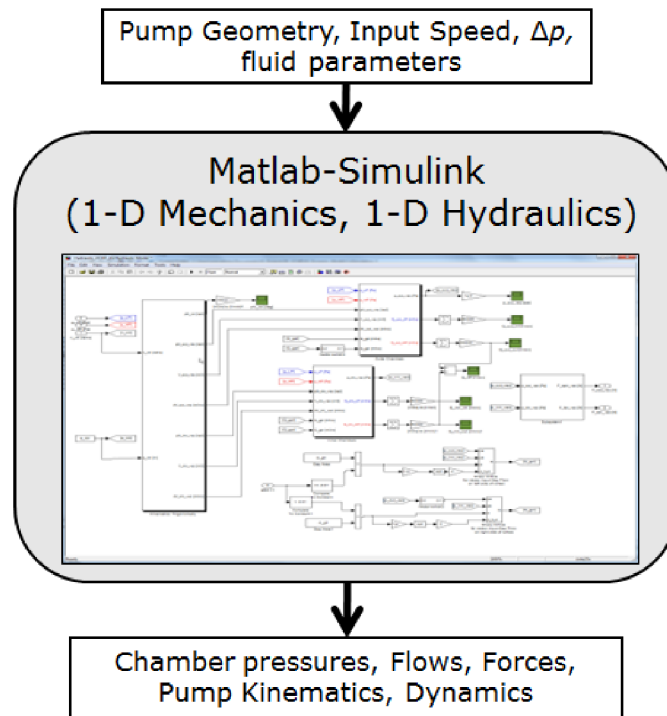


Fig. 5.1: One dimensional (1-D) modelling approach for mechanics and hydraulics in Matlab-Simulink environment.

The second model option is a CFD (Compute Fluid Dynamics) model. The available CFD software Pumplinx can produce more sophisticated models (three dimensional models) but the simulation time of these models is much longer and thus not suitable for time consuming optimization methods and especially dynamics effects like roller movements

in the slot or very small flow areas can be simulated with significant difficulties only. The CFD model was set up, but this model was used only for validation of the 1-D simulation model outputs. The example of performed CFD calculation in Pumplinx environment can be seen in Fig. 5.2.

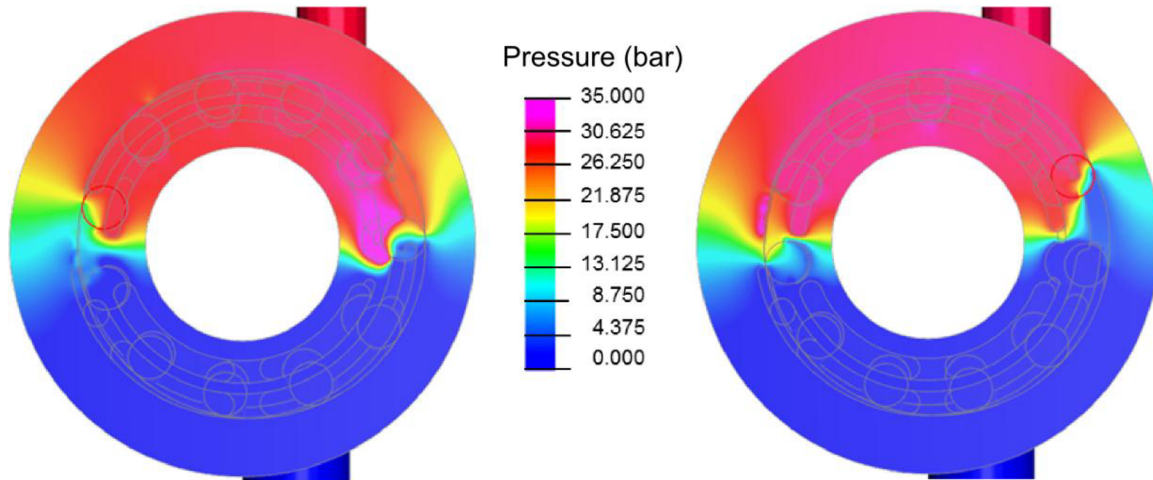


Fig. 5.2: Pressure distribution in gap between port plate and pump calculated in CFD software Pumplinx for pump speed 3400 min^{-1} , oil temperature $50 \text{ }^\circ\text{C}$ and Δp is 35 bar and different rotor positions.

Developed 1-D model in Simulink can be used for other engineering purposes like a system simulation or co-simulation with Multi Body Simulations (MBS) software like an ADAMS. Model approach is shown in Fig. 5.3.

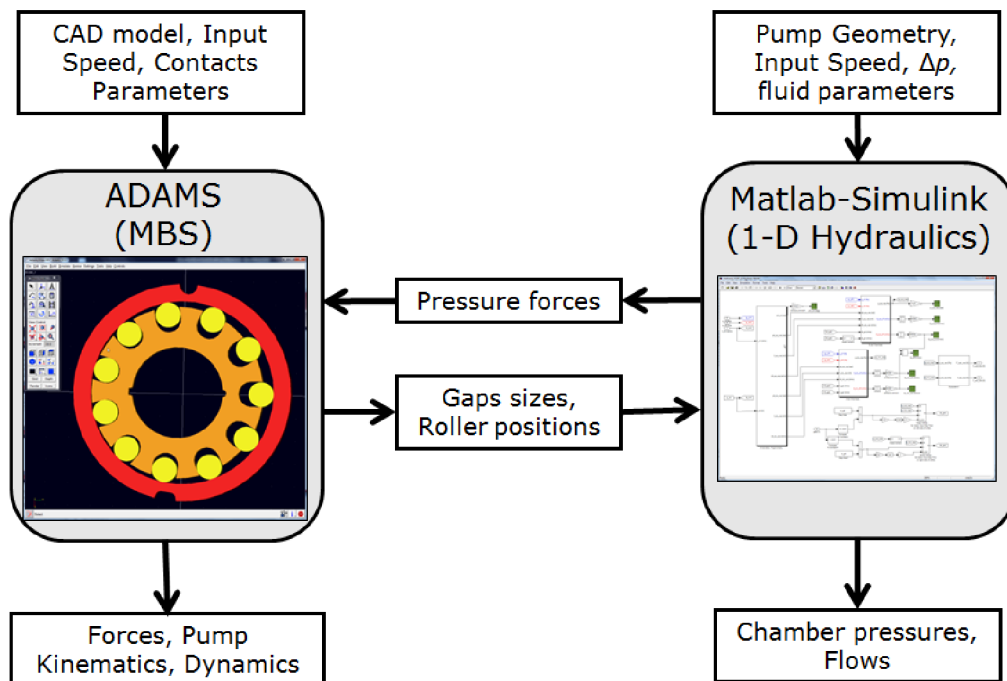


Fig. 5.3: Model approach for co-simulation between 1-D hydraulic model (Matlab-Simulink) and MBS model (ADAMS).

The hydraulic part of the 1-D simulation model connected with a MBS model can provide more information about pump mechanics than only a 1-D hydraulics-mechanics modelling but the complexity of the simulation model provides more unknown parameters

and lower model stability, especially for a big number of optimization loops. This approach was tested and provided similar results like a 1-D hydraulic-mechanic model. Co-simulation can be recommended for an optimization, focused more on the pump mechanics and dynamics especially for contacts modelling.

The CFD model provided more information about flows and pressure distribution in comparison with the 1-D hydraulic model, which can be also demanded in some cases. The CFD simulation and 1-D hydraulic co-simulation with MBS were partially tested and both methods provide some benefits and can be applied on the variable roller pump in the future according to specific simulation requests.

The very complex sophisticated simulation and optimization tools for axial piston machines are developed in Maha Research Center by Ivantysynova and co-authors, for example in [47], [48], [49]. Andrea Vacca and co-authors work on sophisticated optimization tools for the gear pumps with very good results [7], [50]. These works are results of long-time systematic investigation. The successful implementation on the roller pump principle requires long term studies.

This work uses the 1-D modelling approach [51] (*Fig. 5.1*) for fulfill thesis goals. This approach is compromise between the "more static" CFD model and the dynamic co-simulation between 1-D hydraulic and MBS model. The used 1-D modelling approach includes a hydraulic and mechanical model in simplified but sufficient way. This model provides the possibility to make fast dynamic systems (control) simulations and provides a relatively easy possibility for the port plate simulation based optimization algorithm implementation. The first step for selected 1-D optimization is 1-D model build up.

5.1 Simulation Method

Fig. 5.4 shows the modeling approach used in the simulation model. All outer and inner chambers were modeled with pressure build up equations presented in Chapter 3.

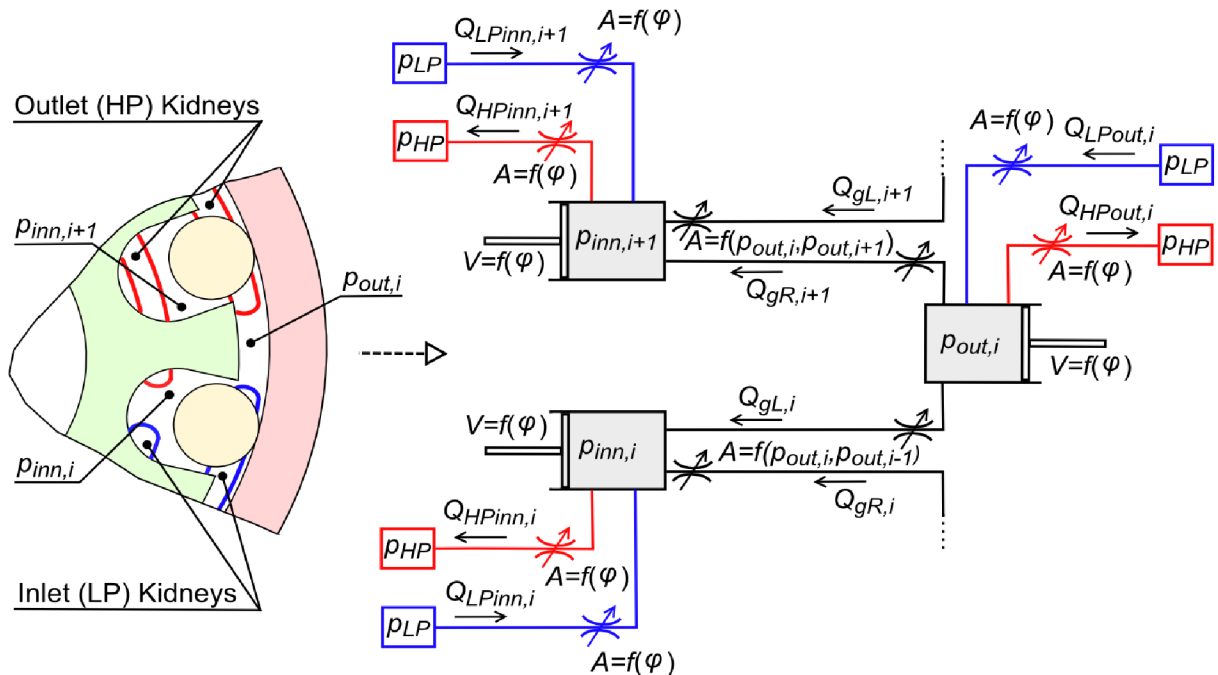


Fig. 5.4: One segment (simplified) of the simulation model.

Flows from high pressure (HP, outlet) and low pressure (LP, inlet) ports to the inner and outer chambers through the kidneys were modeled by orifice equations. The leakages from inner to outer chambers were modeled in the same way. The simulation model considered internal leakage, compression losses and index losses caused by not ideal timing between kidney angles and chamber dead point centers. The cylinders in *Fig. 5.4* represent the chambers, modeled with pressure build up equations and the orifices represent the flow restrictions, modeled with orifice equations.

The model was realized in a Matlab-Simulink environment; (Attachment A1). The inputs into the model are the parameters (dimensions) of the pump, the inlet pressure p_{LP} and outlet pressure p_{HP} and the pump rotor speed n_{rot} .

The outputs of the model are the flows through kidneys Q_{LPinn} , Q_{HPinn} , Q_{LPout} , Q_{HPout} , the slot gap flows Q_{gL} , Q_{gR} , the pressures in the chambers p_{inn} , p_{out} , the roller radial stroke x_{Rrol} , the speed \dot{x}_{Rrol} , the acceleration \ddot{x}_{Rrol} and the radial force acting on the roller F_{ncam} which is important for the optimization focused on pump wear. All outputs were arranged as a vector arrays for easier post processing.

The cam ring dynamics is not included due to fact, that all optimization measurements are performed with a fixed cam ring, it means that the displacement (PC) control is not mounted, but the valve plate optimization requires a prediction of the cam ring forces for the control design. Especially the steady state spring force acting on the cam ring is very important. The spring force size and direction provides information about the PC control functionality. It is necessary to ensure, that the resultant spring force will act against the spring – cam ring pushes towards the spring otherwise the control will not be functional. The used approach with a fixed displacement enables the optimization simplification. Especially number of simulation runs was reduced.

The equations for the cam ring forces and finally for the spring force (Chapter 3.4) were implemented into a Simulink model (Attachment A2), which is also connected to the hydraulic (chamber pressure calculation) model, developed in previous section. The input parameters for the spring force calculations are inner, outer pressures p_{inn} , p_{out} , pump geometry, roller forces and speed.

The outputs are pressure forces acting on the cam ring and the spring force acting on the cam ring. The spring force calculation with a previous part of the simulation model produces the valuable simulation tool for pressure profiles, outlet flow, internal leakages, and spring force prediction. The friction between rollers and cam ring was neglected due to higher speed and stability of the simulation model.

The mathematical description of the simulation model (generally 1-D hydraulic simulations) demands a variable step and stiff solvers. The used solver was ode23tb as is shown in *Tab. 5.1*. It is necessary to ensure that the maximal solver step size will be small enough to capture all-important dynamical effects in the pump. The simulation stop time was adjusted according to the pump speed. Each simulation run simulates two rotor revolutions, during first one revolution, the transient and initialization effects occurred, the second rotor revolution produced correct results, which were saved and used for result evaluation.

Tab. 5.1: Solver settings of Simulink model.

Solver Options	
Type	Variable –step
Solver	Ode23tb (stiff/TR-BDF2)
Max step size	1e-5
Min step size	Auto
Initial step size	Auto
Relative tolerance	1e-4
Absolute tolerance	Auto
Solver reset method	Robust
Shape preservation	Disabled
Number of consecutive min steps	1
Solver Jacobian method	auto
Zero-crossing control	Local settings
Algorithm	Non-adaptive
Number of consecutive zero crossings	1000

5.2 Optimization Method

The optimization in this work is based on the simulation model described in previous sections and the theory-principle from work [52]. This optimization method was selected due to good experiences from the axial piston valve plate optimization. The optimization was driven by two requests. The first one was the increase of the pump volumetric efficiency and the second was the increase of cross port flow and possibility to make the pressure profile more smooth and wear marks smaller instead of volumetric efficiency. From the previous section it is clear that the volumetric efficiency optimization was realized with port plates (with kidneys design). It means that the output from the optimization has to be a new port plate design (kidney design) which dimensions are included in optimization result vector.

The optimization result vector contains 20 kidneys variables (port plate design parameters). Each variable of this vector corresponds to one design parameter such as notch depth or notch start-end angle. These design parameters fully define each notch design, which directly influences the volumetric efficiency, roller forces, cross port leakages, pressure profiles... etc. Each notch is defined by: start angle (rotor angle where notch starts), end angle (rotor angle where notch ends and main kidney starts) and notch cross section area (depth). There is an assumption that the outer edge of the notch has the same radial positions as a main kidney. It is necessary to ensure that the final notch design is realistic and possible to manufacture what is ensured by constrains in optimization script. The better overview on the optimized kidney-notch design offers *Fig. 5.5*.

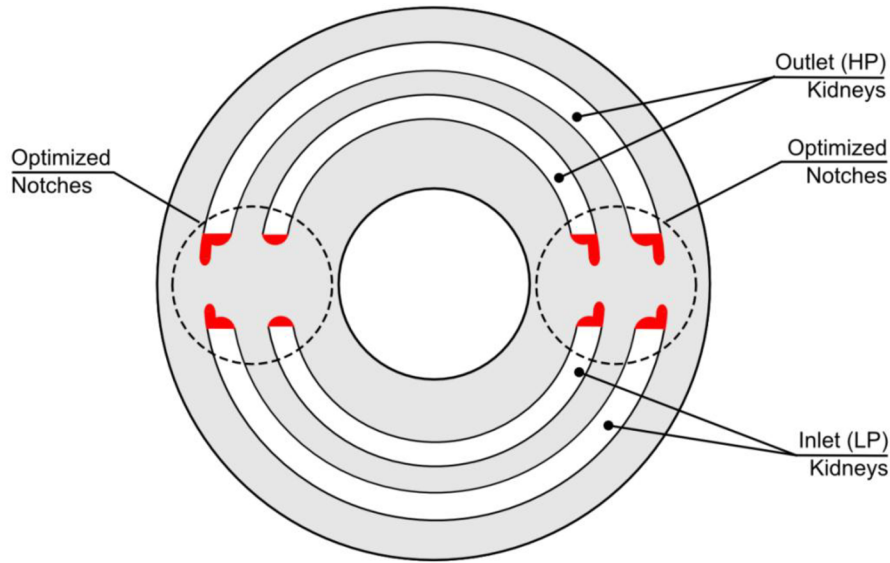


Fig. 5.5: Port plate with optimized kidneys - notches.

The quality criteria vector G_n consists of nine parameters $G_1 \dots G_9$ which are calculated from simulation results. This vector is necessary for the optimization results evaluation. The first four variables of this vector are the notches cross port sections and outlet (HP) charge pressure changes. The next quality criteria variables are the cross-port leakages, the maximal radial gradient force on the roller, maximal radial force on the roller, minimal roller radial force and the resultant force on the cam ring spring. The purpose of this quality criteria vector is to ensure the demanded cross-port flow (volumetric efficiency) with acceptable pressure profile, roller force and spring force with real port plate design. It means design which is possible to manufacture. The quality criteria vector gives an overview about the observed pump parameters during pump optimization. The quality criteria vector G_n is the input to the following equation:

$$\lambda = \frac{1}{\sigma} \cdot \ln \left(\sum_{n=1}^{L_G} e^{\sigma \cdot \frac{G_n}{c_n}} \right) \quad (5.1)$$

The function λ , called as a parameterizing function, is a function which is minimized during optimization cycle. The coefficient σ is setup to value to 20. The target value vector c_n has the same length L_G as the quality criteria vector G_n . The setting of the target value vector is one of the most difficult tasks during the optimization. A suitable setup of the value vector is a question of experiences.

The resultant value of the function λ corresponds to the port plate design quality according to quality criteria parameters and target values defined in vectors G_n and c_n . It means, that port plate design with a lower function λ value corresponds more to parameters defined in the target value vector. Theoretically the minimum of the function λ corresponds to the best port plate design according to quality criteria vector.

The previous function λ provides only information based on the simulation results about port plate quality in the way that a lower number means a design which fits target parameters better. Then the optimization function which minimizes the function value is a clear solution for optimization cycle. The Matlab function "fminsearch" function for a similar purpose. This function returns a result vector that is a local minimizer

of the parameterizing function described in previous lines. The Fig. 5.6 presents graphically the optimization loop. At the first step initial kidney design parameters are sent to the Matlab "fminsearch" function, which calls a function which contains three parts.

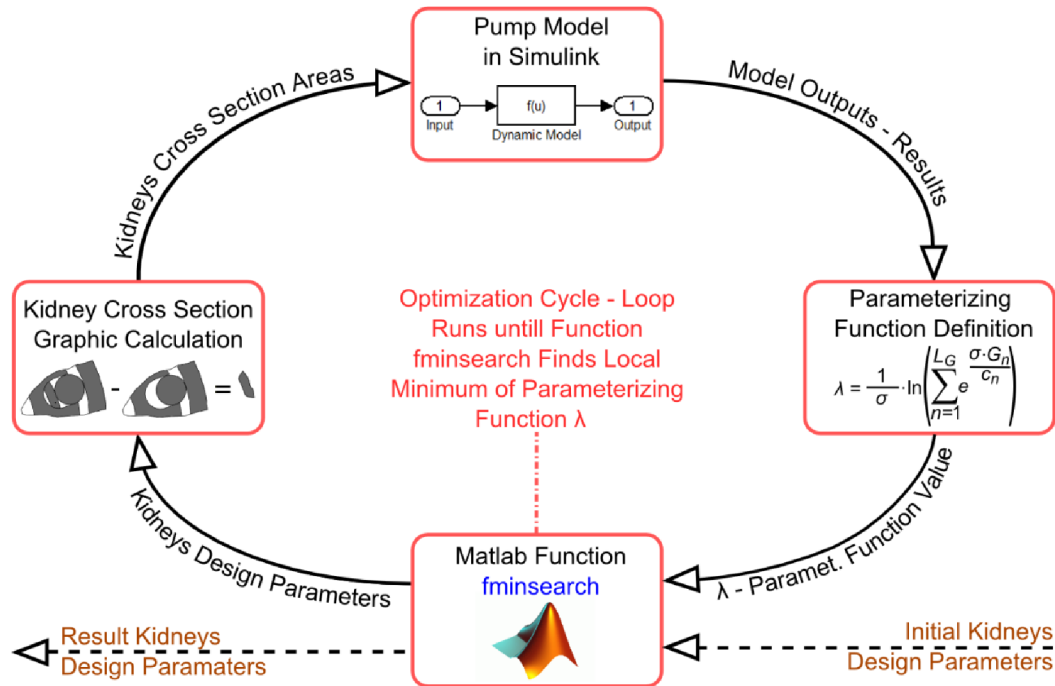


Fig. 5.6: Optimization cycle-loop in Matlab-Simulink

The first part is a kidney cross section graphic calculation. The output from the cross section calculation is sent to the pump model in Simulink. The Simulink pump model simulates the pump behavior with a defined port plate design, pump design and operating conditions – typically conditions where charge pump operates (delta pressure about 25 bar, pump speed 2000 min^{-1} and inlet oil temperature 50°C). The model results are sent to the third part where the function λ is calculated based on simulation model results and the user defined target value vector. All information (port plate/kidney design parameters, quality criteria vector G_n and function λ value) are saved and the λ value is sent to the Matlab "fminsearch" function, which checks if the actual λ value is a local minimum of the parameterizing function λ (which also includes pump model in the end). If this value is a local minimum of this function, the result kidney design parameters are returned from "fminsearch" and represent the optimization results. Otherwise, "fminsearch" adjust kidney design parameters and the optimization cycle runs again. It is necessary to mention that this optimization takes a lot of time or it is unsuccessful in some cases. Saving of each optimization cycle-loop run enables to evaluate results manually, interrupt cycle or take sub-results if they are consider as a sufficient.

5.3 Simulation and Optimization Results

The simulation based optimization produced two port-plate designs. The first design was focused on the increase of the volumetric efficiency and the second design was focused on the chamber pressure profile smoothing. The starting point for optimization was the port plate design A which was designed based on the intuitive approach and testing of many variants of designed hardware.

The port plate design B and C were designed by the developed simulation/optimization tool which significantly shortens port plate design time; especially in comparison with first design A. Design B was optimized for a higher volumetric efficiency – lower cross port leakage, design C was optimized for a smooth chamber pressure profile. This pressure profile smoothing was achieved by a slight increase of the cross port leakage. The initial design A and both optimized designs B and C are shown in *Fig. 5.7*.

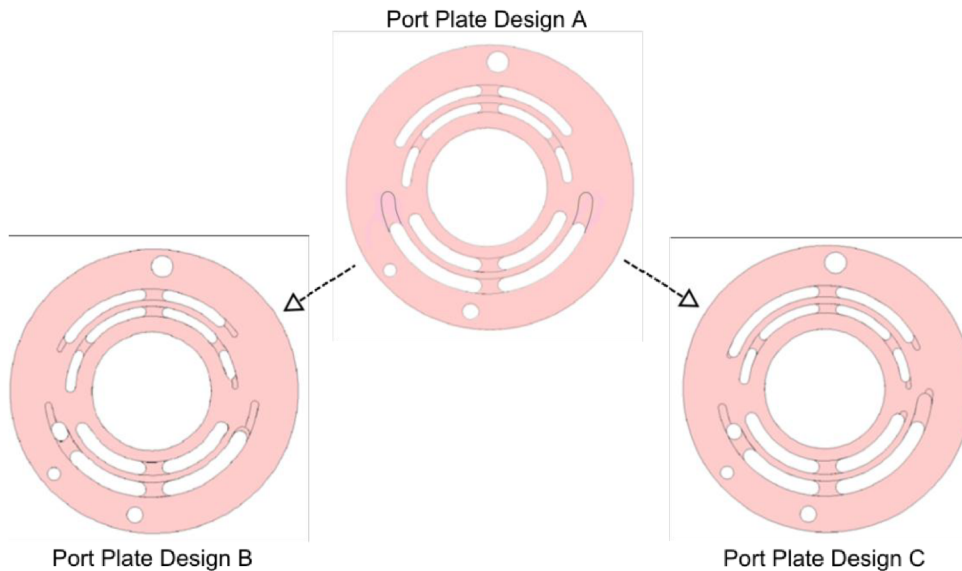


Fig. 5.7: Initial port plate design (A) and two optimized port plate designs (B,C)

The examples of the simulation results are presented in the following figures: *Fig. 5.8*, *Fig. 5.9* and *Fig. 5.10*. These presented results show the pump behavior at speed 2000 min^{-1} , delta pressure 25 bar, inlet oil temperature 50°C and free air contain in the oil 1 %. The top graph in each figure presents the pump effective flow. The second graph presents the total volumetric losses and the third presents the internal leakage. Significant 11 peaks in each of these graphs can be identified, caused by 11 rollers in the pump.

The pressure profiles in the outer and inner chambers correspond to the kidney timing (angles). It can be seen that port plate design B has a higher effective flow and lowest volumetric losses which was demanded during optimization. The port plate C has the lowest effective pump flow together with the highest volumetric losses and internal leakage. The chamber pressure profiles with design C shows a decrease of the pressure overshoots, also by increase of the internal leakage. The port plate C pressure profile is the smoothest with an acceptable effective flow.

The main differences between all three designs are in the effective flow. The chamber pressure profiles were not measured due to difficulty. Generally, it was not required because all measurements confirmed acceptable a pump wear and pump vibrations. Nonstandard vibrations, noise or harshness were not observed. System testing confirms noise and vibrations at the standard level comparable with the standard g-rotor. It is necessary to say that it is good to have a design with a more smooth pressure profile, especially for applications which operates in critical conditions. It can happen that some applications will require different port plate designs due to possible problems with vibration, harshness or noise. The similar approach is used for axial piston pumps, where the valve plate has to be sometimes modified. The simulation results of proposed designs fulfill the optimization requests.

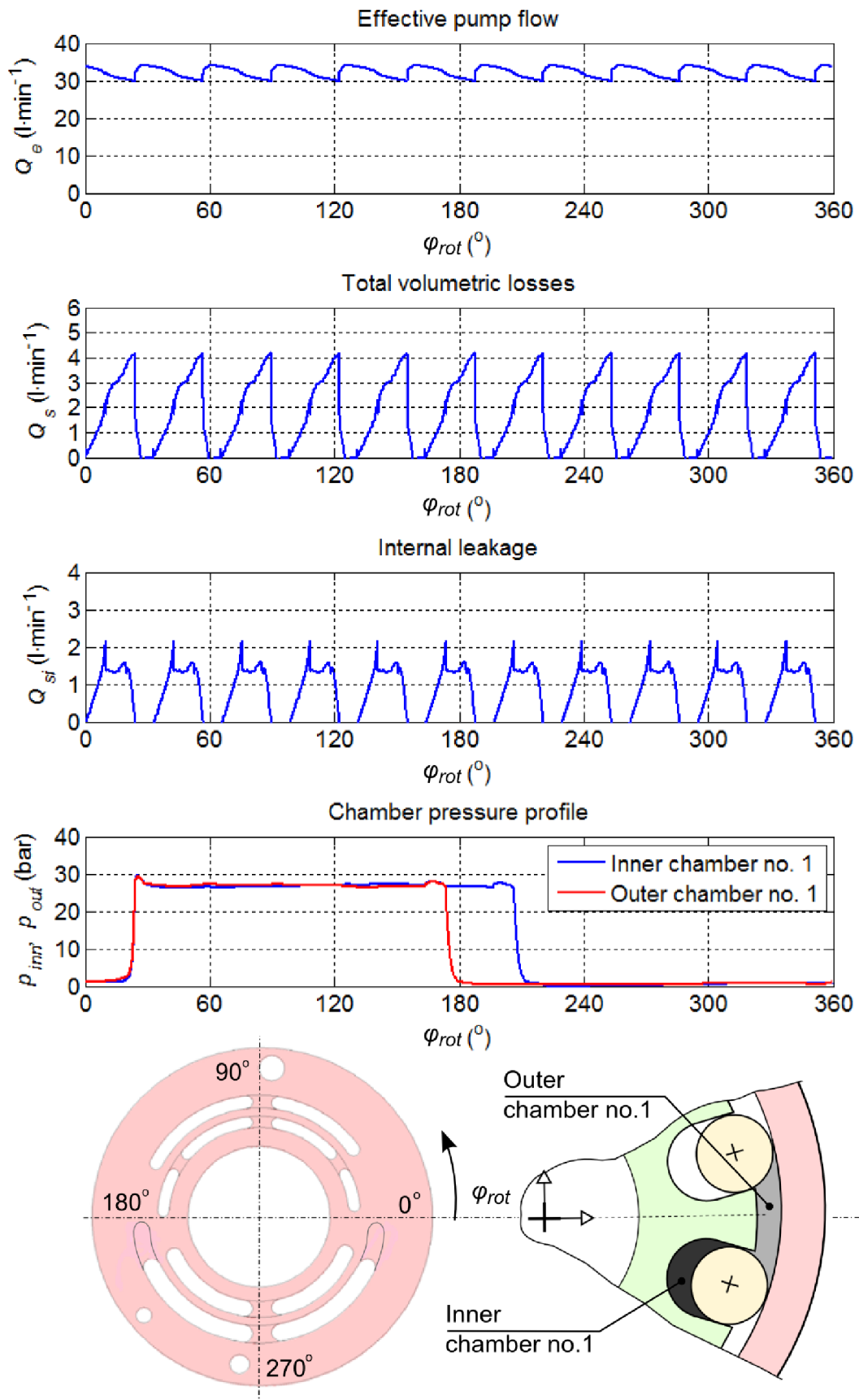


Fig. 5.8: Simulation results of initial port plate A.

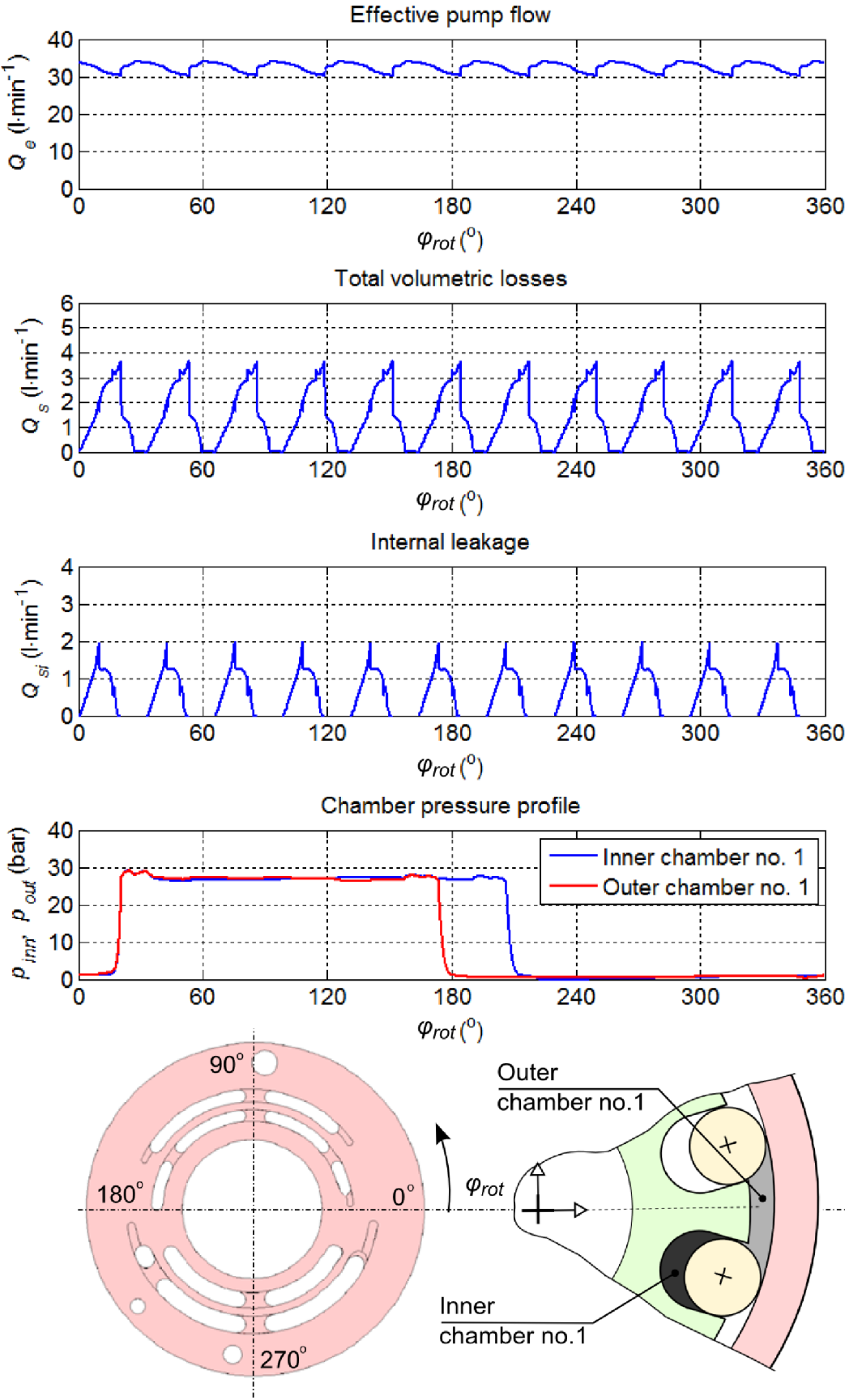


Fig. 5.9: Simulation results of optimized port plate B.

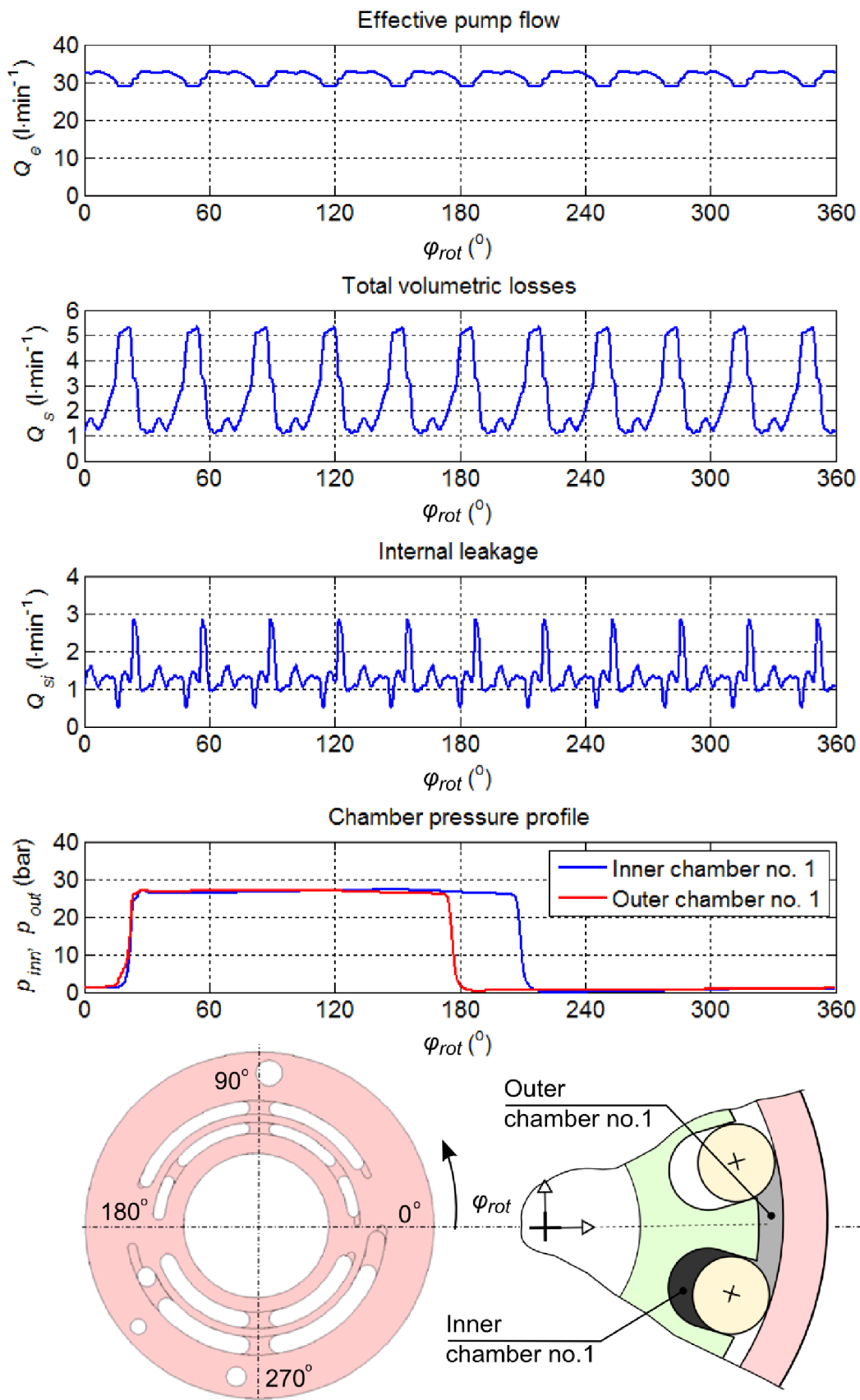


Fig. 5.10: Simulation results of optimized port plate C.

The next parameter which was monitored during simulation and can be plotted is the spring force acting on the cam ring.

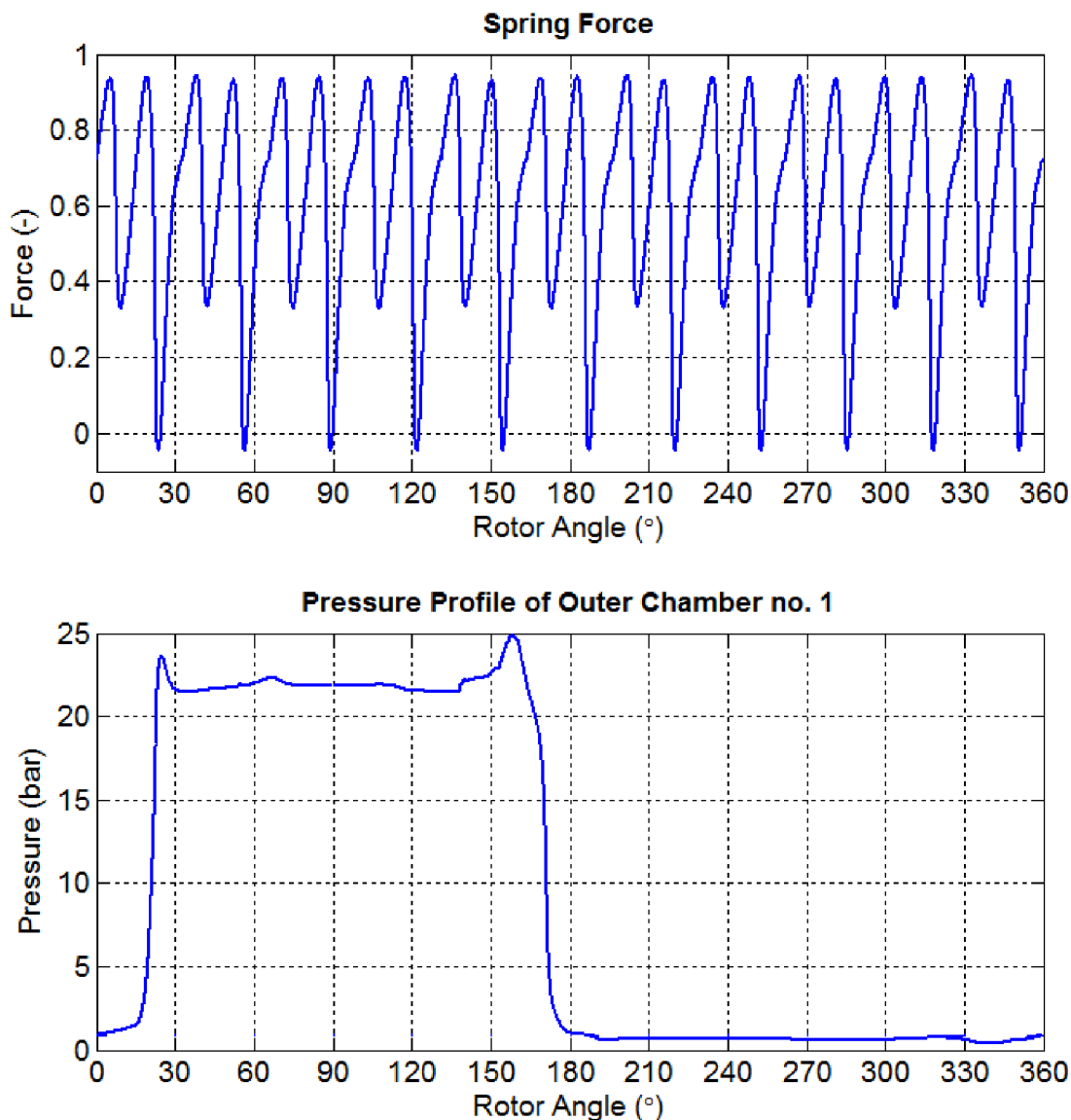


Fig. 5.11: Spring force (top) and chamber pressure (bottom) simulations at a pump speed of 2000 min^{-1} , Δp of 20 bar and maximal displacement.

The cam ring spring force simulation for the port plate design A in Fig. 5.11 shows the shape of the spring force (at normalized scale) during one rotor revolution at full pump displacement. Eleven significant peaks can be seen which correspond to the eleven rollers. A more detail look into simulation results shows 22 peaks, which correspond to eleven rollers and two transition areas (Outlet \rightarrow Inlet, Inlet \rightarrow Outlet). This spring force oscillation is caused by the pressure profile in the chamber which is changing according to the port plate timing. The big decrease of the spring force is repeating each approx. 33° , which is corresponding to the rollers ($360^\circ/11$ roller), because each 33° of revolution the outer chamber is ported from low to high pressure, having a direct impact (reduction) on the spring force, down to negative values. The porting from high to low pressure, visible in the smaller dips down to 35% has, because of the moment balance, a smaller impact on the spring.

All simulations of the final port plate design show similar behavior and values of the spring force during pump revolution, as was demanded, so they are not individually displayed here.

5.4 Verification Method

Simulation and optimization results are validated in two areas. The first area is the validation of the volumetric efficiency. This was realized by comparison between simulation results and measurements of proposed designs. The second validation area is focused on the spring force (cam ring forces) verification.

5.4.1 Volumetric Efficiency

The variable roller charge pump was mounted into an experimental hardware which consists of the variable charge pump housing (in this case end cap) and TMP (transit mixer pump) housing. The TMP housing ensured simple connection to the test stand shaft, but housings brought some additional friction losses which have to be measured and subtracted from the measured shaft torque. Both housings can be seen in *Fig. 5.12*.

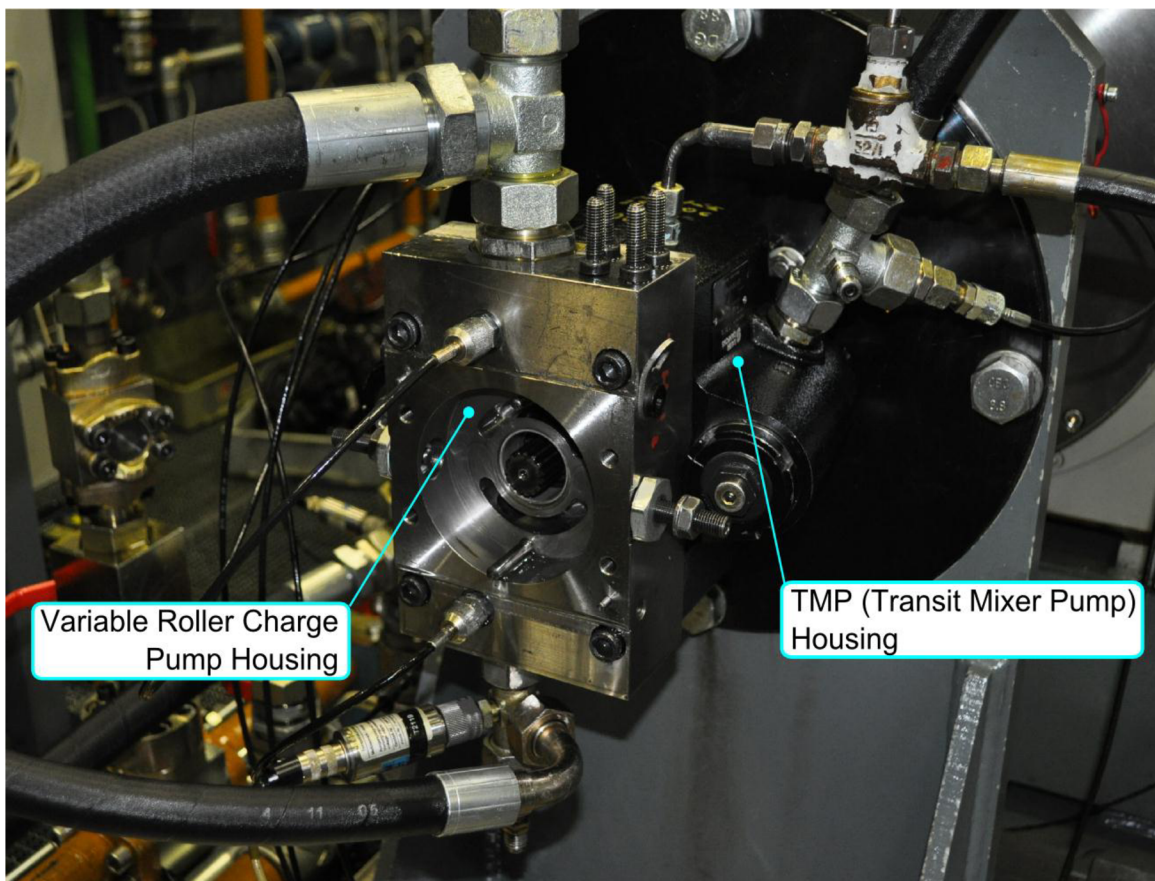


Fig. 5.12: Variable roller charge pump housing mounted on the test stand.

All measurements were performed at the performance test stand. This test stand is equipped with a main drive an electric motor with 500 kW. The speed of this drive is controlled precisely with a frequency inverter. The Electric motor with this power offers sufficiently ideal speed source for the variable roller pump. The test stand is equipped with all

necessary equipment like another smaller drive for inlet filling issues, tank, filtration, oil heaters and coolers. It is important to say, that the test stand was developed for similar measurements and test engineers have a multi-year experiences with similar measurements. Due to this all efficiency measurements were performed very easily and professionally with suitable measurements devices. All sensors have a suitable accuracy and resolution for efficiency measurements.

The new two port plate designs B and C were produced according to the optimization results in the previous section. The pump prototype hardware with the best manufacturing tolerances was selected for measurements purposes. During efficiency measurements, only port plates were changed on the test hardware, minimizing other factors which can influence measurements results.

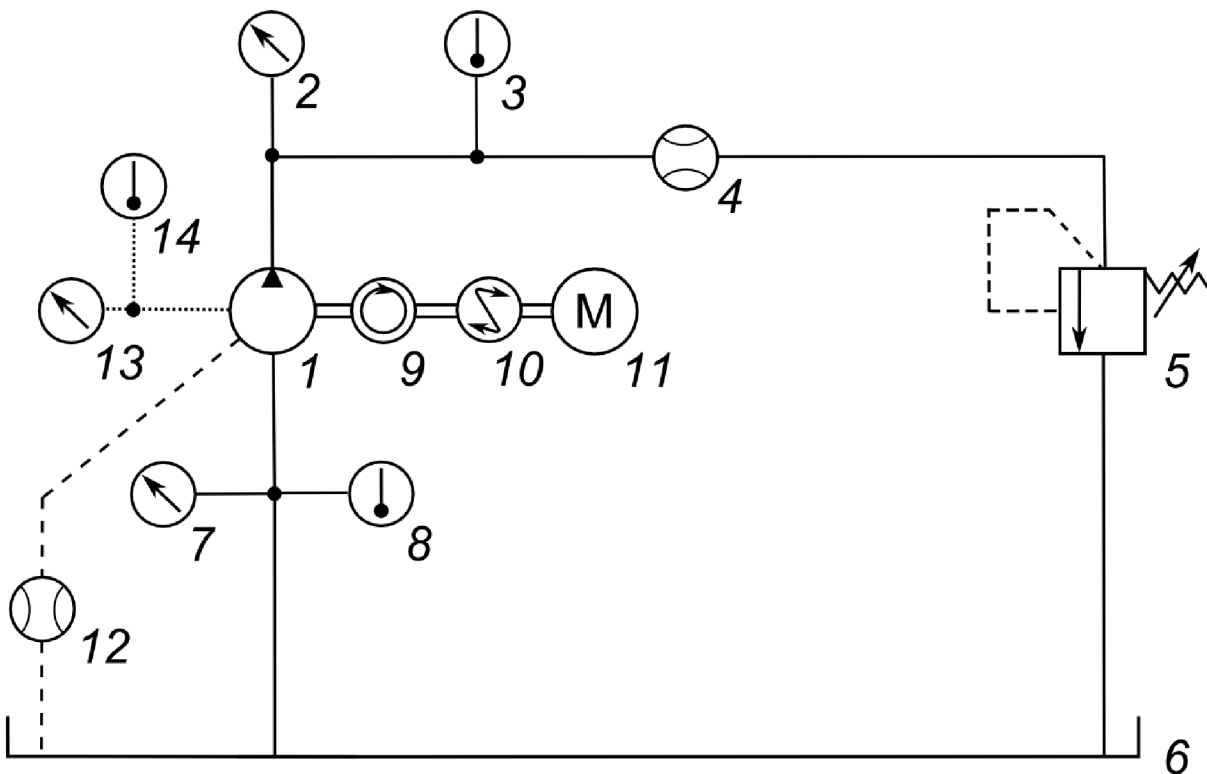


Fig. 5.13: Hydraulic circuit for simulation measurements.

1- variable roller charge pump, 2 – outlet pressure sensor, 3 – outlet oil temperature sensor, 4 – outlet flow meter, 5 – loading relief valve, 6 – tank, 7 – inlet pressure sensor, 8 - inlet temperature sensor, 9 – speed sensor (encoder), 10 – torque sensor, 11 – main electric motor, 12 – case flow meter, 13 – case pressure sensor, 14 – case temperature sensor.

The purpose of the previous hydraulic circuit (*Fig. 5.13*) is to evaluate (calculate from measured values) volumetric, hydro-mechanical and overall efficiency of the variable charge pump system. The best way how to evaluate the efficiency is a measurement with disabled control. It corresponds to the optimization where maximal displacement was considered as well.

The simplified hydraulic circuit diagram that was used, is shown in *Fig. 5.13*. More detailed hydraulic circuit diagram is attached in the attachment A5. The list of used sensors and components is shown in *Tab. 5.2*.

Tab. 5.2: Used components in the measurements.

No. in diagram	Type	Producer	Range	Accuracy
1	Variable roller charge pump	-	-	-
2	Pressure sensor P3MB	HBM	0...50 bar	± 0.5 %
3	Temperature sensor Pt 100	Hydrotechnik	-50...200 °C	± 1 % of final value
4	Flow meter OMG 32	KRAL	1..150 l·min ⁻¹	± 0.1 % of rate
5	Relief valve VP01	DENISON Hydraulics	-	-
6	Tank	EVPU	-	-
7	Pressure sensor P3MB	HBM	0...10 bar	± 0.5 %
8	Temperature sensor Pt 100	Hydrotechnik	-50...200 °C	± 1 % of final value
9	Speed meter HG18	HUBNER	0...7031 min ⁻¹	± 0.3 % (Time difference method)
10	Torque meter 1604-2K	Honeywell	0...225 N·m	± 0.25 %
11	Electric motor 500kW	VUES	-	-
12	Flow meter OMG 20	KRAL	0.3..45 l·min ⁻¹	± 0.1 % of rate
13	Pressure sensor MBS 33	Danfoss	0...10 bar	± 1 %
14	Temperature sensor Pt 100	Hydrotechnik	-50...200 °C	± 1 % of final value

The measurement system contains a variable charge pump *1* with fixed displacement connected to the main electric drive *11*, which propels the investigated pump *1*. The shaft between the variable roller charge pump and the electric drive is equipped with a speed and torque sensors (*9*, *10*). The external leakages from the pump are measured with flow meter *12*. The pump case pressure and case oil temperature are measured by sensors *13*, *14*. The variable roller charge output is connected to the relief valve *5* which ensures constant output (charge) pressure at the pump outlet. The relief valve output is connected to the tank *6*. The variable roller charge pump outlet pressure, temperature and flow are measured with sensors *2*, *3*, *4*. The pressure and temperature sensors (*7*, *8*) measured suction pressure and oil temperature. During measurements the suction pressure was almost constant; therefore external inlet charging was not applied. The physical realization of the testing circuit is shown in *Fig. 5.14*.

The used sensors are connected to the measuring device CRONOS from IMC which provides the conversion from analog to digital signals. All channels used Buterworth's filters.

Standard sampling time for all sensors is 1 ms. For the less used channels it is possible to decrease the sampling time (increase the sampling rate). The CRONOS device is connected to the PC through Ethernet connection. The data are saved on the hard drive, where ONLINE FAMOS software is installed and used for online measurements processing and monitoring according to Fig. 5.15.

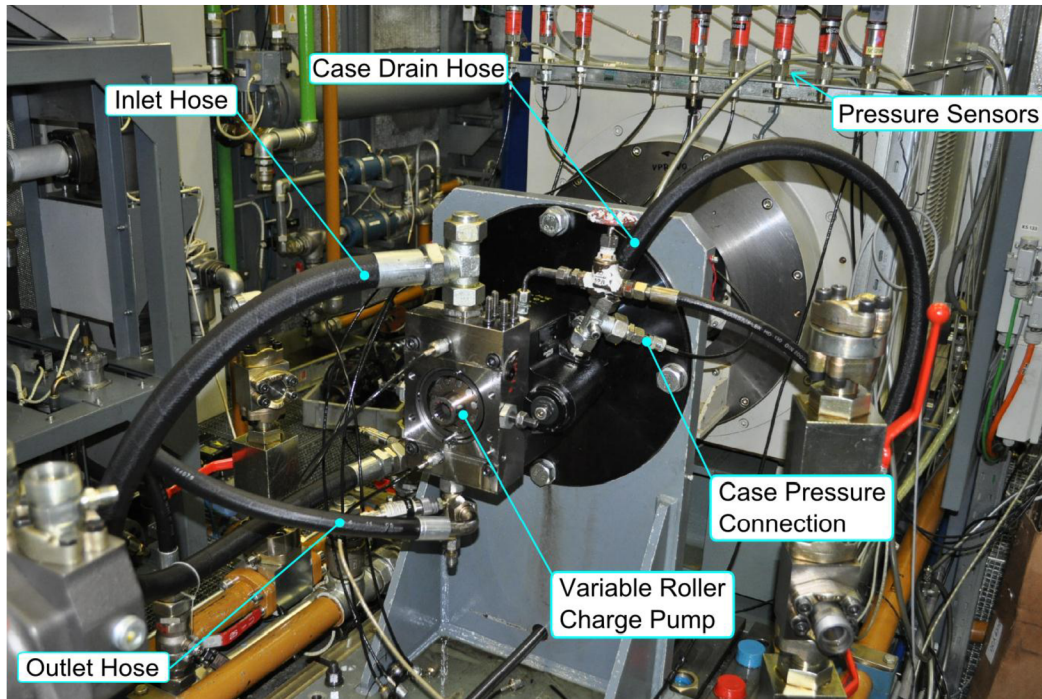


Fig. 5.14: Realization of the testing circuit in test lab.

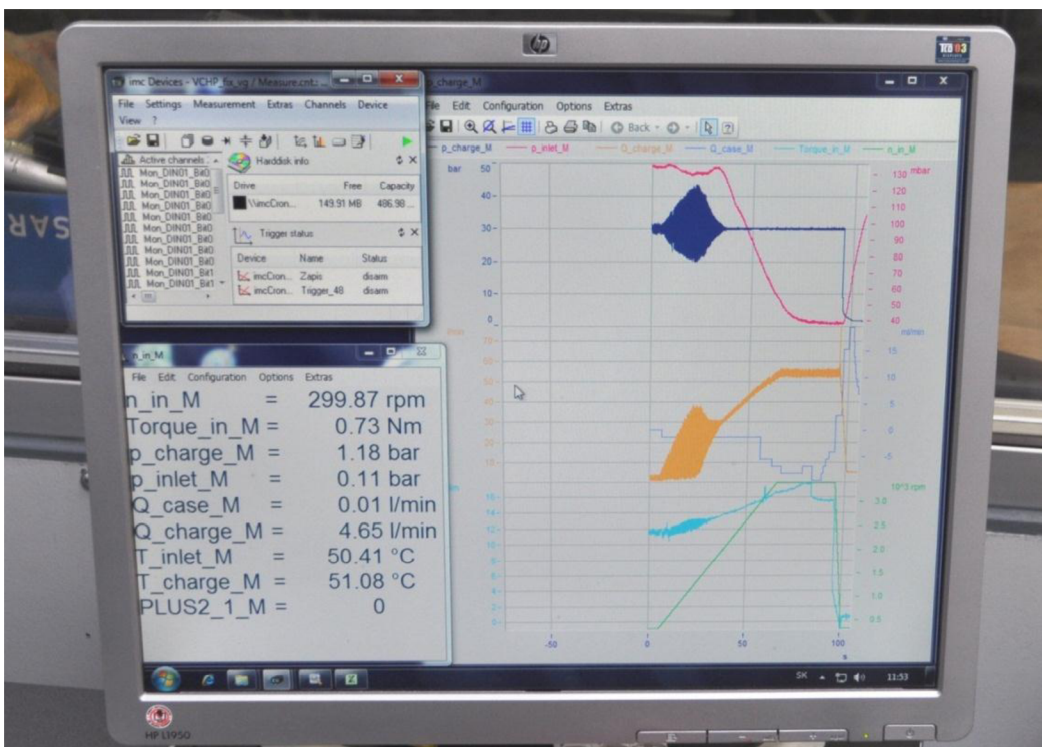


Fig. 5.15: Online measurements monitoring.

The pump efficiency is evaluated from steady state measurements (point measurements). At first step the pre-defined operation conditions (delta pressure, speed, displacement, temperature) of the variable roller charge pump are set. Inlet oil temperatures were set in first case to 50°C and to 80°C in second case. The input oil temperature is controlled by hydraulic oil cooler. The pump displacement was adjusted to three different displacement values: maximal, half and minimal displacement, ensured by screws which push against the cam ring. The charge pump delta pressure varies from 10 bar to 40 bar (10, 15, 20, 30, 40 bar), done by a load relief valve. The input shaft speed was set from 400 min⁻¹ to 4000 min⁻¹ (400, 500, 600, 800, 1000, 1500, 2000, 2500, 3000, 3500, 4000 min⁻¹). Thus, for each temperature 165 measurement points were performed. Together it results into 330 measurements for each port plate type.

The measured device includes not only pump but it includes also parts such as bearings (shaft bearings in the housings). It is necessary to ensure that the efficiency measurements include only parts connected directly with investigated pump. The bearing friction torque characteristic was obtained from measurements where the pump torque is measured without rollers and no delta pressure for various speeds and oil temperatures. The bearing friction torque is subtracted from the measured shaft torque. Then the resulting torque value corresponds to the pump torque only

The selected measurement conditions cover the complete charge pump operation conditions and present the efficiency measurement matrix. This matrix provides sufficient overview about the pump performance and efficiency. The conditions which were not measured are normally interpolated from measured data or approximated according [53] for example. Correct efficiency measurement is the base for the pump loss modeling (efficiency) and the performed measurement provides very good base for this purpose. Part of the measured values was used for optimization result validation in Chapter 3.4. The measured data were also used for system model build up (based on Polymod [53]).

5.4.2 Control Spring Force

The spring force measurement is one of the most challenging tasks in the test lab. The circuit configuration was used the same as for efficiency measurements; it means that the pump is running against an adjustable relief valve. This relief valve enables to change delta pressure according to measurements needs. The pump speed is controlled by the prime mover.

Originally there was the idea to measure the spring force with a force transducer, but this approach wasn't successful due to design problems and other problems such as vibration and force transducer range. Later in the Chapter 5.3 in *Fig. 5.11* is an example, which shows that the resultant force significantly varies during rotor rotation and in some rotor positions this force become negative.

The best possible way is to implement a hydraulic cylinder and a piston on the cam ring according to *Fig. 5.16*. The main idea is based on the principle that compression spring is replaced with hydraulic cylinder and piston, which is jointed to cam ring. The resultant cam ring forces press the hydraulic fluid in the hydraulic cylinder, which results in a pressure build up in the cylinder.

Theoretically, at steady state conditions, the pressure in the hydraulic cylinder multiplied by the piston area corresponds to the mean value of the spring force. The pump has

to be equipped with a displacement sensor for precise cam ring stroke (pump displacement measurements). The external pressure source allows the cam ring stroking – change pump displacement, it means that the measurements can be performed for different displacements.

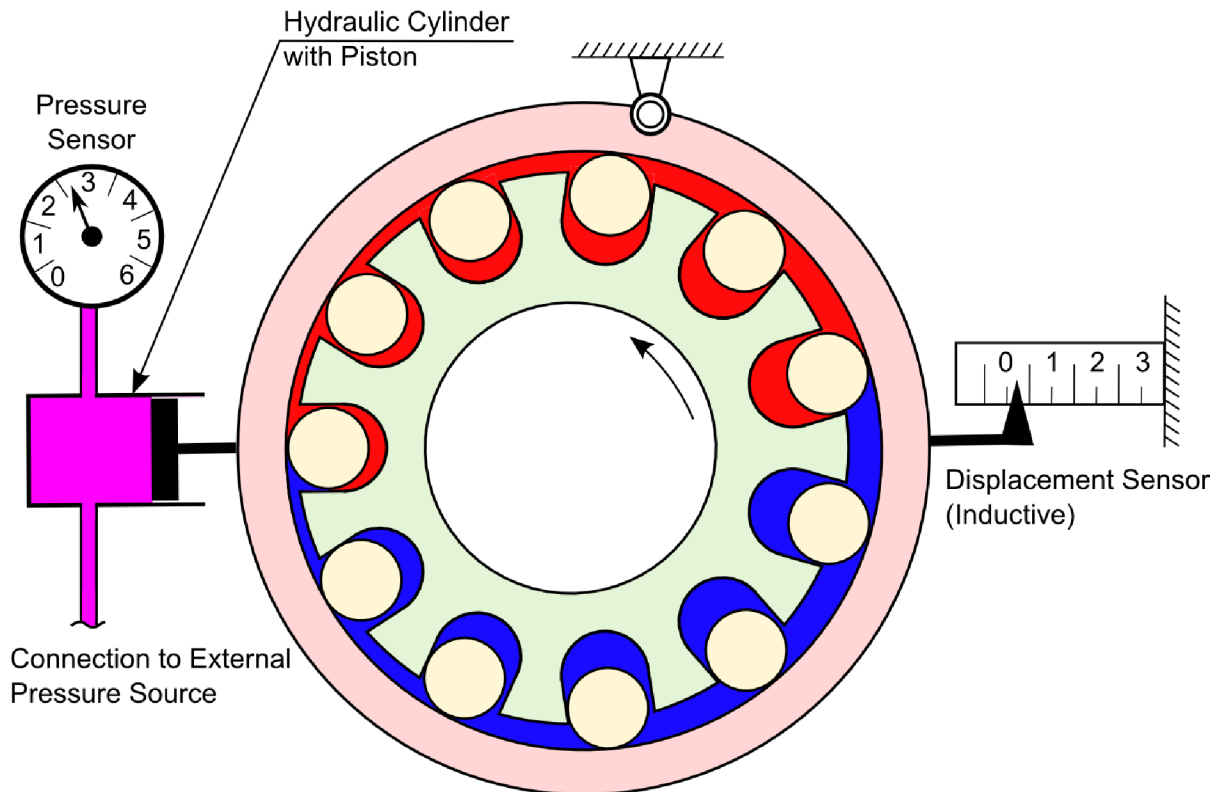


Fig. 5.16: Schematic view on the pump configuration during spring force measurements.

This simple displacement control shows significant hysteresis behavior due to the pump control design and the friction between cam ring and port plates. All "spring force" measurements were performed only with port plate design no. 1 with oil temperature 50°C. The pump speed and delta pressure values were adjusted according to tests demands.

At the beginning of the measurements, the pump was running at the constant speed, constant delta pressure and in the minimal pump displacement ensured by atmospheric fluid pressure in the hydraulic cylinder. Slow pressure increase in the hydraulic cylinder caused a cam ring movement and an increase of the pump displacement. This movement wasn't smooth in all conditions. The pump speed, pump flow, delta pressure, suction pressure, suction oil temperature, outlet oil temperature, pump torque, cam ring displacement (pump displacement) and hydraulic cylinder pressure were recorded during tests. The sampling frequencies of channels were 10 ms and sampling frequency for cylinder pressure was 0.1 ms. The hydraulic circuit diagram is shown in attachment A6.

The *Fig. 5.17* shows a picture taken from the spring force measurements. Some devices on the picture, such as kidney pressure sensors were not connected to the measurement device. Pump is in the experimental housing connected to the transit mixture pump for easy coupling with the prime mover. The test stand configuration corresponds to the pump efficiency measurements presented in previous section.

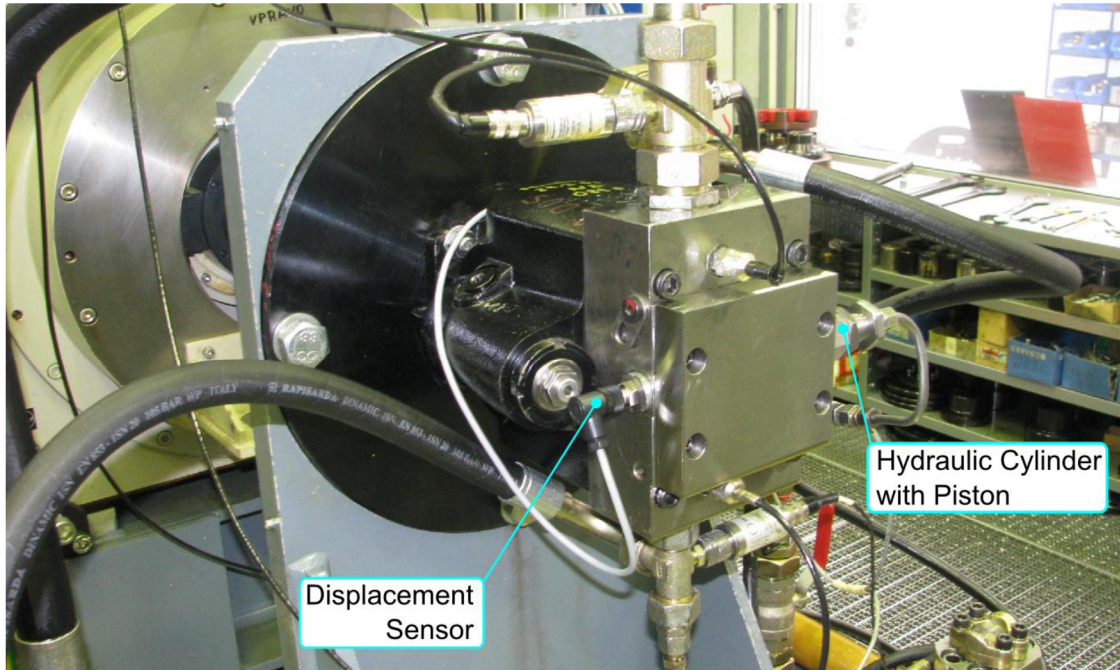


Fig. 5.17: The variable charge pump during spring force measurements.

5.5 Verification of Simulation Results

The error of measurement is basically a combination of sensors errors and digital errors due to A/D conversion of signals. This error has to be evaluated before results verification. The accuracy of the used sensors, based on the calibration, can be seen in *Tab. 5.2*. The accuracy of the performed measurements depends on the accuracy of all applied sensors (*Tab. 5.2*) and the discretization error that occurs during the conversion of the analog into a digital signal. Since each channel has a fixed bit width (12 bits ... 4096 digits) to represent the measured values, this causes a discretization error for each channel. *Tab. 5.3* shows the digital resolution of the measured values.

Tab. 5.3: Digital resolution of the used sensors.

Number in circuit diagram	Sensor	Final value	Analog resolution	Digital resolution
2	Pressure sensor P3MB	50 bar	5 bar/V	0.01221 bar/digit
3, 14	Temperature sensor	100 °C	10 °C/V	0.02441 °C/digit
4	Flow meter OMG 32	150 l·min ⁻¹	1.5 (l·min ⁻¹)/V	0.03662 (l·min ⁻¹)/digit
7	Pressure sensor P3MB	10 bar	1 bar/V	0.00244 bar/digit
9	Speed meter HG18	5000 min ⁻¹	50 (min ⁻¹)/V	1.22070 (min ⁻¹)/digit
10	Torque meter 1604-2K	225 N·m	2.25 (N·m)/V	0.05493 (N·m)/digit
13	Pressure sensor MBS 33	10 bar	1 bar/V	0.00244 bar/digit

For every sensor an overall error (*Tab. 5.4*) is calculated that consists in the majority of cases of a constant part caused by the discretization error (*Tab. 5.2*) and a proportional (*Tab. 5.3*) to the signal increasing sensor error.

Tab. 5.4: Overall sensor errors.

Number in circuit diagram	Sensor	Measured value	Overall error of the measured value (absolute)	Overall error of the measured value (relative)
2	Pressure sensor P3MB	30 bar	± 0.16221 bar	± 0.541 %
3, 14	Temperature sensor	50 °C	± 0.52441 °C	± 1.049 %
4	Flow meter OMG 32	50 l·min ⁻¹	± 0.08662 l·min ⁻¹	± 0.173 %
7	Pressure sensor P3MB	1 bar	± 0.007244 bar	± 0.724 %
9	Speed meter HG18	2800 min ⁻¹	9.6207 min ⁻¹	± 0.344 %
10	Torque meter 1604-2K	15 N·m	± 0.09243 N·m	± 0.616 %
13	Pressure sensor MBS 33	1 bar	± 0.01244 bar	± 1.244 %

ISO 4409 classifies the conditions for steady state measurements according to *Tab. 5.5*.

Tab. 5.5: Permissible variations of mean indicated values [54].

ISO 4409			
Parameter	Tolerance Class A	Tolerance Class B	Tolerance Class C
Temperature	± 1 K	± 2 K	± 4 K
Speed	± 0.5 %	± 1 %	± 2 %
Torque	± 0.5 %	± 1 %	± 2 %
Volume flow rate	± 0.5 %	± 1.5 %	± 2.5 %
Pressures below 2bar	± 0.01 bar	± 0.03 bar	± 0.05 bar
Pressures above 2 bar	± 0.5 %	± 1.5 %	± 2.5 %

The sensors used within the steady state measurements are able to fulfil the requirements of the standard ISO 4409 class B (*Tab. 5.5*). Except some operating parameters, which were obtaining the edge of the parameter range, the accuracy of the sensors exceeds in the majority of test points the requirements.

The first measurements of the prototype pump with different port plates (ver. A, B, C) were realized on a hydraulic parametric test stand, described in the previous section. All port plates were tested in the same way. The pump was loaded by a relief valve with constant delta pressure setting and constant pump speed. The inlet oil temperature was constant at 50 °C.

Tab. 5.6 presents example of the results in comparison with simulation results. There is effective flow difference in simulations and measurements due to differences between real

pump displacement and calculated pump displacement. The displacement of the pump approximated from measurements was bigger than volume which was calculated in the simulation. It was caused by very sensitive part tolerances of the prototype unit.

The measurements show that the effective flow of the pump new design increases or decreased according to optimization demands (as shown in *Tab. 5.6*) with acceptable wear marks. In the end, the measured volumetric efficiency of the pump shows the same tendency as the simulation results. Simulated flows show lower numbers than measured primary due to the external leakage neglection. Port plate B measurements show a higher effective flow for a higher delta pressure than for a lower delta pressure. Probably it was caused by the different port plate pressure balance, which makes the port plate sealing effect better at higher delta pressures.

Tab. 5.6: Comparison of simulated and measured effective flows.

Port plate version	Speed	System pressure	Simulation		Measurement	Deviation
			Effective flow	Volumetric losses	Effective flow	
	n_{rot}	Δp	Q_e	Q_s	Q_e	
	(min^{-1})	(bar)	($\text{l}\cdot\text{min}^{-1}$)	($\text{l}\cdot\text{min}^{-1}$)	($\text{l}\cdot\text{min}^{-1}$)	(%)
A	1500	15	24.10	1.39	25.12	-4.1
A	1500	30	23.90	1.59	24.33	-1.8
A	2800	15	45.56	2.01	47.67	-4.4
A	2800	30	45.30	2.27	47.38	-4.4
B	1500	15	24.31	1.18	25.61	-5.1
B	1500	30	24.09	1.40	25.81	-6.7
B	2800	15	45.93	1.64	48.17	-4.7
B	2800	30	45.67	1.90	49.10	-7.0
C	1500	15	23.45	2.04	23.74	-1.2
C	1500	30	22.91	2.58	22.26	2.9
C	2800	15	44.90	2.67	45.61	-1.6
C	2800	30	44.40	3.17	45.01	-1.4

The volumetric efficiency-tendencies for the designed port plates can be also seen from measurements in *Fig. 5.18*, where output flows versus pump speed at constant Δp (top graph for 15 bar and bottom for 20 bar), maximal pump displacement and constant inlet oil temperature at 50 °C are plotted.

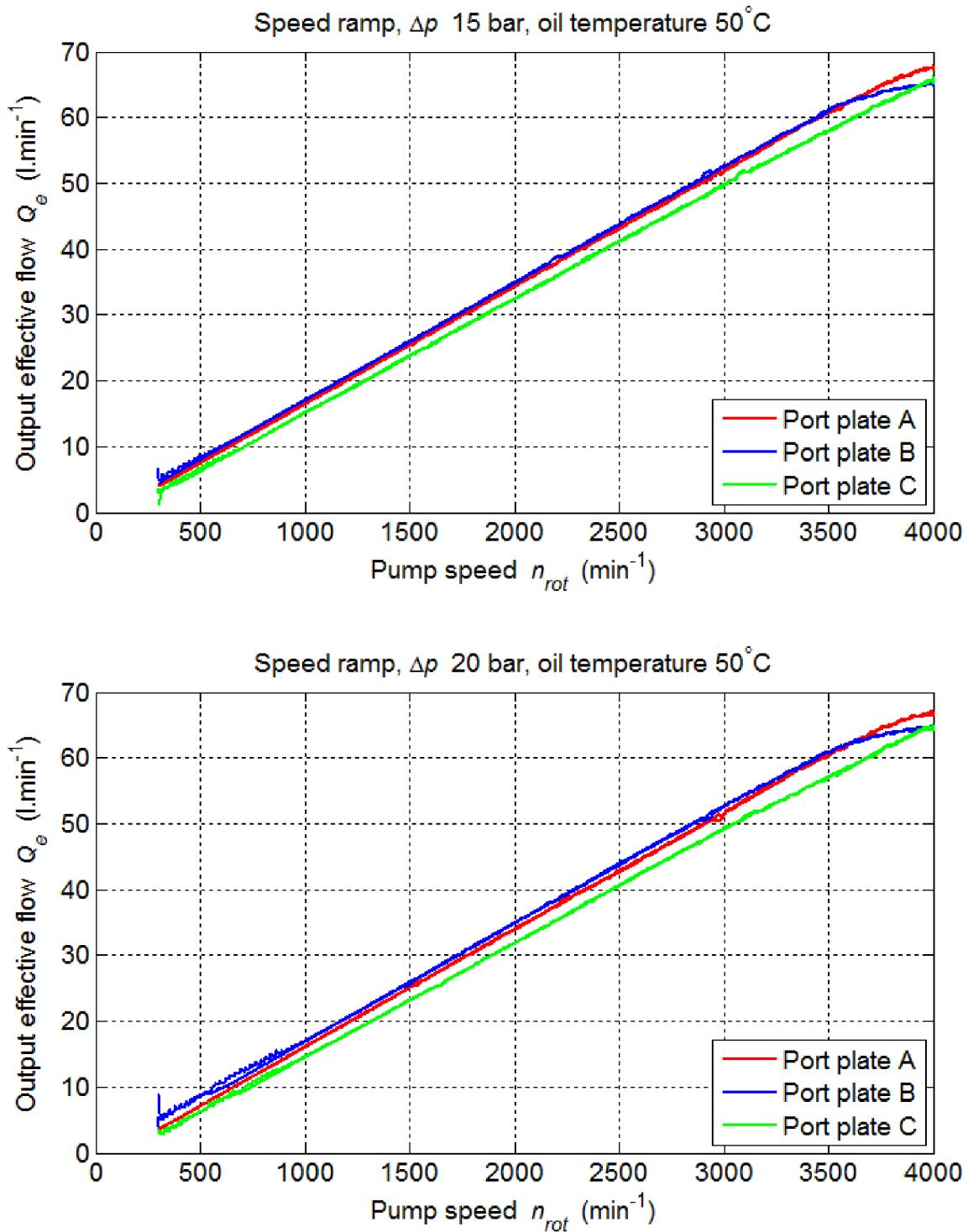


Fig. 5.18: Flow vs. Speed characteristics of tested port plates at different pressures. Port plate A is red color, port plate B is blue color and port plate C is green color.

The Fig. 5.18 shows a decrease of the volumetric efficiency at higher speeds due to filling losses especially for the port plate versions A and B. From a system point of view, the decrease of volumetric efficiency is not significant and occurs at high speeds, where pump doesn't operate. These filling losses can be predicted with CFD model.

The spring force values recalculated from the cylinder pressure at maximal displacement were used for a comparison between simulations and measurements. The maximal displacement was used due to good experimental results and simple hysteresis identification which was subtracted from measured values (to get comparable data with simulations, which don't consider friction). The delta pressure values from 15 to 25 bar and speed values from 1000 to 3000 min^{-1} were selected due to fact, that the charge pumps operates typically in these conditions.

This comparison in *Fig. 5.19* confirms a good agreement between simulations and measurements. The biggest deviation (at 1800 min^{-1}) is probably caused by dynamic effects which are not included in hydraulic model. It can be caused by many factors such as Eigen frequencies of the measured system or roller pump.

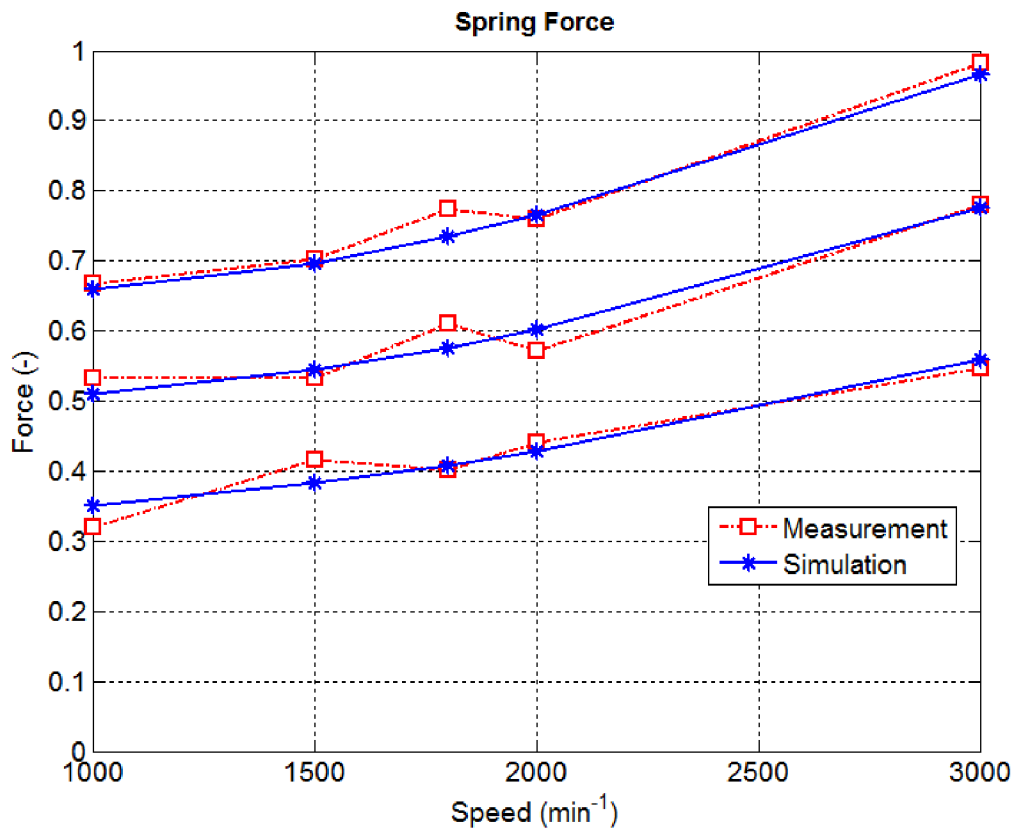


Fig. 5.19: Comparison between mean spring force simulations and measurements in normalized scale in different operating conditions.

Generally, it seems that this small deviation at specific speed doesn't have a significant impact on the system performance. Similar effects are observed in axial piston pumps where the control pressure in servo system at specific speed shows also some dynamical system influences.

6 MODELLING OF HYDROSTATIC DRIVETRAIN FOR POWER SAVING EVALUATION

Previous lines confirmed that the variable roller pump can be used in HST (Hydrostatic transmission). The next lines deal with a variable roller pump application as a charge pump and its power saving evaluation.

A hydrostatic transmission (HST) is a special kind of continuously variable transmission (CVT). It allows changing a gear ratio continuously with usage of displacement control of a pump (eventually of a motor). An example of a HST, shown in *Fig. 6.1*, is the variable displacement swash plate pump (1) and variable bent axis motor (2) connected in a circuit through working loop A and working loop B. The pump is the source of the fluid energy and the motor is the source of the mechanical energy. Other components in the circuit are added to obtain certain operating features [2]. The output flow of the axial piston pump is controlled by varying the swash plate angle per control (in *Fig. 6.1* electrical) command, which is the input for the pump control (3), which controls via servo pressure the pump displacement. Generally the control command can be electrical, mechanical or hydraulic.

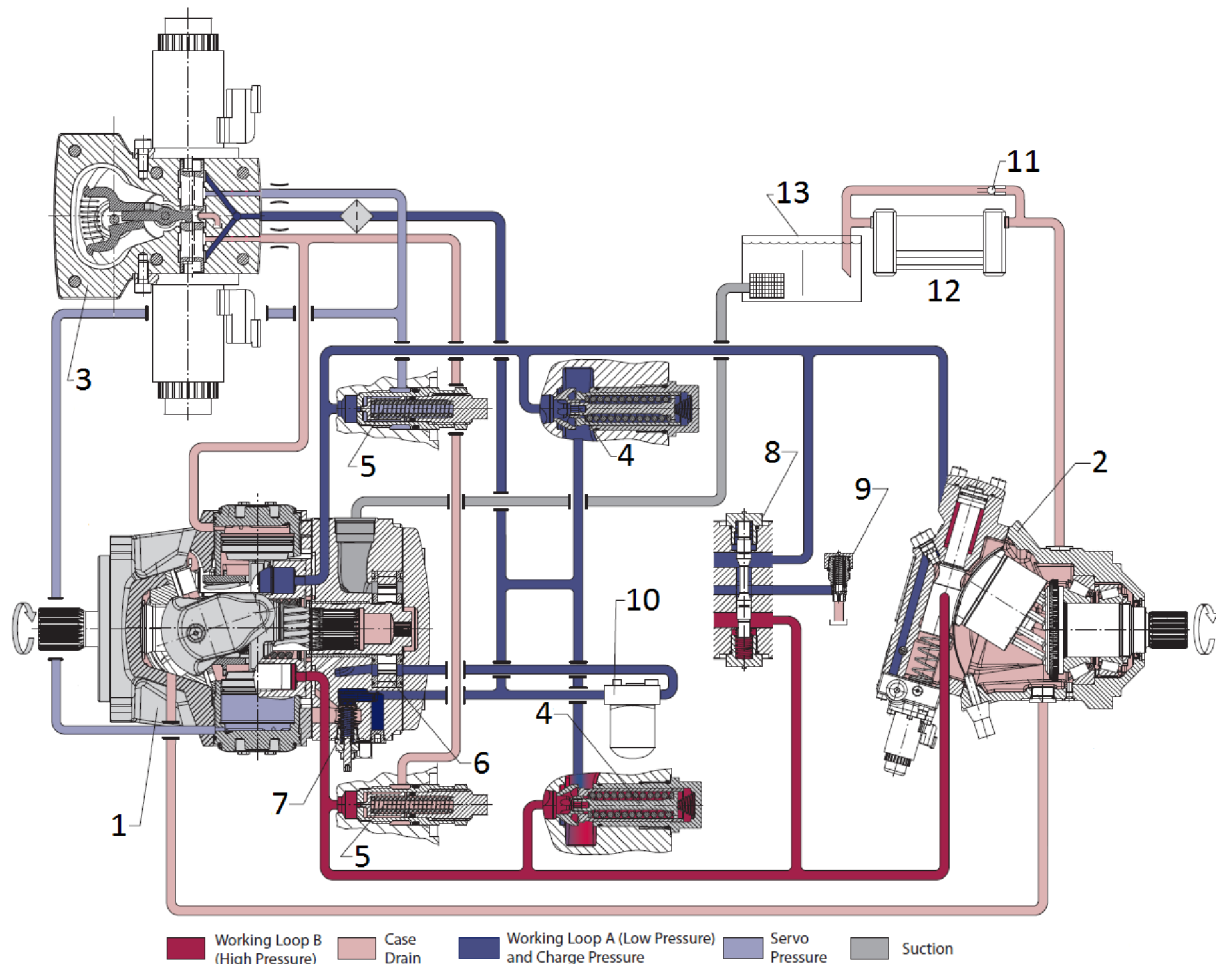


Fig. 6.1: Hydrostatic transmission produced by Danfoss Power Solutions company [55]. 1-variable displacement pump, 2-variable displacement motor, 3- pump displacement control, 4-charge check/high pressure relief valve (HPRV), 5-pressure limiter valves (PL), 6-charge pump, 7-charge pressure relief valve (CPRV), 8-loop flushing shuttle valve, 9-loop flushing relief valve, 10-charge pressure filter, 11-heat exchanger bypass valve, 12-heat exchanger, 13-reservoir.

The check valve/high pressure relief valves (4) (multifunction valves) have two main effects. They control (limit) the maximum loop pressure to some design value. This high pressure protection is fast, but in the end it causes a power dissipation (heat generation), when the valves are active. The second function of these valves has to ensure the charging of the working loops. It means to enable a flow from the charge pump to a working loop, when the pressure in the working loop is lower than the charge pressure. The next pressure protection of the working loops is ensured by pressure limiter valves (5). The pressure limiters are non-power dissipative high pressure controls and therefore limit the heat generated in the system. Unlike a relief valve, they are a slower protection because the pressure limiter changes the displacement of the pump in response to a high system pressure. The charge pump (6) is absolutely necessary in a HST. It has to ensure functions associated with its volume flow rate and charge pressure. This topic will be discussed more later. The charge pressure relief valve (7) ensures maximal charge pressure in the circuit.

The integral part of the motor, loop flushing (LF) shunt spool (8) is used to separate working loop A and working loop B pressures. The system delta pressure will cause the shuttle spool to shift, selecting the low system pressure side to flow to the loop flushing relief valve (9). Use the loop flushing option in Installations that require fluid to be removed from the low pressure side of the system circuit due to cooling requirements and also used to facilitate the removal of contaminants from the loop. Some cooling may be achieved by heat radiation from the housings, pipe work and tank surfaces, and intermittent heat inputs may be absorbed by the tank volume, but for most mobile machines the worst conditions need to be catered for (normally road drive). Sufficient charge flow needs to be provided to carry heat to the cooler fast enough to keep temperatures at acceptable levels. The purpose of the charge pressure filter (10) in the circuit is to ensure suitable cleanliness level of the hydraulic oil. The next important component in the circuit is the heat exchanger (12), which has to keep the fluid within recommended temperature limits. The heat exchanger bypass valve (11) is usually used to limit backpressure during cold starts. The last important component in the circuit is the reservoir (13), which in addition to the provider of the charge pump inlet with a constant source of fluid, it also helps remove air from system and cool the fluid. The reservoir also provides make-up fluid for volume changes associated with fluid expansion or contraction, possible cylinder flow and minor leakage.

The described type of HST is produced in the different sizes, due to a very big portfolio of vehicle sizes. The simple connection of a variable pump and a variable motor could be found mainly in telehandlers, wheel loaders and backhoe loaders. For example, the more complicated HST could be found in combine harvesters and sprayers. Some vehicle types equipped with a HST are shown in *Fig. 6.2*.

Almost all mobile machines equipped with a closed circuit hydrostatic transmission are powered by the engine. In the simple drivetrain equipped with a hydrostatic transmission (shown in *Fig. 6.1*), the engine is connected to the variable pump via input shaft. The gearbox (wheel) is connected to the motor via output shaft. The displacement control of the pump determines whether the vehicle is moving forward, backwards or is stationary. The pump output is increased by pump stroking, thereby increasing the speed of the motor (the speed of the motor could be also increased by the decrease of the motor displacement).

The result is that the vehicle can be speeded up and slowed down by the pump displacement control (eventually by motor displacement control). The rotation of the motor shaft can be reversed by moving the pump swash plate through the neutral position and

shifting it in the opposite (negative) direction, which causes fluid to flow in the opposite direction and the motor to rotate in the opposite direction, thus reversing the vehicle [2].



*Fig. 6.2: Typical applications of HST.
a) telehandler, b) wheel loader, c) combine harvester, d) sprayer.*

Basically two types of HST control (control of transmission ratio) are used in drivetrains. The first type is the primary controls, when the pump displacement is controlled only. The second type is the combined control when the pump and motor displacements are controlled [30].

Main advantages are that the HST provides improved maneuverability and CVT (continuously variable transmission) ability, which are normally demanded for mobile working machines. The next advantage of the HST is the flexibility of the drivetrain installation. The good example of the flexible drivetrain installation is a combine harvester or sprayer, where the installation of the conventional mechanical drivetrain will be very difficult. The maneuverability, CVT ability and installation flexibility are important for vehicle productivity, but they are provided at cost. The efficiency of a HST is always lower than a discrete-gear transmission, which typical value is about 95% or bigger. A hydrostatic transmission has a total efficiency about 80% and the newer designs up to 90% in some specific operating conditions, but none can approach the efficiency of a discrete transmission. Due to higher fuel costs, HST efficiency becomes more important for the vehicle manufacturer. These situations on the market result in very high pressure on the HST

manufacturer to increase total the efficiency of HST and thus decrease the efficiency difference between HST and conventional mechanical (discrete-gear) transmission. This increase could be achieved by the efficiency increase of the pump and motor but it can be achieved by other components efficiency increase also, which don't participate on the power transmit from the engine to the wheel, but they ensure the correct function of the HST transmission.

One of these components is a charge pump [2]. The charge pump is a critical component of the hydrostatic transmission. Without a charge flow and charge pressure, the HST will cease to function. A charge pump is normally a small fixed pump implemented in the housing of the pump shown in *Fig. 6.1* and in a hydraulic circuit diagram of the simplified HST in *Fig. 6.3*. Both pumps (main and charge) operate with the same input shaft speed due to same shaft.

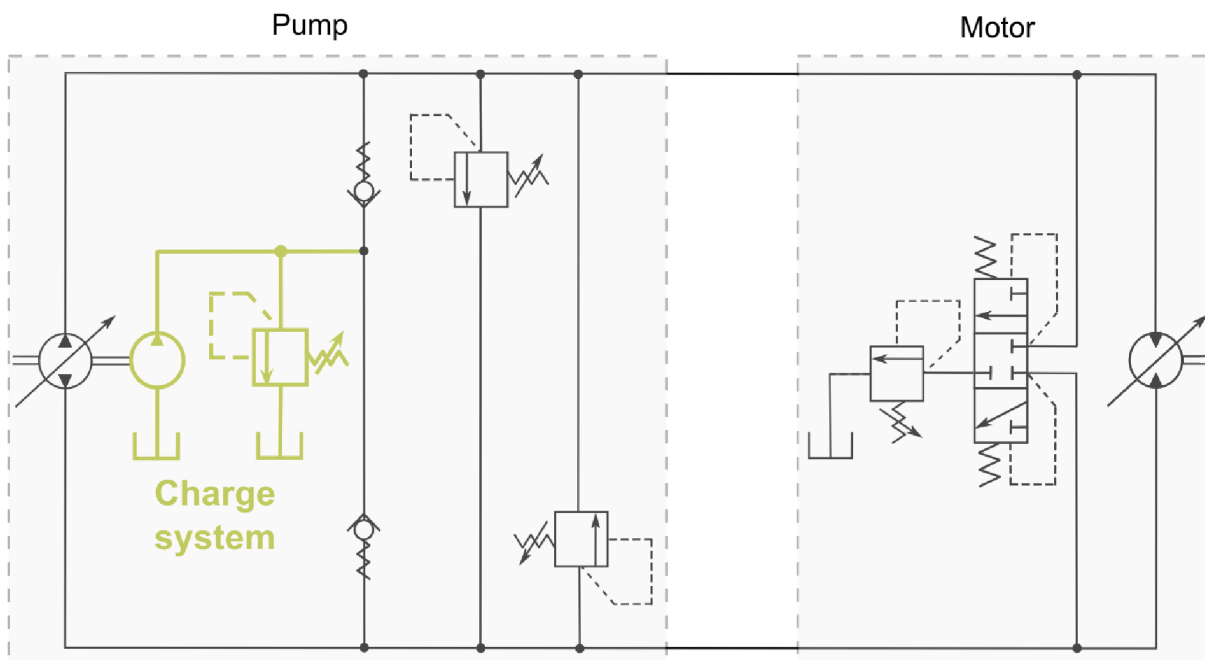


Fig. 6.3: Hydraulic circuit diagram of the simple HST.

The charge pump purposes connected with charge pump volume flow rate are:

- Replenish loop fluid lost through volumetric efficiency of the pump and motor (and other components).
- Replenish loop fluid lost through the loop flushing valve.
- Provide fluid due to bulk modulus effects.
- Provide flow to activate the servo control units.
- Provide flow to the pump control for proper operation.
- Provide a flow source for auxiliary circuit functions such as parking brake, motor displacement control...

All these charge flows and charge pressure requirements have to be accommodated in each mode of system operations, otherwise system provides poor performance and could be damaged.

6.1 Variable Roller Charge Pump in HST

Application of a VCP (variable charge pump) instead of a FCP (fixed charge pump) into standard-conventional charging system (shown in *Fig. 6.4*) brings design changes into conventional HST.

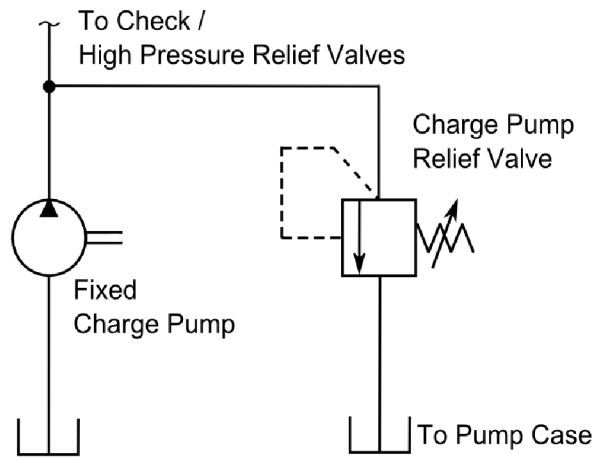


Fig. 6.4: Conventional (FCP) charging system for HST (Variant A).

The charge pressure in a conventional charging system (FCP) is controlled by a charge pump relief valve (CPRV). The charge pressure in HST with a VCP is adjusted by the VCP control (pressure compensated control), which results in the remove of the charge pressure relief valve or in a more preferred increase of CPRV setting (safety function). Disabling of the CPRV function results in a pump flushing flow decrease what is not acceptable in systems with higher power losses due to cooling requirements. There are generally two easy possibilities how to provide the pump flushing flow. The first one is to increase the motor flushing flow and connect the motor drain port with the pump drain. It means that the hot oil from the motor case will be used for pump case cooling which is not preferred.

The next possibility is to use a simple (bypass) orifice which connects the VCP outlet with the pump case and ensures constant flushing flow to the pump case. The motor (loop) flushing system in HST is not influenced by the VCP. The modified system with a VCP and bypass orifice hydraulic circuit is shown in *Fig. 6.5*.

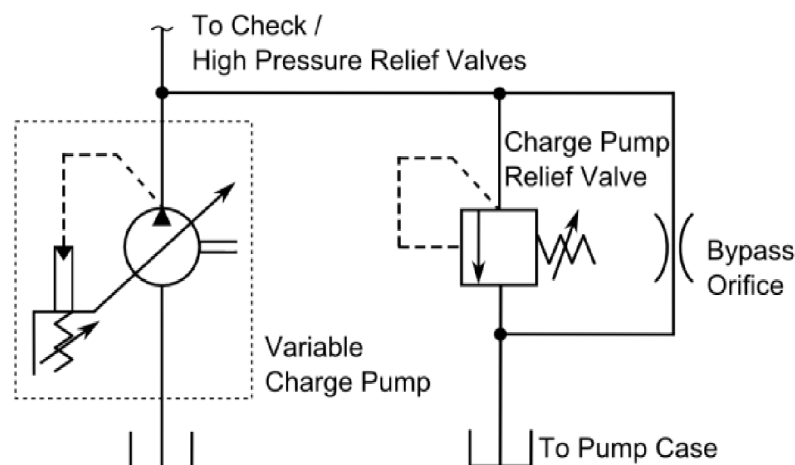


Fig. 6.5: VCP with bypass orifice application (Variant B).

These changes enables the operation of a HST with VCP in the similar way as a HST with a fixed charge pump which was confirmed by a system flywheel test shown in *Fig. 6.6*. The first-top graph presents the command to the displacement control of the pump. The second graph shows servo and charge pressures. The third graph present the pressures in the working loop (system hoses) A and B. The last graph shows pump and motor absolute speed.

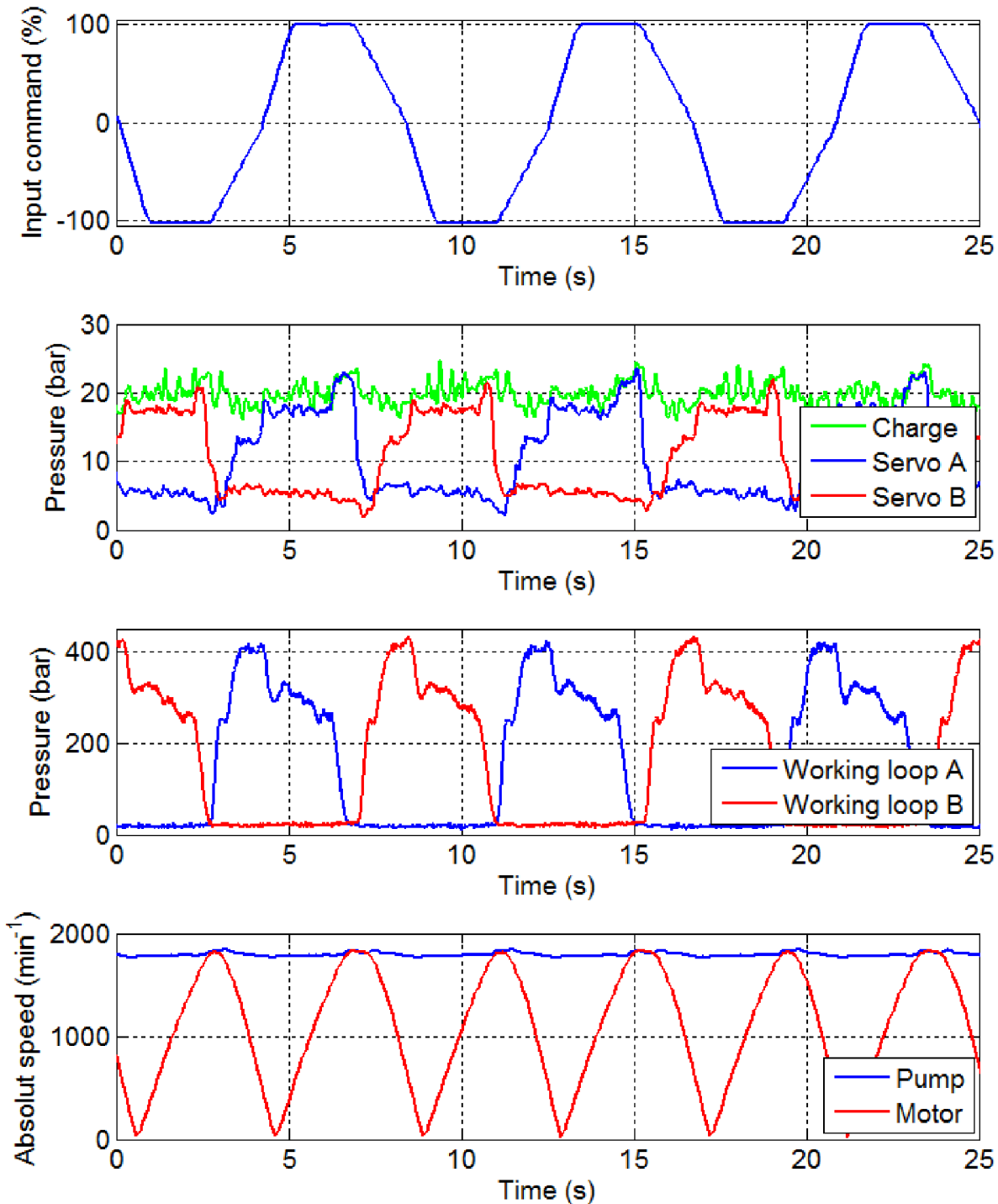


Fig. 6.6: Flywheel system test with variable charge pump.

The presented flywheel system test uses a HST containing a variable displacement pump (89 cm^3) controlled by a manual displacement control and connected via hoses to the fixed motor (89 cm^3), loaded with flywheel with an inertia $3.84 \text{ kg}\cdot\text{m}^2$. The pump runs at 1800 min^{-1} constant speed. The motor speed varies according to the pump displacement. The VCP with a bypass orifice was mounted in the pump housing. It can be seen, that the charge pressure profile in *Fig. 6.6* is not ideal but sufficient for the charge pump function.

This system brings a noticeable a power saving only in the cases when the engine/pump has a high speed and FCP delivers more flow than required which has to be wasted in the CPRV valve. The VCP is able to adjust the output flow according to the oil demands in the circuit and that decreases the power consumption. Probably a similar scenario occurs when the vehicle is in the idle mode (standing), motor flushing is not active and almost all FCP flow is wasted in the CPRV because the low HST performance does not require a high flushing/cooling flow. Theoretically both scenarios provide a potential for power savings but generally this potential is low because of many mobile machines do not operate long time in idle mode.

Base on the previous consideration it looks clear that the application of a VCP with variable pump flushing system (*Fig. 6.7*) and loop (motor) flushing system (*Fig. 6.8*) have a significant effect on the power savings.

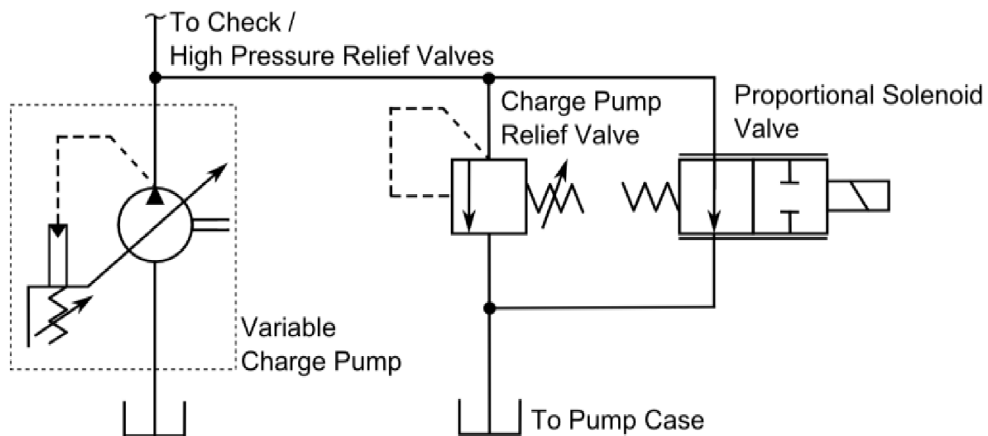


Fig. 6.7: Proposed variable pump flushing system (Variant C).

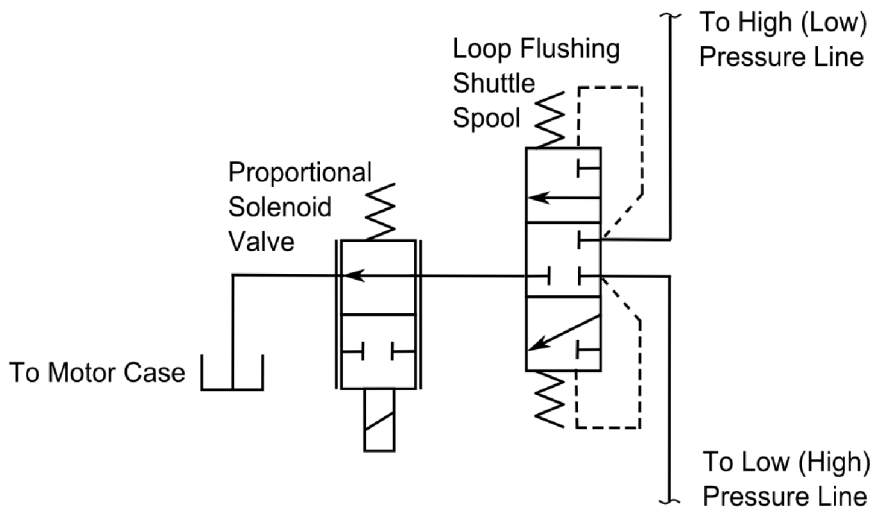


Fig. 6.8: Proposed variable loop flushing system (Variant C).

Due to this it is necessary to include a variable flushing system for the pump and the motor-loop. Ideally, proportional flow control valves, which will adjust the flow according to the oil temperature or HST performance, could be used. A variable pump flushing system should decrease the current to the proportional solenoid with pump case oil temperature increase. The same principle should be used for a variable loop flushing system, but the solenoid current should be depending on the motor case oil temperature or loop oil temperature. An intelligent pump and loop flushing system allows less waste of flushing flow and saving of energy. Cheaper thermostat valves could by also considered.

A better overview about VCP power savings gives the next figure. The Fig. 6.9 presents the measured potential of power savings achieved with a VCP (displacement 100% and 50%) in comparison with a FCP (gear rotor with displacement 100%).

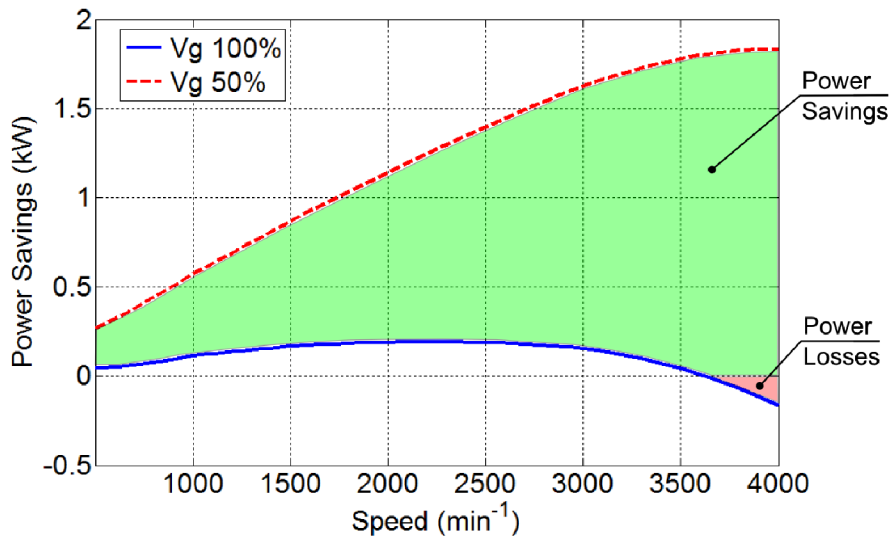


Fig. 6.9: Measured power saving potential.

The measurements were performed with a 17 cm³ FCP and VCP units (presented curve is difference between VCP and FCP power input), charge pressure 31 bar and suction oil temperature 50 °C. The blue curve in this graph presents a negligible power savings due to higher VCP overall efficiency and the red curve presents significant power savings due to displacement decrease. The green area presents possible VCP power savings with the assumption of a VCP displacement reduction from 100 % up to 50 %. The area bordered by the red and blue line contains also red area which presents power losses. These losses occur only in high speeds when the VCP displacement is not reduced and the VCP efficiency is lower than the FCP efficiency. Practically these conditions don't occur often due to the fact that the pump displacement is reduced mainly in high speeds.

It is necessary to consider that a VCP system not only loads the engine with lower power but the VCP system produces less losses what finally decreases the demand for flushing flow (cooling flow).

6.2 Simulation Model of the Drivetrains

According to Fig. 6.9 it is clear that the VCP has a power saving potential in HST drivetrains. The power savings due to the increase of the charge pump efficiency (blue line) cannot bring a significant effect, especially in low pressure applications and so it is not focus

of this work. The full VCP power saving potential occurs with the decrease of the VCP displacement; it means that power saving potential is depending on the real HST demand for charge pump flow. One possible way how to calculate VCP power savings is a drivetrain simulation. The modeling of the drivetrain is separated in two parts. The first part is the hydro-mechanical drivetrain modeling. The output from the first part is coupled with the output from the second part of the modelling which is the thermal model of the hydrostatic transmission.

6.2.1 Hydro-Mechanical Drivetrain Model

The hydro-mechanical drivetrain model was developed based on previous papers. The structure of the simulated drivetrain is shown in *Fig. 6.10*. The whole model is based on the one dimensional principle. The model was built modularly and it can be simply modified. The model parts are described in the following paragraphs. The purpose of this model was a prediction of the drivetrain efficiency but simple dynamics was also included.

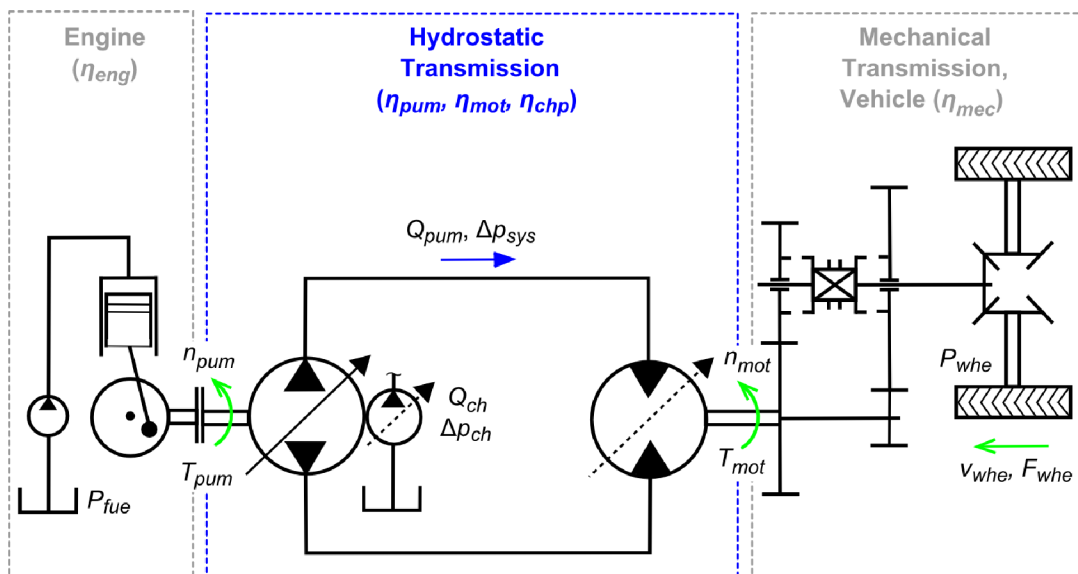


Fig. 6.10: Simulated drivetrain structure.

- **Engine**

The engine model is based on the work developed in [5], [6], [56], [57]. This model equipped with an engine speed regulator considers the engine dynamics based on measurements. The model includes a map of the engine torque and fuel consumption. The base equation for the engine shaft speed can be written in this form:

$$(I_{eng} + I_{pum}) \cdot \dot{\omega}_{pum} = T_{eng} - T_{pum} - T_{dam} \quad (6.1)$$

where I_{eng} and I_{pum} represent rotational inertias of the engine and pump. According to the figure, the pump rotational speed ω_{pum} is the same as the engine shaft speed. The engine produces torque T_{eng} . The HST pump loads engine with torque T_{pum} (this torque includes also the torque from charge pump) and damping torque T_{dam} . In the case of a pump gear between the HST pump and the engine, the previous equation has to be modified. Inputs to the model are speed command, HST pump torque and the output is the fuel consumption, actual engine power and engine/HST pump speed.

- **HST and Charge Pump**

The HST efficiency model together with the charge pump efficiency model is based on Polymod. The Polymod approach, developed by Ivantysynova and Mikeska in [53], is based on a mathematical approximation of steady state measurements. The similar possibility how to predict unit efficiency with lower accuracy is described in [58]. Losses in the pump, motor and charge pump model predicts the efficiency of the HST. Losses in the hydraulic hoses between pump and motor are included too. The model considers the dynamics of the (HST) pump servo system, pump control, motor control, motor loop flushing system and charging system (CPRV valve or VCP cam ring dynamics). The dynamic part of the HST model is based on one-dimensional/ control volume modelling which consists of orifice equations, pressure build up equations and equations of motion, which can be found in [20], [21] and [26]. The model parameters were adjusted according to the measurements to achieve sufficient agreement between measurements and simulations. The VCP simple PC control model is based on the developed linearized control system model.

- **Mechanical Transmission and Vehicle**

The model of the vehicle and the mechanical transmission was developed according to equations mentioned in [5], [6], [59], [57]. The model considers constant mechanical transmission efficiency and uses a simplified one dimensional vehicle model according to the equation (6.2).

$$m_{veh} \cdot \dot{v}_{veh} = \frac{T_{mot} \cdot i_{mec} \cdot \eta_{mec}}{r_{whe}} - m_{veh} \cdot g \cdot \sin(\vartheta) - m_{veh} \cdot g \cdot f_{rol} \cos(\vartheta) \cdot \text{sign}(v_{veh}) \quad (6.2)$$

An equation neglects an air resistance (which is not significant for mobile working machines) and use simple calculation of the wheel rolling resistance. The vehicle mass is represented by m_{veh} , vehicle longitude speed by v_{veh} , motor torque by T_{mot} , mechanical transmission ratio by i_{mec} , mechanical transmission efficiency by η_{mec} (or by inverted value in the case of the braking mode), wheel radius by r_{whe} , slope angle by ϑ , gravitational constant by g and rolling resistance coefficient is corresponding to the variable f_{rol} .

6.2.2 HST Thermal Model

The thermal model coupled with a hydro-mechanical one dimensional model is used for a determination of the cooling / loop flushing requirements in the HST. Due to simulation speed requirements the thermal approach is also based on the one-dimensional approach.

Generally, it can be concluded that one dimensional hydro-mechanical model building is sufficiently described in the available literature. The situation is different with a one dimensional thermal model of hydrostatic drivetrains. The majority of authors focus on working hydraulics but the modeling approach can be also used in hydrostatic transmission modeling. The older works such as [24], [60], [61], [62], and newer from Maha fluid power research center [63], [64], used for the thermal model development in this work.

The general equation (6.3) of control volume energy E can be written [64]:

$$\frac{dE}{dt} = \sum \dot{m}_{in} \cdot h_{in} - \sum \dot{m}_{out} \cdot h_{out} + \dot{q} - \dot{W} \quad (6.3)$$

where the input oil mass flow is \dot{m}_{in} with the enthalpy h_{in} and the output oil mass flow from the control volume is \dot{m}_{out} with the input enthalpy h_{out} . The heat rejection rate from the control volume is \dot{q} and \dot{W} is the work rate. After some replacement and simplification according to [64], final equation can be derived as:

$$\frac{dT}{dt} = \frac{1}{\rho \cdot c \cdot V} \cdot \left(\sum \dot{m}_{in} \cdot h_{in} - \sum \dot{m}_{out} \cdot h_{out} + \dot{q} - \dot{W} \right) + \frac{v \cdot \gamma \cdot T}{c} \cdot \frac{dp}{dt} \quad (6.4)$$

where T is the oil temperature, ρ is the oil density, V is the oil volume, c is the specific heat, p is the pressure of the oil in the control volume, v is the kinematic viscosity and γ is the thermal volumetric expansion coefficient.

The main advantage of the control volume approach in hydraulic and thermal modelling is that this approach enables to connect the hydraulic model with the thermal model. The equation (6.4) is modified according to the simulated vehicle and then this modified equation is connected with the relevant hydraulic part of the model. The thermal model output is the oil temperature and the inputs are: ambient temperature, power loss and flows in and out of the control volume which are assumed as equal. The simulation model assumed that all power losses (P_{loss}) in the circuit are transferred into heat of the hydraulic oil. Each hydraulic component in the thermal part of the simulation model (hose, pump, motor and tank) is a connection of two node equations (fluid mass equation and component mass equation) which are a modification of the equation (6.4) according to Fig. 6.11.

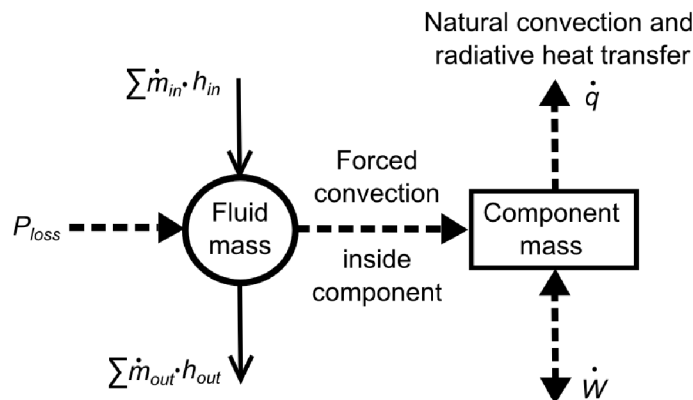


Fig. 6.11: Thermal modeling approach for hydraulic components with fluid mass node and component mass node [64].

The forced convection heat transfer occurs inside of the components and it is a connection between fluid mass node and component mass node. The conductive and radiative heat transfer equations connect each component mass node to the surrounding (with ambient temperature). In the end, this connection gives the fluid mass passive conductive and radiative cooling (\dot{q}) through the component mass node. Base on the Fig. 6.1 and Fig. 6.11, the general thermal model was setup. The model considers only basic components in the hydrostatic transmission.

The model inputs are flows and pressures calculated in the hydraulic-mechanical model, power losses calculated from pressure drops over components, efficiency (kit) power losses calculated in Polymod, material properties, geometric properties and performance properties (for example cooler power) of used components. Outputs from the model are the temperatures of the hydraulic oil in the circuit and they are used in the hydraulic-mechanical part of the model which makes a close coupling between the thermal part of the model and the hydraulic-mechanical part of the model.

It is necessary to ensure, that the control volume approach calculates the pressures and flows corresponding to the thermal model demands. The thermal model has to ensure the law of mass flow conservation. The used approach is suitable for developing of a thermo-hydraulic-mechanical model. If fast pressure changes were not expected, the equation (6.4) can be rewritten to a more suitable form. Following equations and constants are taken from Al-Natour's dissertation work [60]. Each component model consists at least from one fluid mass and one component mass. The general equation for the fluid mass temperature T_F can be written in this form:

$$\frac{dT_F}{dt} = \frac{\sum Q_{in} \cdot c_{oil} \cdot \rho_{oil} - \sum Q_{out} \cdot c_{oil} \cdot \rho_{oil} + \sum P_{loss} - \sum \dot{q}_{FC}}{V_F \cdot \rho_{oil} \cdot c_{oil}} \quad (6.5)$$

Oil mass flows (flow rate) to the fluid mass (control volume) is Q_{in} , Q_{out} represent inlet and outlet oil flows from the fluid mass (control volume). P_{loss} are efficiency losses which occur in the hydraulic system. They are calculated from pressure drops and the unit losses through Polymod. The specific hydraulic oil heat capacity is named as c_{oil} and the hydraulic density as ρ_{oil} . The volume of fluid mass or with other words the control volume fluid volume is represented like V_F in this equation. The heat transfer between the fluid mass node and the component mass is named as a \dot{q}_{FC} . This forced convection can be calculated based on the equation

$$\dot{q}_{FC} = h_f \cdot A_f \cdot (T_F - T_C) \quad (6.6)$$

Where A_f is the inside surface area used for forced convection, h_f is the forced convection heat transfer coefficient, which depends on the Nusselt number [60]. The component mass temperature (T_C) can be calculated from equation (6.7).

$$\frac{dT_C}{dt} = \frac{\dot{q}_{FC} - \dot{q}_{CA}}{m_c \cdot c_c} \quad (6.7)$$

The right side of this equation contains the component mass m_c , the specific heat constant of the component material c_c , the forced convection \dot{q}_{FC} and the natural convective-radiative heat transfer \dot{q}_{CA} . This convective-radiative heat transfer \dot{q}_{CA} is described in equation (6.8), where the dependency on the natural heat convection coefficient h_n , surface area A_n , emissivity of the black body ε , Stefan-Boltzmann constant σ_{SB} and temperature difference between component mass and outside ambient temperature T_c can be seen [60].

$$\dot{q}_{CA} = h_n \cdot A_n \cdot (T_C - T_A) + \varepsilon \cdot \sigma_{SB} \cdot A_n \cdot (T_C - T_A)^4 \quad (6.8)$$

The first part of the equation's right side corresponds to the convection heat transfer and the second corresponds to the radiation heat transfer. The radiation heat transfer for low temperatures can be neglected and normally for low temperatures it is part of the natural heat convection coefficient h_n . The conductive heat transfer between the HST and other vehicle components was not considered. Conductive heat transfer was used only for the heat transfer calculation between charge pump housing and pump housing.

Base on the approach described in previous equations, all components shown in Fig. 6.12 were covered. The pump oil case temperature, gallery oil temperature, high/low (system) pressure hoses oil temperature, motor case temperature, drain hose oil temperature, tank oil temperature and suction hose oil temperature together with their component mass temperatures were described. The used approach neglects temperature distribution

in the components but on other hand, this approach is able to calculate the average oil temperature in each simulated component. The cooling subsystem consists of the motor and the pump drain ports which are connected to the tank. The oil from the tank is cooled in the cooler (heat exchanger) which is located at the inlet of the tank. The cooler model was implemented as a look up table. The output cooling power is a function of temperature difference between ambient/air temperature and input oil temperature, fan speed and cooler flow [65]. The cooler model doesn't include own dynamics in this simulation model. Ambient temperatures were assumed as constant. The forced, natural convection and radiative heat transfer were modelled according to [60]. This work contains also tables with parameters for the one dimensional thermal modeling. The simulation model doesn't consider working hydraulics.

The next *Fig. 6.12* shows the structure of the thermal model: the considered hydraulic oil flows, heat transfers and power losses. The pump at the top left corner consist of the two fluid nodes and two mass nodes representing the oil pump case volume, the gallery oil volume, the pump mass and the charge pump mass which are coupled together. Flow inputs for the gallery fluid node are: the charge pump suction flow from Tank Q_{sucCP} and the flow from high pressure relief valves, which flows from the high pressure line through the high pressure relief valve (HPRV) to the fluid gallery Q_{HPRV} . The flow outputs are the charge pump leakage Q_{caseCP} , the pump control flow Q_{contP} (which firstly flows to the control, which is not thermally modeled), the charge pump relief valve flow (in case of VCP bypass orifice flow) Q_{CPRV} and the check flow Q_{check} . The flows Q_{CPRV} , Q_{contP} , Q_{caseP} with the pump leakage Q_{leakP} deliver oil to the pump case, where this oil is heated up with the part of the pump losses P_{lossP*} (kit losses and pressure drops), the pump control losses $P_{lossConP}$, the part of charge pump losses $P_{lossCP*}$ and the part of the CPRV losses $P_{lossCPRV*}$. Hot oil from the pump case is drained with Q_{caseP} flow flowing through drain hoses to the tank. The oil in the gallery is heated up with the $P_{lossHPRV}$, the rest of the charge pump losses $P_{lossCP*}$ and the rest of the CPRV losses $P_{lossCPRV*}$. Some energy left the pump housing through the pump surface according to the *Fig. 6.12*.

The oil in HP, LP hoses (Loop A, B) is heated up with the part of the pump/motor losses P_{lossP*} / P_{lossM*} , the check valves losses $P_{lossCheck}$ and losses which occurs in the hoses $P_{lossHose}$. The relatively cold oil from the gallery replace oil losses in the HP, LP hoses, pump, motor kits with Q_{check} flow. This flow covers concretely the pump leak flow Q_{leakP} , theoretically the high pressure relief valves flow Q_{HPRV} , the motor leak flow Q_{leakM} , the motor control flow Q_{contM} and the loop flushing flow Q_{LF} . The hose material also provides some possibility to transfer the part of the heat from the oil to the surroundings. The loop flushing flow, Q_{LF} , motor control flow Q_{contM} and Q_{leakM} flows to the motor case, where are heated up by part of the motor losses P_{lossM*} , the motor control losses $P_{lossConM}$ and the loop flushing losses P_{lossLF} . The motor case drain flow Q_{caseM} drains hot oil from the motor case to the tank together with the pump case drain flow Q_{caseP} . Flows through hose bring some power losses but on other hand it provides also possibility to cool oil thought the hose-component mass as an each component. The case flows come to the tank, where the most of the oil is available. The pump case flow and the motor case flow come to the tank separately through drain hoses. The oil in the tank is cooled with the cooler P_{cool} and then continues in suction hoses to the charge pump, finally oil flow loop is closed. Each component provides at least passive cooling (tank provides active cooling with cooler) with a heat rejection through component masses. The index * means that the power loss is divided between fluid nodes. For example the pump loss is divided between the loop node and pump case node.

This simplified approach calculates oil temperatures for the pump case, gallery, HP/LP (loop) hoses, motor case, drain hoses and suction hoses. It also provides overview about mass components temperatures. Developed model provides enough information necessary for cooling performance evaluation.

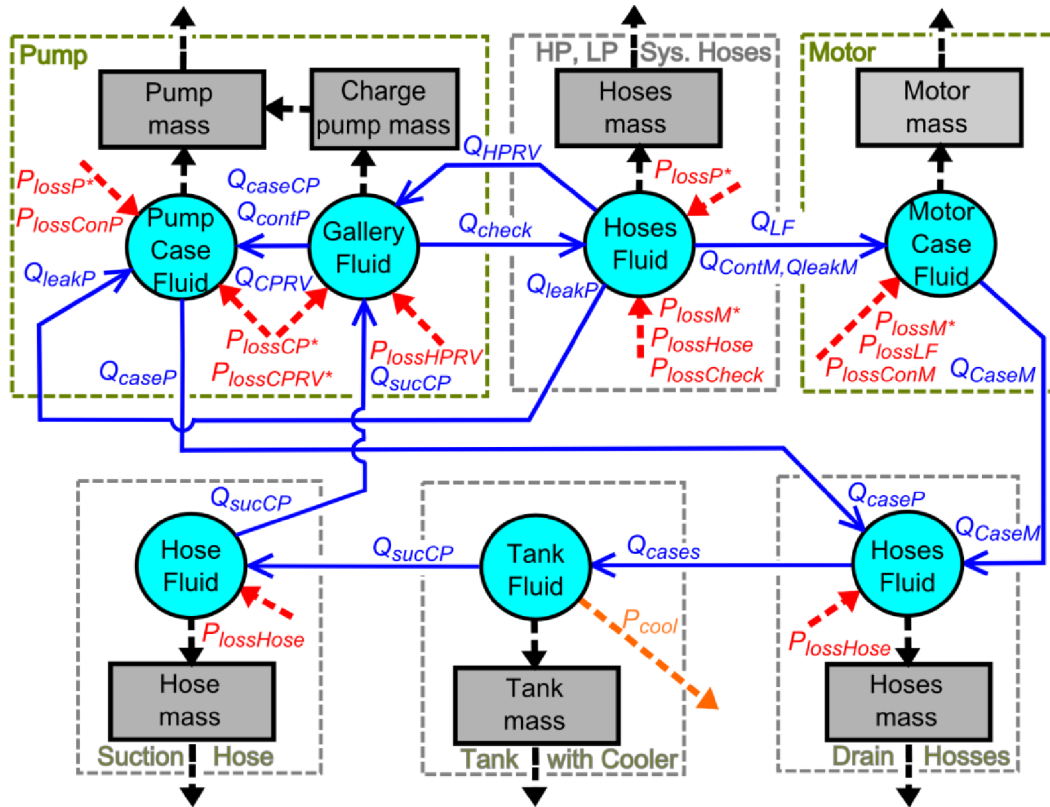


Fig. 6.12: Principle of used HST drivetrain thermal modelling.

6.2.3 Drivetrain Model Implementation

The analyses in this work consider the influence of a VCP application. The whole evaluation of the power saving potential is based on the system simulation of the combine harvester and the telehandler, which were chosen for further analysis. So, two different vehicle types with two different working conditions and different FCP sizes will be analyzed at the next pages. The base structure of drivetrains is shown in Fig. 6.10. The HST in the considered drivetrains consists of one motor and pump, where pump is connected to the engine and the motor is connected to the mechanical transmission which propels wheels. The cooling system was described in the previous chapter and the cooling structure was considered the same for the combine harvester and telehandler. Naturally, the simulation parameters were setup according to the vehicle type and working conditions.

The simulation model was implemented in Matlab-Simulink. The drivetrain models were built with modular structure which can be seen in attachment A3 (complete drivetrain model) and attachment A4 (thermal subsystem). The model's subsystems are built according to the physical structure of the vehicle. This structure allows an easy model rebuilding and problem finding is accelerated. Each subsystem in the model contains corresponding set of the equations, derived in the previous chapters. The telehandler model was built analogically [66]. The main differences are in the used parameters of the simulated drivetrain components.

6.3 Verification of Simulation Model

The verification of the simulation model is primary based on the comparison between the simulation results and the measurements. The simulation results have to follow measurements and all simulated characteristics have to have physical background. Intuitive approach based on the experiences can be also useful. Only some of measurements could be published due to measurements performed on the customer machines. The dynamic behavior of the hydro-mechanical model was validated with telehandler measurements. The measurements were performed for relatively short cycles; due to this the thermal model validation for these conditions doesn't make a sense.

An example of the drivetrain model accuracy is shown in *Fig. 6.13*, where two acceleration cycles of the telehandler were compared. The telehandler driver controls vehicle speed via the pedal, which sets demanded engine speed. The pump and motor displacements are controlled according to the engine speed and delta system pressure. The demanded speed was input for the simulation.

First two graphs show the telehandler engine and the vehicle speed. It can be seen, that the first vehicle acceleration from standing up to $10 \text{ km}\cdot\text{h}^{-1}$, starts at 9 s and it ends at 27 s. The second acceleration starts at 38 s and finishes at 60 s. The maximal telehandler speed corresponds to the first gear, which was shifted during whole drive. The resulting system pressure Δp_{sys} shows a relatively low value due to measurement (and simulation) conditions. The telehandler was driving on the road without any slope which has direct impact on the system pressure. The solid surface results in the low wheel rolling resistance coefficient, which also has a positive impact on the system pressure. The maximum system pressure value was about 150 bar. The next graph to last presents the charge pressure behavior where the pump speed dependency can be seen. The maximal charge pressure, more than 31 bar, occurs at the maximal pump speed. The last graph presents the pump and the motor displacement behavior. The logic of the motor and the pump displacement control is depending on the selected control system.

The different example used for the model validation is shown in *Fig. 6.14*. The telehandler drives down the hill with shifted second gear. The first graph presents the engine speed and the second graph presents telehandler speed. The engine speed is controlled by a driver again. The slight engine speed overshoot between 15 s and 25 s is not shown in simulation model due to different drag torque used in the simulation. The vehicle accelerated from 7 s up to 12 s when the speed settled about at $28 \text{ km}\cdot\text{h}^{-1}$. During acceleration the system pressure rises up to 250 bar. Due to downhill drive the slight telehandler acceleration continues up to 22 s when the maximal telehandler speed about $30 \text{ km}\cdot\text{h}^{-1}$ was achieved. The negative system delta pressure during the telehandler drive also confirms downhill drive. The next graph in *Fig. 6.14* shows charge pressure behavior. The significant pump speed dependency can be seen again. This is caused by charge pump relief valve, which p - Q characteristic is not ideal. The pump displacement and the motor displacement characteristics can be seen in the last graph. The behavior of the pump and motor is corresponding to the driving mode which was selected on the vehicle.

Both telehandler simulation results follow measurement results very well. The hydro-mechanical part of the simulation model was discussed in the past in [56], [59], [66] also and the general approach was validating in another works such as [5], [6].

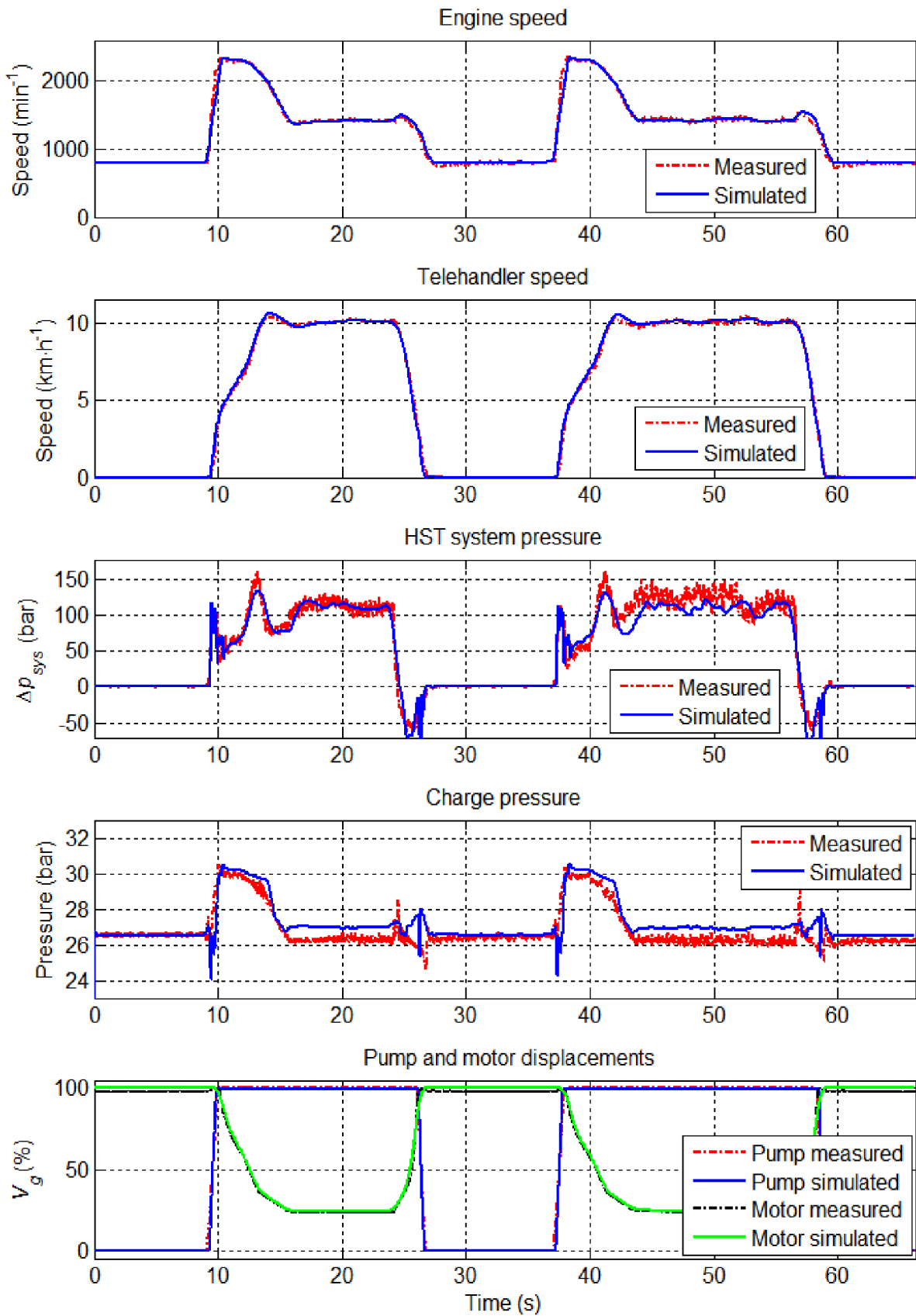


Fig. 6.13: Comparison of telehandler measurements and simulation during two acceleration and deceleration cycles.

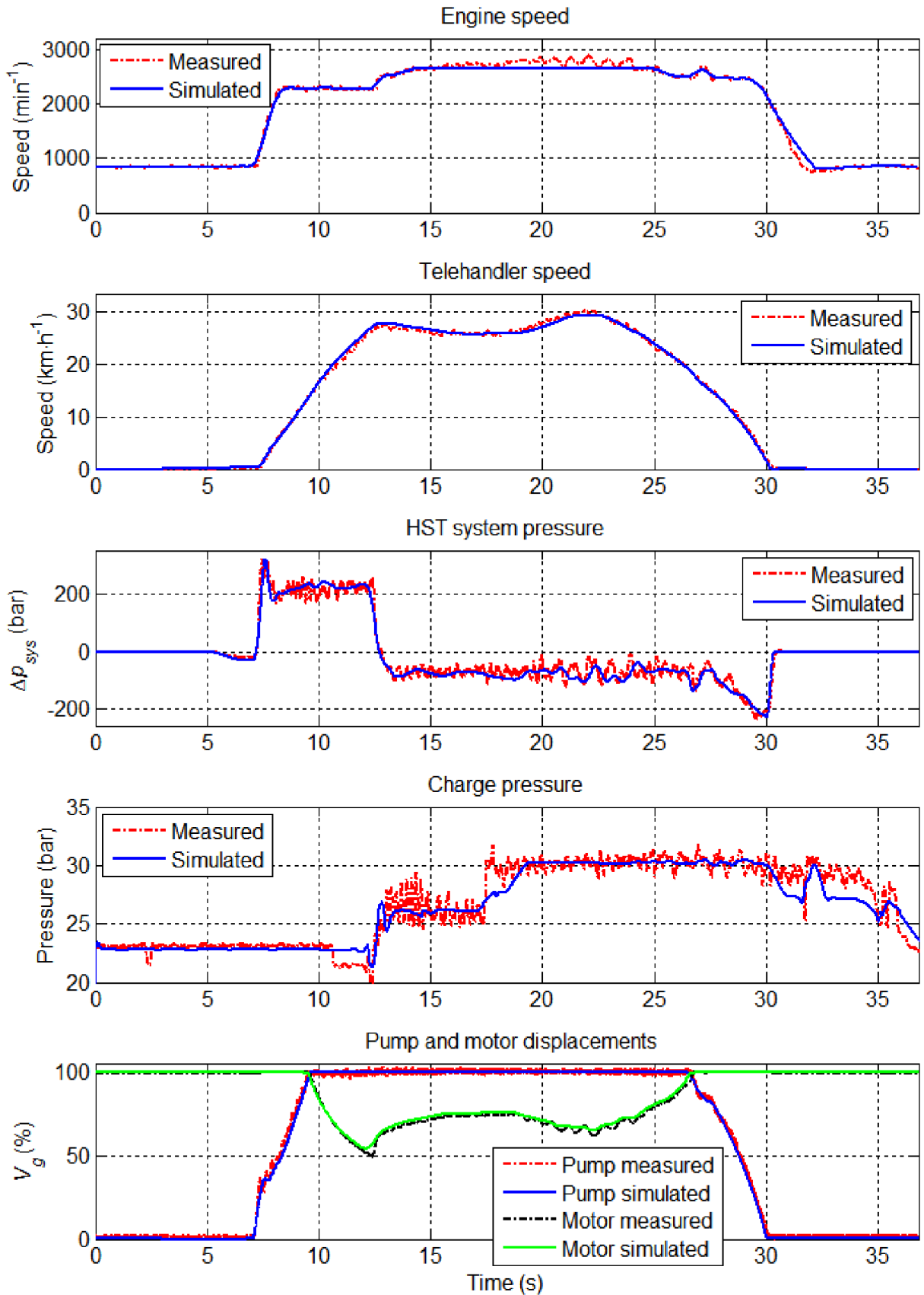


Fig. 6.14: Comparison of telehandler measurements and simulation during downhill drive.

The thermal part of the simulation was validated with combine harvester simulations. Steady-state measurements of the combine harvester with FCP were available only. Combine harvesters measurements simulate steady state combine harvester drive on the road (transporting) and field with constant speed (harvesting). Measurements were performed at the customer machine; therefore the details might not be mentioned. Some of the simulation results which were used for validation are shown in following two figures: *Fig. 6.15*, *Fig. 6.16*.

The first *Fig. 6.15* shows hydraulic oil temperatures during field drive - harvesting. During harvesting combine harvester runs at the constant speed about $8 \text{ km}\cdot\text{h}^{-1}$. The engine speed is almost 3000 min^{-1} and the delta system pressure about 150 bar.

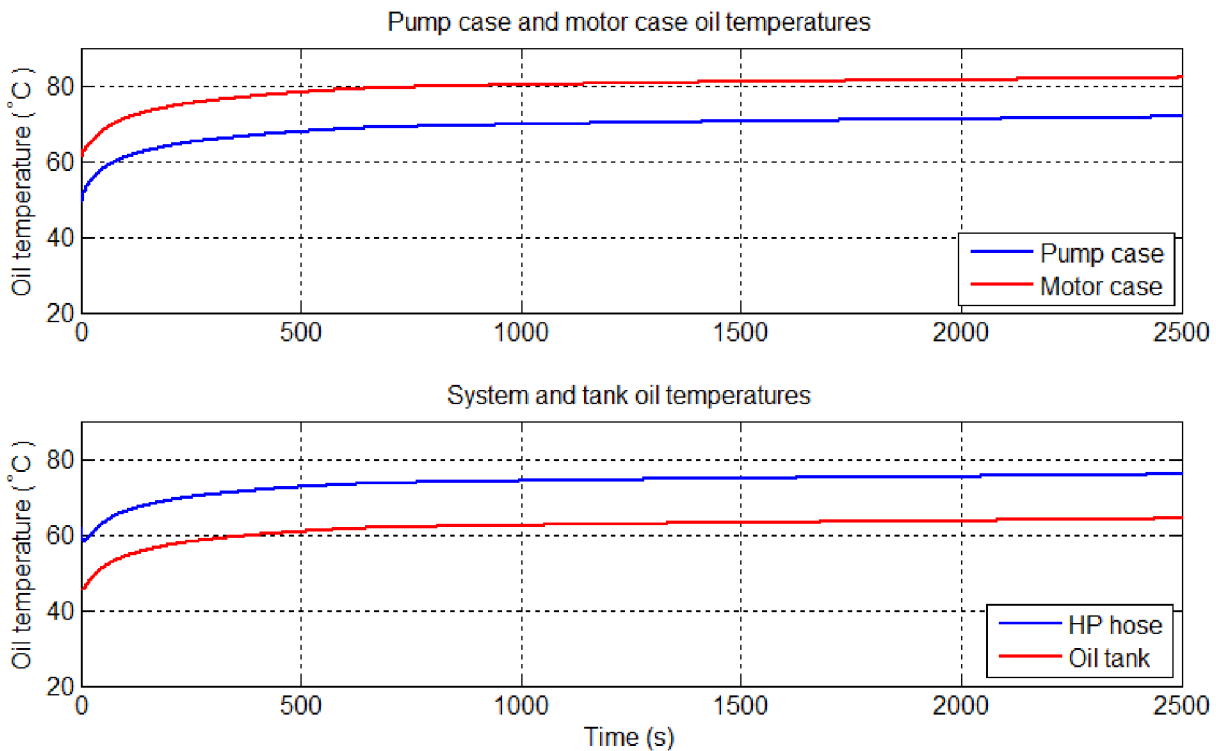


Fig. 6.15: Simulated combine harvester oil temperatures during field drive.

According to the measurements, the steady temperature of the pump case oil is 73.4°C and the temperature of the motor case oil is 82.3°C . The simulation model shows the steady pump case oil temperature 72.1°C and the steady motor case oil temperature 82.4°C . The measured steady temperature of the oil in the HP hose is 79°C . The simulation provides only the average temperature of the oil in the HP and LP hose called as the loop temperature, which value is 76.2°C . This value lower due to the fact, that the oil in the LP hose has normally lower temperature. The measured steady temperature of the oil in the tank is 63.9°C and the simulated temperature is 64.6°C .

The second simulation shown in *Fig. 6.16* simulates combine harvester drive (transport) on the road. The thermal behavior is shown in *Fig. 6.16*. It can be seen that the temperatures are lower than during field drive. The engine speed during road drive is constant and its value is about 1400 min^{-1} . The vehicle speed is about 30 km/h with third gear. System delta pressure is about 140 bar. Lower temperatures are caused by lower power losses in HST – lower heat generation.

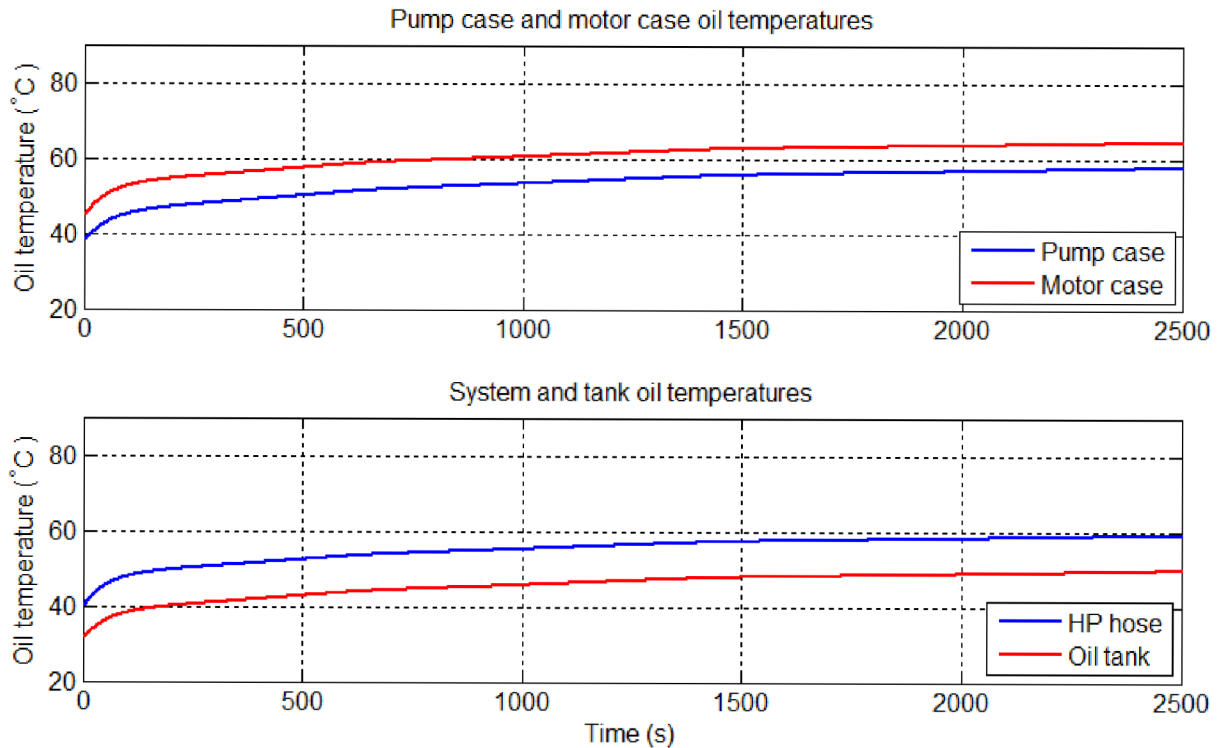


Fig. 6.16: Simulated combine harvester oil temperatures during road drive.

The measured steady oil temperature is 60.5°C in the pump case and 65.7°C in the motor case. The simulation model shows 58°C the pump case oil temperature and 64.7°C the motor case oil temperature. According to the measurements, the measured HP hose oil temperature is 61°C and the simulation provides the average temperature of the both system hoses 59.4°C. The measured tank oil temperature is 51°C, which is very close to the simulated value 49.9°C.

Generally, the temperatures show very good agreement between measurements and simulations in the steady state (final) conditions. Simulated oil temperature increase shows good agreement with measurement too. At the specific conditions, simulations show that the simulated oil temperature increase up to 10% faster than measurement shows. Probably it was caused by model simplifying (neglecting of the heat conduction between HST, using only static model of the cooler or other mentioned above).

All simulation model validations show that the used simulation approach is suitable and both drivetrain models calculate reasonable and acceptable results especially for VCP power saving evaluation.

7 POWER SAVING POTENTIAL




The power saving output is one of the most important outputs of this work. The resultant power saving potential can be easily recalculated to the energy, fuel, emission or cost savings if the relevant data are available. The next important outputs from the simulation are information about the operating parameters like pressures, temperatures, speeds etc. These parameters provide first information about the VCP system suitability and durability for the selected vehicle.

The evaluation of the VCP power saving potential is based on the simulations for typical operating conditions of the selected vehicles [33]. The different vehicle parameters or the different operating conditions can result into different power savings. Due to this, it is necessary to determine parameters of the simulated vehicles and their operating conditions, which are simulated.


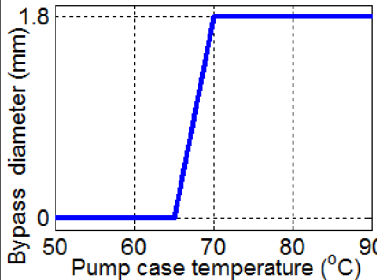
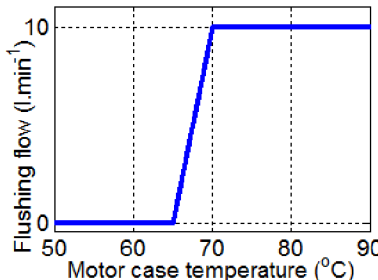
7.1 Analyze Vehicles and their Operating Conditions

The first vehicle is a telehandler which is approximately a two times smaller vehicle with a smaller FCP with the displacement 17 cm^3 , but engine speed varies much during working cycle. Transporting (street drive) was considered also. Parameters of the telehandler used for the power saving evaluation are shown in *Tab. 7.1*. Telehandler flushing parameters are shown in *Tab. 7.2*. The charge pressure setting was approximately 30 bar. The loading of the telehandler cannot be considered as a steady state drive because the vehicle speed varies during this cycle significantly. The ambient air temperature in simulations was assumed as constant ($25 \text{ }^\circ\text{C}$).

Tab. 7.1: Drivetrain parameters of the simulated telehandler.

	Telehandler Parameters			
	Vehicle mass	9000 kg	Pump size	78 cm^3
	Engine power	75 kW	Motor size	110 cm^3
	Wheel radius	0.48 m	Number of gears	2
	Transporting			
	Engine speed	2600 min^{-1}	Pump stroke	100 %
	Vehicle speed	$40 \text{ km}\cdot\text{h}^{-1}$	Motor stroke	50 %
	Gear	2nd	Δp system	165 bar
	Loading			
	Engine speed	$800 \dots 1600 \text{ min}^{-1}$	Pump stroke	100 %
	Vehicle speed	$0 \dots 8 \text{ km}\cdot\text{h}^{-1}$	Motor stroke	25... 100 %
	Gear	1st	Δp system	0... 250 bar



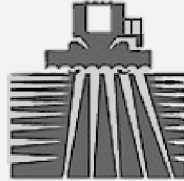
Tab. 7.2: Flushing system parameters of the simulated telehandler.

Telehandler Flushing System Parameters					
	Flushing system	CP	Bypass orifice diameter	Loop flushing flow	
	A	FCP 17 cm ³	None (flow ensured by the CPRV)		10 l·min ⁻¹
	B	VCP 17 cm ³		1.8 mm	10 l·min ⁻¹
C	VCP 17 cm ³				


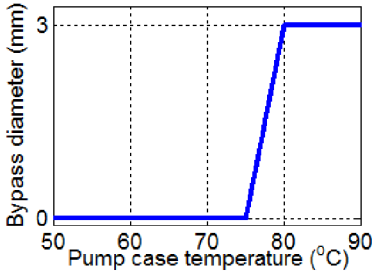
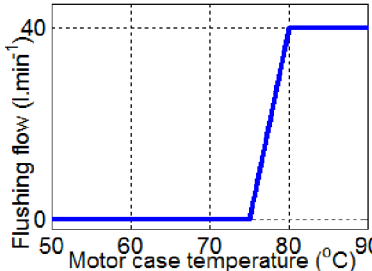
The second simulated vehicle is a combine harvester which practically works only in two modes: harvesting and transporting. The parameters used for the VCP power saving potential evaluation are shown in Tab. 7.3. Used parameters of flushing systems are shown in

Tab. 7.4. Both modes can be considered as steady state, because the combine harvester drives with constant speed on fields and streets for longer time. The simulated vehicle normally uses a relatively big FCP with 40 cm³ displacement. The charge pressure setting was approximately 27 bar.

Tab. 7.3: Drivetrain parameters of the simulated combine harvester.

	Combine Harvester Parameters			
	Vehicle mass	20000 kg	Pump size	165 cm ³
	Engine power	300 kW	Motor size	160 cm ³
	Fr. wheel radius	0.85 m	Number of gears	3
	Transporting			
	Engine speed	1400 min ⁻¹	Pump stroke	100 %
	Vehicle speed	35 km·h ⁻¹	Motor stroke	45 %
	Gear	3rd	Δp system	170 bar
	Harvesting			
	Engine speed	2100 min ⁻¹	Pump stroke	100 %
	Vehicle speed	8.5 km·h ⁻¹	Motor stroke	100 %
	Gear	1st	Δp system	160 bar

Tab. 7.4: Flushing system parameters of the simulated combine harvester.

Combine Harvester Flushing System Parameters					
	Flushing system	CP	Bypass orifice diameter	Loop flushing flow	
	A	FCP 40 cm ³	None (flow ensured by the CPRV)		40 l·min ⁻¹
	B	VCP 40 cm ³	3 mm		40 l·min ⁻¹
C	VCP 40 cm ³				

7.1.1 Telehandler Results for Loading

The first telehandler mode, Y loading cycle (standard working cycle where material is loading on the trailer by wheel loader/telehandler), was simulated with a standard FCP system and a VCP system. The simulated Y cycle is shown in Fig. 7.1.

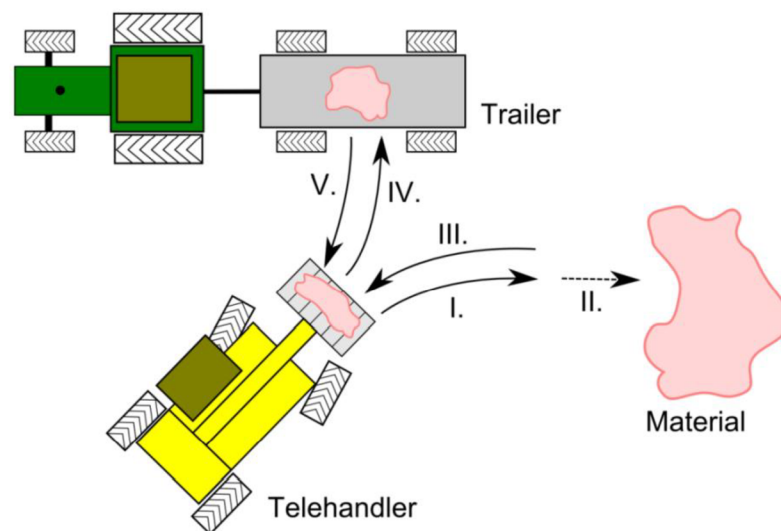


Fig. 7.1: Simulated telehandler Y loading cycle. I. – forward drive to material, II.- slow forward drive – loading, III. – reverse drive with material, IV.-forward drive to trailer, V-reverse drive without material.

This cycle consists of several movements: In the first movement, (I.) telehandler drives forward to approach the material for loading. The second movement (II.) presents the slow forward drive to load the telehandler's bucket with the material. When the material is loaded the telehandler has to move away from material which occurs in reverse drive (III.). When

the reverse drive is finished, the telehandler has to stop. This configuration is shown in *Fig. 7.1*. The forward drive (IV.) gets the telehandler closer to the trailer where the material is loaded on the trailer. When the material is on the trailer and the bucket is empty, the telehandler moves with reverse drive (V.) back to the initial position and the whole cycle repeats.

For the Y cycle simulations presented in *Fig. 7.2* and *Fig. 7.3*, a constant oil temperature of 70 °C is assumed due to the short Y cycle. The rolling resistance corresponds to the asphalt road surface. In this case the power saving potential for the VCP system with the standard loop flushing system and pump bypass orifice for the Y cycle is up to 0.4 kW, depending on the vehicle performance. The highest power savings occur during the pump speed increase when the FCP system delivers more flow than required. This additional flow is then used for pump flushing but the VCP destrokes in these conditions and ensures an almost constant flushing flow for the pump, in similar way the loop flushing works. The *Fig. 7.3* shows the telehandler Y cycle simulation with disabled flushing flows which represents the situation when the oil temperature is lower than setting and the variable flushing orifices are closed. The power saving for these (more theoretical) conditions was up to 1.3 kW again in dependence on the vehicle performance during the cycle.

Previous simulations give the idea about the power savings borders than the idea about real power savings in the operating conditions. Normally the oil in the circuit heats up and power savings change with oil temperature. Due to this, 100 loading cycles were simulated. These simulations, for the standard FCP system and VCP system with standard loop flushing system and 1.8 mm bypass orifice, are shown in *Fig. 7.4*. The ambient temperature was assumed constant 25 °C. The mean power saving at 10th cycle is 0.33 kW and at 100th cycle is 0.28 kW. The oil temperature for VCP and FCP are almost identical. In this case the cooling performance of the VCP with 1.8 mm bypass orifice corresponds to the standard FCP system. Temperatures curves are almost identical. Based on this, it can be concluded that the achieved power saving is based on the VCP efficiency increase, not on the cooling reduction.

The variable flushing system simulation for 100 loading cycles is shown in *Fig. 7.5*. The mean power saving at 10th cycle is 0.9 kW and at 100th cycle it is 0.6 kW. The power saving and oil temperature differences between 10th and 100th cycle are more significant. This was caused by the variable pump and loop flushing system which openings are almost closed at 10th and the VCP displacement is significantly reduced. The maximal power saving occurs at the beginning when the flushing flow is reduced and the oil heats up quickly. At these reduced conditions, vehicle runs only for limited time, thus the saved energy in the CP is not significant. At the beginning, the main pump and motor can bring some additional power saving due to the fast increase of the loop temperature, which has a positive impact on the overall HST drivetrain efficiency.

Following increase of the oil temperature results into demand for more cooling flow and the VCP displacement increase which increases the power consumption and decreases the power saving. The absolute mean power saving with variable flushing is still higher than the flushing system with a bypass orifice what is paid by an acceptable increase of the oil temperature (set by the variable flushing system setting).

From previous Y cycle telehandler simulations can be assumed that the maximal VCP power saving for simulated conditions varies between 0.3 kW and 0.9 kW according to the cooling performance. The mean power saving 0.3 kW is possible to achieve without increase of the oil temperature. The further power saving increase requires oil temperature increase.

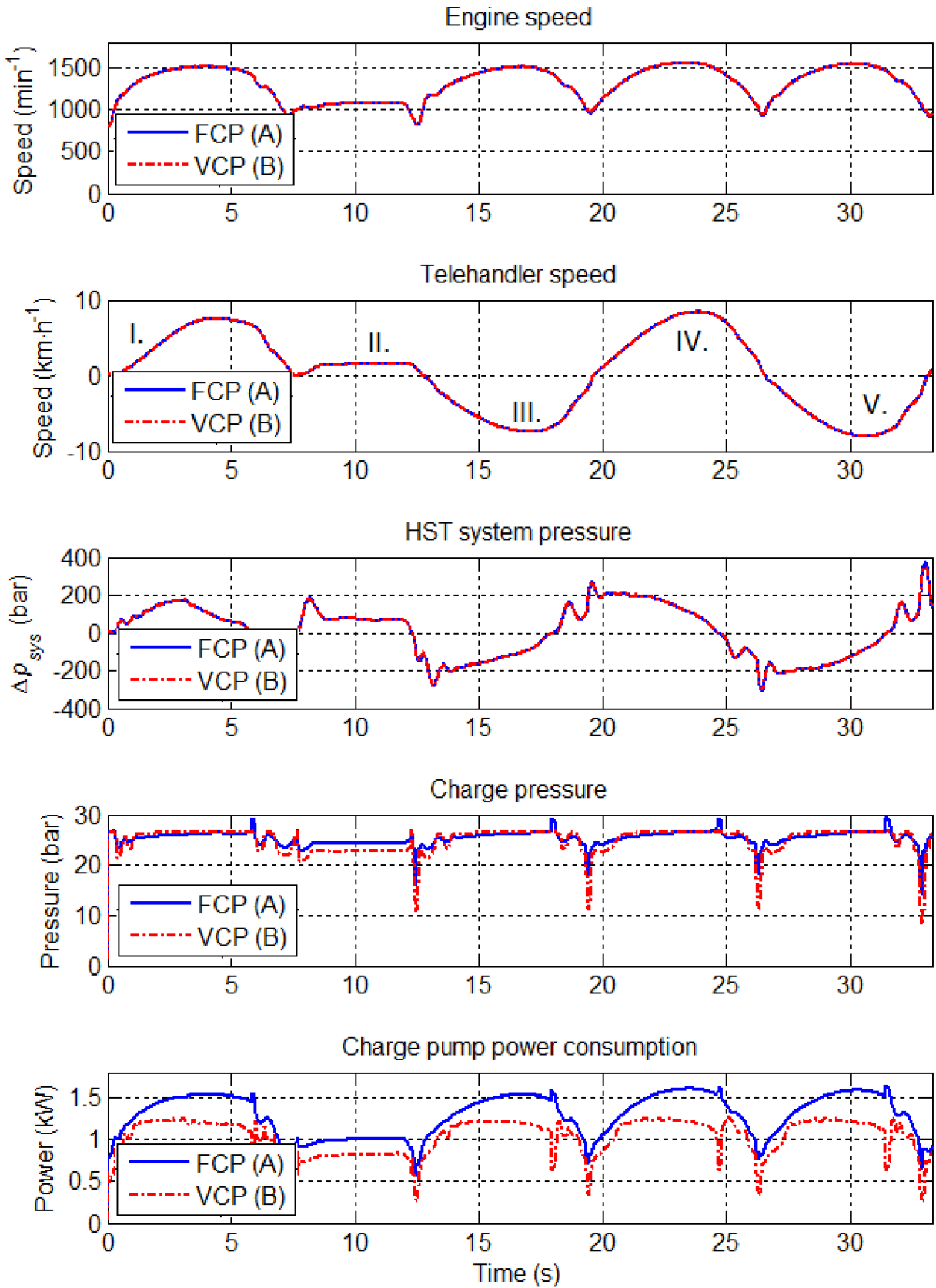


Fig. 7.2: Telehandler Y cycle simulations for the standard FCP system (A) and VCP system (B) with the standard LF system and pump bypass orifice (1.8 mm) with constant oil temperature.

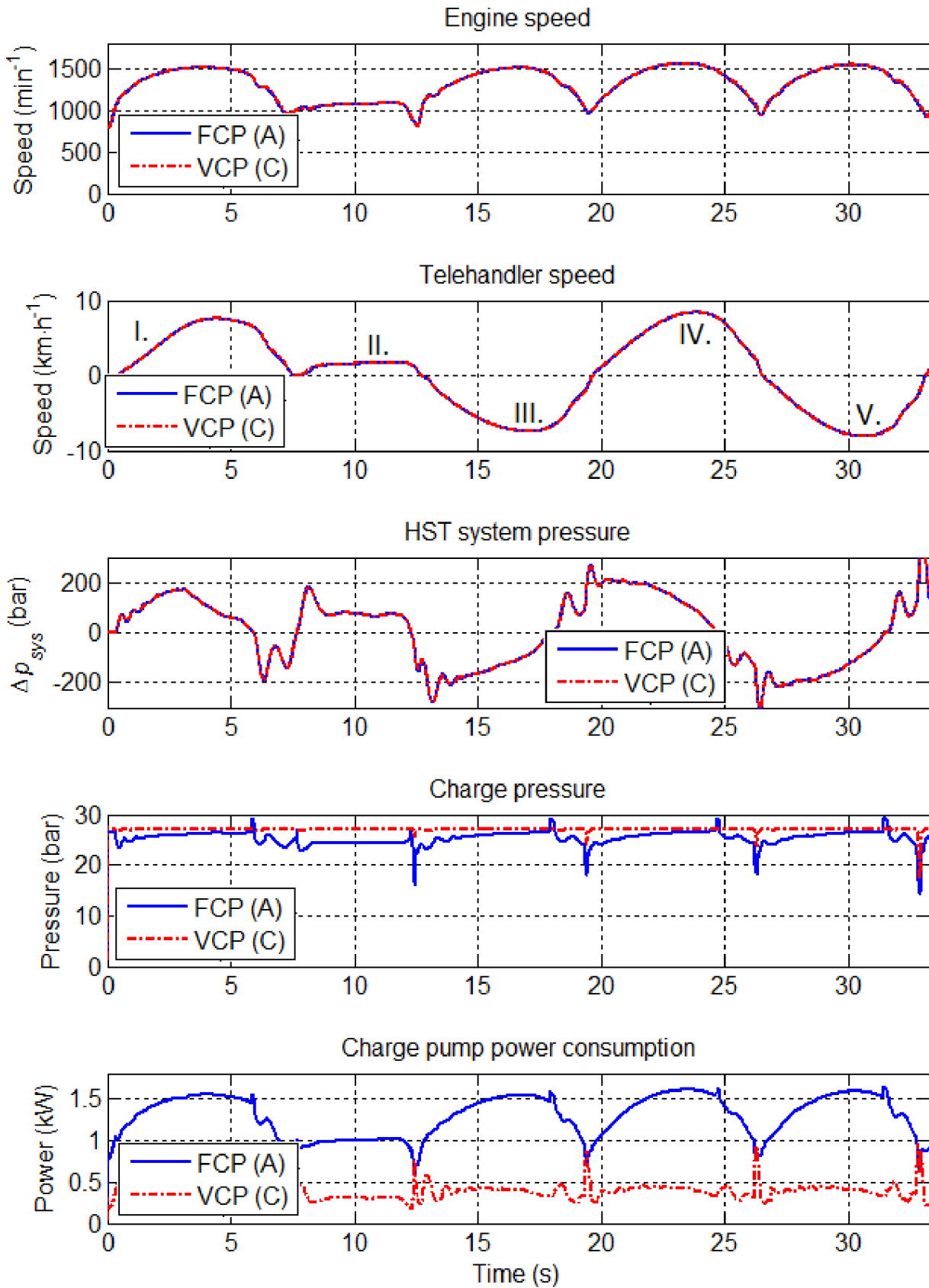


Fig. 7.3: Telehandler Y cycle simulations for the standard FCP system (A) and VCP system (C) with disabled pump and LF (or fully closed variable flushing system) with constant oil temperature.

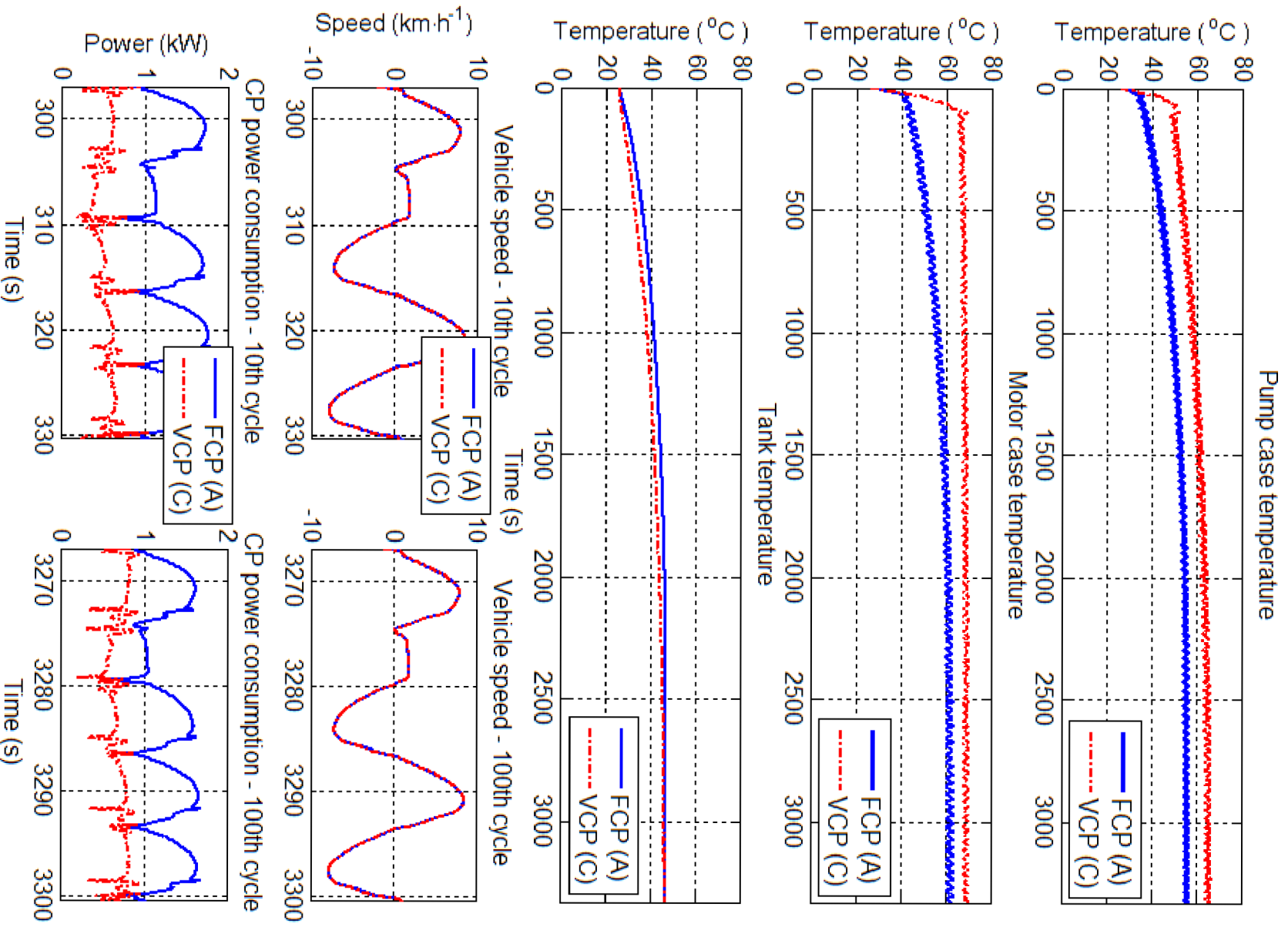


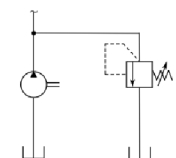


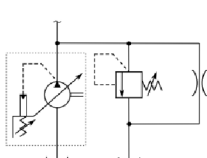


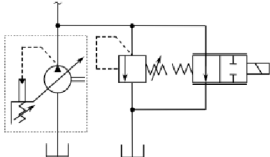


Fig. 7.5: Teledriller Y cycle simulations for the standard FCP system (A) and VCP system (C) with variable pump and LF system fully opened at 80 C.

7.1.2 Telehandler Results for Transport

The second telehandler mode is the maximal speed road drive (Tab. 7.5). This cycle corresponds to the fast telehandler drive on the road. The transport drive confirmed that the flow used for the pump flushing can be at maximal engine speed reduced. The VCP displacement could be reduced also which brings the power saving of approximately 1.2 kW. The variable flushing system with 80 °C setting brings power saving of 1.4 kW in simulated conditions.



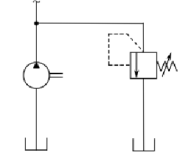
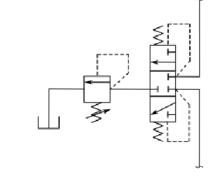


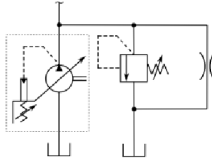
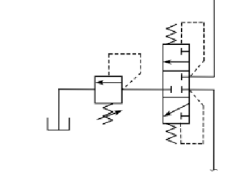


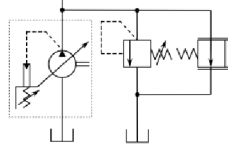
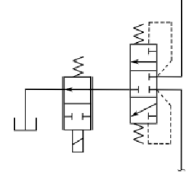
Tab. 7.5: Telehandler transport drive simulations.

	A: FCP 17cm³ (standard system)				
Charge pressure	29.9 bar	Pump case temperature	57.8 °C		
Displacement	100 %	Motor case temperature	81.6 °C		
Power in	3.11 kW	Pump case flow	28.0 l·min ⁻¹		
		Motor case flow	13.2 l·min ⁻¹		
	B: VCP 17cm³ with bypass orifice (1.8 mm bypass orifice)				
Charge pressure	29.6 bar	Pump case temperature	63.2 °C		
Displacement	59 %	Motor case temperature	82.1 °C		
Power in	1.94 kW	Pump case flow	11.2 l·min ⁻¹		
		Motor case flow	13.2 min ⁻¹		
	C: VCP 17cm³ with variable pump and loop flushing system, (settings 80 °C)				
Charge pressure	29.6 bar	Pump case temperature	67.5 °C		
Displacement	51 %	Motor case temperature	82.9 °C		
Power in	1.74 kW	Pump case flow	7.4 l·min ⁻¹		
		Motor case flow	13.2 l·min ⁻¹		

7.1.3 Combine Harvester Results for Transport

The first harvester simulation is transport drive, where the combine harvester drives at max speed on the road, after 30 minutes' drive simulation results were taken. The street drive represents approximately 40% of the vehicle working time.

Tab. 7.6: Combine harvester transport drive simulations.



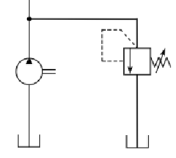
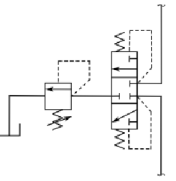


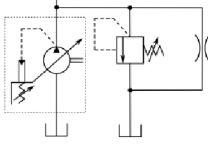
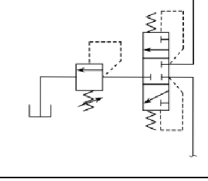


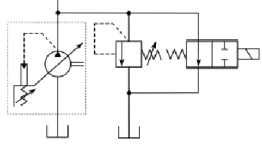
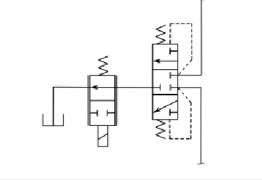
	A: FCP 40cm³ (standard system)			
Charge pressure	23.7 bar	Pump case temperature	56.3 °C	
Displacement	100 %	Motor case temperature	65.5 °C	
Power in	4.37 kW	Pump case flow	27.5 l·min ⁻¹	
		Motor case flow	45.1 l·min ⁻¹	
	B: VCP 40cm³ with bypass orifice (3 mm bypass orifice)			
Charge pressure	27.5 bar	Pump case temperature	56.6 °C	
Displacement	99 %	Motor case temperature	64.7 °C	
Power in	4.54 kW	Pump case flow	25.8 l·min ⁻¹	
		Motor case flow	47.8 l·min ⁻¹	
	C: VCP 40cm³ with variable pump and loop flushing system, (settings 80 °C)			
Charge pressure	27.6 bar	Pump case temperature	75.1 °C	
Displacement	45 %	Motor case temperature	77.4 °C	
Power in	2.36 kW	Pump case flow	8.6 l·min ⁻¹	
		Motor case flow	37.3 l·min ⁻¹	

The power saving of the VCP (Tab. 7.6) without variable flushing flow (bypass orifice and standard loop flushing system) is a negative value -0.17 kW; it means that VCP is not able to save power on the transport driving in comparison to the FCP, which is caused by higher charge pressures. The PC control of VCP is able to keep the charge pressure at a higher level than the charge pressure with the FCP. If the PC control of the VCP will be set lower (at the same level as the FCP), then the VCP will be able to save small amount of input power due to the higher overall efficiency. The biggest impact on the drivetrain at transporting drive has a variable flushing system (orifices). Both variable flushing systems (motor and pump flushing) have thermal setting at 75-80 °C (from closed to full opened flow area). This change allows controlling the flushing flow based on the motor/pump case temperature and brings a power saving about 2 kW with acceptable temperature (1.25 kW for variable flushing setting 65-70 °C).

7.1.4 Combine Harvester Results for Harvesting

The next mode (*Tab. 7.7*) is harvesting mode (60% of working time) where the bigger VCP power saving about 1.7 kW (without the variable flushing systems) occurred due to a decrease of the VCP displacement. It can be seen, that the pump and motor case temperatures are comparable to the FCP system.

Tab. 7.7: Combine harvester harvesting simulations.

	A: FCP 40cm³ (standard system)			
Charge pressure	27.5 bar	Pump case temperature	62.6 °C	
Displacement	100%	Motor case temperature	77.3 °C	
Power in	7.35 kW	Pump case flow	54.0 l·min ⁻¹	
		Motor case flow	50.9.1 l·min ⁻¹	
	B: VCP 40cm³ with bypass orifice (3 mm bypass orifice,)			
Charge pressure	27.6 bar	Pump case temperature	66.6 °C	
Displacement	73 %	Motor case temperature	76.7 °C	
Power in	5.65 kW	Pump case flow	28.3 l·min ⁻¹	
		Motor case flow	47.8 l·min ⁻¹	
	C: VCP 40cm³ with variable pump and loop flushing system, (settings 80 °C)			
Charge pressure	27.6 bar	Pump case temperature	76.5 °C	
Displacement	56 %	Motor case temperature	79.4 °C	
Power in	4.58 kW	Pump case flow	13.4 l·min ⁻¹	
		Motor case flow	45.2 l·min ⁻¹	

The variable flushing system results in a decrease of the VCP displacement (reduction of the flushing flow) and finally, the VCP with a variable flushing system brings power saving up to 2.8 kW with the motor and pump case temperatures up to 80 °C.

Previous simulations show different power savings in dependence on the vehicle type, conditions and charging system configuration but all results show significant dependency of the power saving on the cooling (flushing) performance.

7.2 Recommendations for Sizing of a Variable Charge Pump in HST

The previous experiences from a VCP system modelling can be concluded into some recommendations for the VCP sizing. In the past, the standard FCP was normally sized as a 10% of pump and motor total displacement [2]. According to this rule, HST circuit with the 78 cm³ pump and 110 cm³ requires the 19 cm³ charge pump. A more detailed approach quantifies all leakages and flow consumption which occurs in the circuit. Together with the detail knowledge of the vehicle application, following approach is proposed.

The leakages of the pump and motor (whole HST) can be simply measured or calculated as a function of the pump speed and the system pressure with the highest oil temperatures which can occur in the selected application. The consumption of the pump control and other subsystems like a motor control, parking brake and other systems can be clearly calculated or measured. During the pump or motor displacement change, the servo pistons oil consumption calculation is necessary to consider as part of the control consumption (Q_{contM} , Q_{contP}). Due to fluid compression losses bulk modulus effects has to be added to the total losses which has to be cover with charge pump as well.

The previous investigations can be done with measurements or simply calculated but the charge pump application requires a loop flushing flow definition. If this flow is unknown, it has to be measured or calculated. The standard FCP is normally oversized and the flow which is not used for covering losses in the circuit flows through the CPRV to the pump case where it helps to cool the pump case. Sometimes, the motor drain is connected to the pump case and this motor case flow, which also contains loop flushing flow, ensures the pump case cooling.

The total demand for cooling flow can be calculated from all power losses which occur in a HST. The power losses can be specified in three ways; experimentally, by rough estimation (about 25-30% of HST input power) or simulated with Polymod [53] or similar tool [58]. The specification of the power losses in the HST has to consider not only the losses in the pump and motor but it has to consider all losses which occur in hoses, fittings and also valves. The used approach assumed that all power losses in a HST convert to increased oil temperature. The maximal oil temperature in the circuit is defined according to the component specification. Normally, the hottest spot in HST is a motor case but for the calculation it is better to use the oil temperature in a system hose (loop temperature) T_{Loop} . For each application, we have also a defined maximum temperature of the hydraulic oil. Then the rough estimation of the cooling flow Q_{CF} , demanded for heat removal from the HST, can be written as:

$$Q_{CF} = \frac{(P_{lossPTotal} + P_{lossMTTotal} + P_{lossHose})}{(T_{Loop} - T_{Tank}) \cdot \rho_{oil} \cdot c_{oil}} \quad (7.1)$$

where the total pump loss $P_{lossPTotal}$ is a loss which occurs in the pump housing, which means it is the sum of kit and pressure drop losses, control losses, charge pump losses, CPRV (bypass, in the case of the VCP) losses, check valve losses and HPRV losses. Similarly, total motor losses $P_{lossMTTotal}$ include kit losses and pressure drops, loop flushing losses and motor control losses. These losses used in the numerator of the equation (7.1) can be measured, calculated using efficiency data or simply estimated with overall efficiencies. Losses, which occur in hoses, are included in $P_{lossHose}$. The sum of all losses in the HST is represented by the numerator of the equation (7.1). The denominator contains the oil density ρ_{oil} , the oil

specific heat c_{oil} and the difference between the tank and loop oil temperatures. This temperature difference ($T_{Loop} - T_{Tank}$) provides information about the cooler effectivity. The hot oil is removed from the HST through the case flows. Thus the sum of the pump case flow and the motor case flow has to be equal to the cooling flow according to:

$$Q_{CF} = Q_{CaseP} + Q_{CaseM} = (Q_{CPRV} + Q_{contP} + Q_{leakP} + Q_{caseCP}) + (Q_{LF} + Q_{contM} + Q_{leakM}) \quad (7.2)$$

The equation (7.1) can be plotted again as a function of the pump speed and it has to be calculated for some typical system delta pressures and maximal allowed temperatures. The calculated cooling flow Q_{CF} includes pump case leakages, motor case leakages according to equation (7.2). The difference between calculated cooling flow and case leakages (Q_{contP} , Q_{contM} , Q_{leakP} , Q_{leakM} , Q_{caseCP}) has to be divided between the loop flushing flow Q_{LF} and the CPRV flow Q_{CPRV} (bypass flow in the case of the VCP). The LF valve setting and bypass orifice sizing have to be based on simulations or measurements, because it is difficult to estimate how much of the total unit loss is converted into heat in the case and into the heat in the loop oil. The LF setting and bypass sizing are also based on oil temperatures (pump case, motor case, loop) requirements. The VCP sizing depends on the whole cooling flow Q_{CF} demand, not on the cooling flow redistribution between the pump case and motor case.

The sum of all leakages and flows mentioned in the previous lines can be plotted as a function of the pump speed as shown in Fig. 7.6. The yellow line (1.) represents the HST charge flow demand without demand for cooling (LF flow and bypass flow). The red curve (2.) represents the HST demand for a cooling flow (from equation (7.1)). Normally the difference between the red curve (2) and the yellow curve (1) is covered by the loop flushing flow and the CPRV flow in the HST.

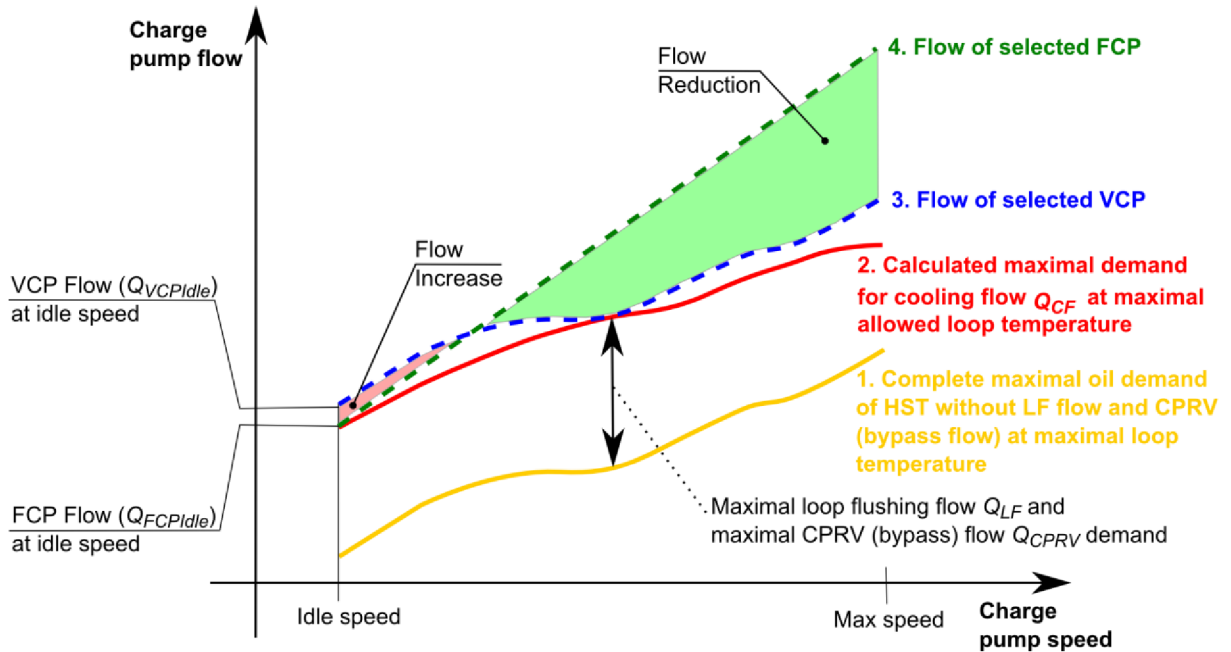


Fig. 7.6: Charge pump flow demands in dependence on the speed.

The flow curve of the designed FCP has to be higher than the red curve. In the presented case the flow curve (4) of proposed FCP is plotted with dotted green line.

The VCP can be designed based on the yellow (1.) curve. The maximal difference between the red (2.) and the yellow (1.) curve is shown by the double arrows in the figure. This flow, which includes the flushing flow and the bypass flow, is taken as constant and added to the yellow line (1.). This results to the blue dotted line (3.) which represents the flow of the proposed VCP.

It can be seen that the VCP flow curve (dotted blue) doesn't follow the red curve ideally, what is caused by the LF and bypass flow, which are considered as constant due to constant charge pressure ensured by the VCP. This caused that the VCP with standard LF system and bypass orifice delivers more flow than is required and more flow than the FCP (red area named as Flow Increase). Theoretically, it can occur only in very rare conditions and probably in the real situations it will never occur. The flow reduction caused by the VCP displacement reduction (green area in the graph) is more significant and it will occur more often. This was also confirmed by previous simulations. The ideal red-curve-following can be ensured only by a variable (intelligent) loop and pump flushing system with a thermal settings corresponding to the maximal allowed oil temperature. The size of the VCP with a variable flushing system should be equal to the VCP size with the bypass orifice and the standard LF system.

The geometrical displacement of the proposed FCP pump or the VCP can be simply calculated from *Fig. 7.7*. This figure shows recalculated theoretical VCP and FCP displacements in the dependence on the pump speed. These displacements were obtained from *Fig. 7.6*. VCP and FCP flows from previous figure (green and blue dotted lines) were divided by the pump speed. In *Fig. 7.7* it can be seen that the FCP displacement is constant and for the VCP displacement, the maximum displacement value has to be chosen. Selected FCP and VCP displacements have to be adjusted according to charge pump volumetric efficiencies.

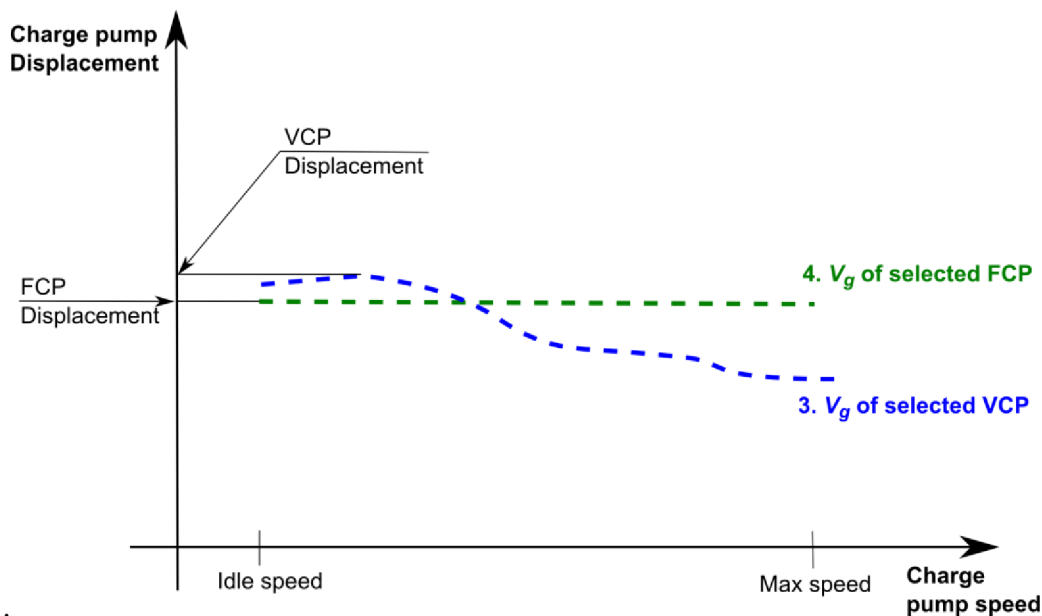


Fig. 7.7: FCP and VCP displacement in dependence on the speed.

It necessary to mention, that the suitable charge pump sizing has to be performed for vehicle operating conditions, where the maximum demand for the charge flow occurs. After the suitable VCP sizing the one dimensional thermal simulations should be performed to confirm the VCP system sizing. Due to the high system complexity measurements will be also required.

The presented approach shows only one example how to set up the charge, LF and bypass system in a HST. Each application can be different and the flow demands of a charge pump can be different in their different operation conditions. Due to this, graphs or calculations shown in *Fig. 7.6* and *Fig. 7.7* have to be evaluated for each application.

This approach doesn't consider effects like heat rejection by componets, heat conduction and etc. But the proposed recommendations for the VCP sizing are on the safe side from the design; of course some safety can be added to the calculation nonetheless.

8 CONCLUSION

The presented thesis gives a holistic view about variable roller charge pumps. At the beginning, the work deals with the theory connected to the selected pump and then continues with the volumetric efficiency modelling and measurements. The work continues with the pump control force analysis and the control comparison. These analyses approach the end with system investigations and finish with the evaluation of the variable charge pump power saving potential in selected mobile machines. The whole thesis can be separated into two parts. The first part is primarily focused on the roller pump and the second part is focused on the system application and power saving evaluation.

At the first part of this thesis, the roller pump functionality was described and the methodology of a 1-D simulation model was developed. The developed simulation model could be used for pressure profile prediction, roller force prediction and cross port leakage prediction which has direct impact on the total volumetric efficiency. The simulation model was successfully used as a tool for optimization of the port plates which was confirmed by several tests. The measurements confirmed the tendency of the effective flow behavior between simulation results and measurements. The developed tool could help to predict the variable roller charge pump volumetric efficiency and in the end, it provides better port plate designs for the roller pumps and solves possible future problems related to the pressure profile. This work provides a good base for next developments in the area of roller pump simulations.

The next model improvement could be achieved by including the external leakage into the model. It should help to calculate more accurately the volumetric efficiency in the simulation model. The implementation of the torque calculation and total efficiency calculation should be a future step in the model development.

Another advantage of the developed model is the cam ring force prediction which could help to improve the performance of actual controls. Also this part of the model was verified. The work deals also with possible controls which can be applied on the variable roller charge pump. Performed basic measurements compared two types of the control and confirmed that the variable roller charge pump is able to work in transmissions with both types of the control. Simulation models provided also explanation of the root reasons for different control performances.

The second part of the work analyzed the potential of a variable charge pump for two typical mobile applications. This part required to perform a 1-D drivetrain simulation model together with thermal behaviour analysis of the HST. The drivetrain simulation of the VCP charging system with a bypass orifice confirms higher power savings only in cases when the pump speed was significantly higher than normal speeds and a relatively constant flushing flow through the bypass orifice to the pump case still ensures suitable cooling. The best simulation results were achieved with variable flushing flows, where the demand for charging flow was adjusted (decreased) according to the HST cooling requirements.

Performed simulations show maximal steady state power savings about 2.8 kW for combine harvester (maximal engine power 300 kW) and about 1.4 kW for telehandler (maximal engine power 75 kW) at simulated conditions. Theoretically further acceptable oil temperature increase could bring further VCP power savings (savings are paid by an oil temperature increase). This idea has to be investigated more because of the leakage increase and other parameter changes due to the oil temperature increase.

Based on previous simulation results, the VCP can only be effective or offer an added value in systems (vehicles) where the full (or a large amount) of the charge flow is not needed in the majority of machine operating time. For example the suitable application could be a HST system where a significant amount of the operating time, the pump runs at zero or very small angle, for example differential steering at track type vehicles or suitable HST application with an oil temperature dependent intelligent flushing (cooling) system. Especially the combination of a suitable HST system and the intelligent variable flushing flow could make with the VCP an interesting solution aimed to decrease the power consumption and in the end the fuel consumption. Theoretically, next system improvements can be achieved with an electronically adjustable PC control, which is able to adjust charge pressure according to the HST demands.

These VCP systems and intelligent flushing (cooling) systems are not used in today's standard HST. The next step is to design and simulate the VCP with the concrete intelligent variable flushing flow and compare fuel savings and VCP system costs, if the VCP implementation is profitable. The electronically controlled PC control for the VCP requires further investigation too.

8.1 Contribution of Doctoral Thesis

From the state of the art point of view, this work brings relatively complex investigation of the variable charge pump design and its system application together with a power saving evaluation. The developed theory and tools will extend the existing state of the art connected not only with the roller pump topic but mainly with variable charge pump systems. The main contribution of this work can be separated into the following points:

- Extension of the variable roller pump theory, which was confirmed by comparison between measurements and simulations [51].
- Development of a methodology for the variable roller pumps optimization with focus on the volumetric efficiency [51].
- Cam ring forces (control spring force) derivation, validated by measurements [34].
- Comparison of selected pressure compensator controls for a variable charge pump and their analysis through linearized VCP control models.
- Novel proposal of variable charge pump implementation into HST [66].
- Power saving potential evaluation for two types of vehicles [66]:
 - Telehandler.
 - Combine harvester.
- Recommendations for pump sizing and proposal of a system layout together with suitable charge systems for maximization of the variable charge pump power savings (variable flushing flow).

The whole work presents a guideline for a sophisticated variable (roller) charge pump development and covers empty spots in the theory. Additionally, methodologies dealing with the variable charge pump design and system applications were shown. Kinematic equations and tool for cross section areas calculation were also implemented into graphic user interface, which is successfully used for VCP design calculations. The value of the knowledge included in this work is highlighted by a real market demand.

REFERENCES

- [1] R. Rahmfeld, *Development and control of energy saving hydraulic servo drives for mobile systems*, Harburg: TU Hamburg - Harburg, 2002, p. 127.
- [2] J. Cundiff, *Fluid Power Circuits and Controls: Fundamentals and Applications (Mechanical Engineering Series)*, Boca Ranton: CRC Press, 2002, p. 533.
- [3] US Environmental Protection Agency, "Clean Air Non road Diesel - Tier 4 Final Rule," US Environmental Protection Agency, [Online]. Available: <http://www.epa.gov/nonroad-diesel/2004fr.htm>. [Accessed 5 August 2012].
- [4] European Commission, "Directives on emissions from non-road mobile machinery," European Commission, [Online]. Available: http://ec.europa.eu/enterprise/sectors/mechanical/documents/legislation/emissions-non-road/index_en.htm. [Accessed 5 8 2010].
- [5] E. A. Prasetyawan, *Modeling, Simulation and Control of an Earthmoving Vehicle Powertrain Simulator*, Urbana, Illinois: University of Illinois at Urbana-Champaign, 2001, p. 143.
- [6] R. Zhang, *Multivariable robust control of nonlinear systems with application to an electro-hydraulic powertrain*, Urbana, Illinois: University of Illinois at Urbana Champaign, 2002, p. 217.
- [7] R. S. Devendram and A. Vacca, "A novel design concept for variable delivery flow external gear pumps and motors," *International Journal of Fluid Power*, vol. 15, pp. 121-137, 27 November 2014.
- [8] I. Nancy and J. Veronis, "Word Sense Disambiguation: The State of the Art. Computational Linguistics 24 (1)," [Online]. Available: <http://sites.univ-provence.fr/~veronis/pdf/1998wsd.pdf>. [Accessed 13 April 2011].
- [9] D. Danardono, K. Kim, E. Roziboyev and C. Kim, "Design and optimization of an LPG roller vane pump for suppressing cavitation," *International Journal of Automotive Technology*, vol. 11, pp. 323-330, 2010.
- [10] N. Zhurba and W. Cleghorn, "Kinematic Solution and Force Layout of a Roller Pump with Internal Outlets," in *Transmission and Driveline Symposium 2000*, Detroit, 2000.
- [11] L. Jiad, Z. Shengchang, D. Hongying, K. X. C. Yulong and Z. Yulin, "Research and Optimization on Slot Profile of Multi Stage and Double-Action Roller Rotary Pump," *Advanced Materials Research*, Vols. 403-408, pp. 3182-3185, November 2011.
- [12] S. C. Zhang, B. B. Lin, J. Lin, H. Y. Deng, Y. C. Zheng and H. S. Fang, "The experimentation study of double-action roller pump for electrical sprayer-used," *Machinery Design & Manufacture*, pp. 33-37, April 2009.

-
- [13] S. C. Zhang, J. D. Lian, H. Y. Deng, Y. L. Ke, X. D. Chen and Y. L. Zhang, "Optimization Design for a Type of Double-action Roller Rotary Pump with High Efficiency," *Oil Field Equipment*, pp. 117-119, Decemeber 2011.
- [14] A. M. Karmel, "A Study of the Internal Forces in a Variable-Displacement Vane-Pump—Part I: A Theoretical Analysis," *Journal of Fluids Engineering*, pp. 227-232, 1986.
- [15] A. M. Karmel, "Modeling and Analysis of the Dynamics of a Variable-Displacement Vane-Pump With a Pivoting Cam," in *American Control Conference*, Minneapolis, 1987.
- [16] A. M. Karmel, "A Study of the Internal Forces in a Variable-Displacement Vane-Pump—Part II: A Parametric Study," *Journal of Fluids Engineering*, pp. 233-237, 1986.
- [17] T. B. Li, *Actuation, Design and Control of a Variable Displacement Vane Pump for Valveless Hydraulic*, Nashville: Vanderbilt University, 2008, p. 49.
- [18] P. Dean, *Modern Control Design for a Variable Displacement Hydraulic Pump*, University of Missouri-Columbia, 2006, p. 104.
- [19] J. Meira, A. Filho, W. Melo and E. Ribeiro, "Startegies for energy savings with use of constatnt and variable oil pump systems," in *Congresso 2011 SAE Brasil*, Sao Paulo, 2011.
- [20] J. Ivantysyn and M. Ivantysynova, *Hydrostatic pumps and motors: Principles, Design, Performance, Modelling, Analysis, Control and Testing*, New Delhi: Akademia Books International, 2001, p. 512.
- [21] E. C. Fitch and I. T. Hong, *Hydraulic Component Design and Selection*, Stillwater, Oklahoma: BarDyne, Inc., 2004, p. 633.
- [22] E. C. Fitch and T. I. Hong, *Hydraulic System Modeling and Simulation*, Stillwater, Oklahoma: BarDyne, Inc., 2001, p. 291.
- [23] N. Manring, *Hydraulic Control Systems*, Hoboken: John Willey & Sons, 2005, p. 446.
- [24] P. Noskievic, *Modelovani a identifikace systemu*, Ostrava: Montanex a.s., 1999, p. 276.
- [25] J. Turza, *Dynamika tekutinovych systemov*, Zilina: Strojnicka Fakulta VSDS Zilina, 1994, p. 226.
- [26] F. Nepraz, J. Nevrlý, V. Penaz and K. Tretina, *Modelovani systemu s hydraulickymi mechanizmy*, Brno: Bosch Rexroth, 2002, p. 173.
- [27] Venom Performance, "Fuel Pumps," [Online]. Available: http://www.venom-performance.com/catalog/fuel_pump.pdf?content=high_flow_fuel_pump. [Accessed 24 August 2014].
- [28] Pentair, "Hypro pumps," Hypro pumps, [Online]. Available: <http://www.hypropumps.com/EngineeredSearchResults.aspx#ProductType=Roller+%26+Gear+Pumps|isAccessory=false>. [Accessed 24 August 2014].
-

-
- [29] F. Pintore, M. Borghi, R. Morselli, A. Benevelli, B. Zardin and F. Belluzzi, "Modelling and Simulation of the Hydraulic Circuit of an Agricultural Tractor," in *8th FPNI Ph.D Symposium on Fluid Power*, Lappeenranta, 2014.
- [30] P. Kucik, I. Strazovec and P. Krissak, *Hydraulicky prenos energie, Mobilne pracovne stroje*, Zilina: EDIS, 2000, p. 384.
- [31] A. Akers, M. Gassman and R. Smith, *Hydraulic Power System Analysis*, Boca Raton: CRC Taylor & Francis, 2006, p. 365.
- [32] P. Chapple, *Principles of Hydraulic Systems Designs*, Oxford: Information Press, 2003, p. 268.
- [33] A. Schumacher, R. Rahmfeld and E. Skirde, "Best Point Control - Energetisches Einsparpotenzial eines Antriebsstrang-Managementsystems," in *VDI Conference Transmissions in Mobile Machines*, Friedrichshafen, 2011.
- [34] P. Zavadinka and R. Grepl, "Cam Ring Force Simulation for Variable Roller Pump," in *Mechatronics 2013*, Brno, 2013.
- [35] Magna, "Variable Flow Oil Pump," Magna International Inc., 2014. [Online]. Available: <http://www.magna.com/innovation/fuel-efficiency/innovation/variable-flow-oil-pump-> [Accessed 19 November 2014].
- [36] ZF Lenksysteme, "Variable Displacement Pump Varioserv," [Online]. Available: http://www.zflenksysteme.com/fileadmin/_migrated/content_uploads/ZF_Varioserv_E_08.pdf. [Accessed 19 November 2014].
- [37] Bosch Rexroth, "Hydraulic Vane Pumps," Bosch Rexroth, [Online]. Available: <http://www.boschrexroth.com/en/us/products/product-groups/industrial-hydraulics/pumps/vane-pumps/index>. [Accessed 19 November 2014].
- [38] Parker Hannifin Corporation, "Vane Pumps," Parker Hannifin Corporation, 2014. [Online]. Available: <http://www.parker.com/portal/site/PARKER/menuitem.7100150cebe5bbc2d6806710237ad1ca/?vgnextoid=f5c9b5bbec622110VgnVCM10000032a71dacRCRD&vgnextfmt=EN&vgnextcatid=16220530&vgnextcat=VANE+PUMPS>. [Accessed 19 November 2014].
- [39] A. Perry, "Application of control theory to the improvement of a vane pump for faster dynamic response," in *Proceedings of the 6th JFPS International*, Tsukuba, 2005.
- [40] H. E. Merritt, *Hydraulic Control Systems*, New York: John Wiley & Sons, Inc., 1967, p. 366.
- [41] N. D. Manring, *Fluid Power Pumps & Motors: Analysis, Design and Control*, New York: Mc Graw Hill Education, 2013, p. 304.
- [42] J. Koreis, *Modelovani prenosu vykonu a informace*, Pardubice: Univerzita Pardubice, 2002, p. 178.
- [43] J. Balate, *Automaticke rizeni, Praha: BEN - technicka literatura*, 2004, p. 664.
-

-
- [44] W. Forsythe and R. M. Goodall, *Digital Control; Fundamentals, Theory and Practice*, London: McGraw-Hill, Inc., 1991, p. 256.
- [45] SAE International, "SAE Standards," [Online]. Available: http://standards.sae.org/j745_200906/. [Accessed 13 September 2014].
- [46] D. Rosinova and M. Dubravaska, *Optimalizacia*, Bratislava: Slovenska Technicka Univerzita v Bratislave, 2007, p. 190.
- [47] K. Dongjune and M. Ivantysynova, "Valve plate optimization focusing on noise reduction in the axial piston machine with high volumetric efficiency," in *7th FPNI PhD Symposium on Fluid Power*, Reggio Emilia, 2012.
- [48] A. Schenk, M. Zecchi and M. Ivantysynova, "Accurate Prediction of Axial Piston Machine's Performance Through a Thermo-Elasto-Hydrodynamic Simulation Model," in *ASME/BATH 2013 Symposium on Fluid Power and Motion Control*, Bath, 2013.
- [49] G. K. Seeniraj and M. Ivantysynova, "Impact of Valve Plate Design on Noise, Volumetric Efficiency and Control Effort in an Axial Piston Pump," in *ASME 2006 International Mechanical Engineering Congress and Exposition*, Chicago, 2006.
- [50] P. Casoli, A. Vacca and G. L. Berta, "Optimization of relevant design parameters of external gear pumps," in *Proceedings of the JFPS International Symposium on Fluid Power*, Toyama, 2008.
- [51] P. Zavadinka and R. Grepl, "Simulation based optimization methodology of Port Plates for Roller Pumps," in *Proceedings of the 7th FPNI PhD Symposium on Fluid Power*, Regio Emilia, 2012.
- [52] G. Kreisselmeier and R. Steinhauser, "Systematic Control Design by Optimizing a Vector Performance Index," *IFAC Symposium on Computer Aided Design of Control Systems*, pp. 113-117, 1979.
- [53] D. Mikeska and M. Ivantysynova, "A precise steady state model of displacement machines for the application in virtual prototyping of power split drives," in *2nd FPNI PhD Symposium on Fluid Power*, Modena, 2002.
- [54] W. Post, *Determination of the steady-state performance of a 20 cm³ Innas Variable Floating Cup Pump*, Eindhoven: Eindhoven University of Technology, 2010, p. 47.
- [55] Danfoss Power Solutions, "H1 family - closed circuit pumps & motors," 2013. [Online]. Available: <http://powersolutions.danfoss.com/Products/PistonPumpsandMotors/H1FamilyClosedCircuitPumpsMotors/index.htm>. [Accessed 22 April 2014].
- [56] P. Zavadinka and P. Krissak, "Modeling and simulation of diesel engine for mobile working machine powertrain," in *Hydraulics and pneumatics 2009*, Wroclaw, 2009.
- [57] U. Kiencke and L. Nielsen, *Automotive Control Systems*, Berlin: Springer-Verlag Berlin Heidelberg, 2005, p. 512.
-

-
- [58] J. Krchnar, J. Koneracky, R. Olsiak, K. Prikkel and K. Stracar, *Technicka diagnostika rotacnych hydrostatickych pohonov*, Bratislava: Slovenska Technicka Univerzita v Bratislave, 2010, p. 119.
- [59] P. Zavadinka and P. Krissak, "Modeling and simulation of mobile working machine powertrain," in *Technical Computing Prague 2009*, Prague, 2009.
- [60] I. S. Al-Natour, *Study of an open circuit hydraulic power system with compact cooler-reservoir unit*, Dublin: Dublin City University, 1992.
- [61] C. G. LI and Z. X. Jiao, "Thermal-hydraulic modeling and simulation of piston pump," *Chinese Journal of Automatics*, vol. IXX, pp. 354-358, 2006.
- [62] A. J. Siders, T. G. D. and J. P. Chapple, "Thermal-Hydraulic Performance Prediction in Fluid Power Systems," *Proceedings of The Institution of Mechanical Engineers Part I-journal of Systems and Control Engineering*, vol. 210, no. 49, pp. 231-242, 1996.
- [63] E. Busquets and M. Ivantysynova, "Thermal-hydraulic behavior prediction of a valve controller wheel loader," in *22nd International Conference on Hydraulics and Pneumatics*, Prague, 2011.
- [64] E. Busquets and M. Ivantysynova, "Cooling power reduction of displacement controlled multi actuator," in *Proceedings of the 7th FPNI PhD Symposium on Fluid Power*, Reggio Emilia, 2012.
- [65] KTR, "KTRComponents for Construction and Agricultural Equipment," [Online]. Available: http://www.ktr.com/fileadmin/ktr/media/Tools_Downloads/kataloge/ktr-kat99BB01.pdf. [Accessed 13 5 2015].
- [66] P. Zavadinka and R. Grepl, "Energy Power Saving Potential of Hydrostatic Drivetrain with Variable Charge Pump," in *8th FPNI Ph.D. Symposium on Fluid Power*, Lappeenranta, 2014.

References cited according to IEEE 2006.

AUTHOR'S PUBLICATIONS

1. P. Zavadinka and P. Krissak, "Simulacny model dieseloveho motora," *Acta Hydraulica et Pneumatica*, pp. 34-38, ISSN 1336-7536, 1/2009.
2. P. Zavadinka and P. Krissak, "Modeling and simulation of mobile working machine powertrain," in *Technical Computing*, p. 13, ISBN 978-80-7080-733-0, Prague, Czech Republic, 2009.
3. P. Zavadinka and P. Krissak, "Modeling and simulation of diesel engine for mobile working machine powertrain," *Hydraulics and pneumatics 2009*, pp. 339-348, ISBN 978-83-87982-34-8, Wroclaw, Poland, 2009.
4. M. Imre, R. Rahmfeld, P. Zavadinka and P. Krissak, "Simulation model of priority flow control valve compared with a flow compensation tests results," *Hydraulika a pneumatika*, pp. 25-28, ISSN 1335-5171, 1-2/2010.
5. P. Zavadinka and P. Krissak, "Dynamicky model vozidla pri prejazde zakrutou," *Hydraulika a pneumatika*, pp. 53-57, ISSN 1335-5171, 1-2/2010.
6. M. Imre, P. Krissak, R. Rahmfeld and P. Zavadinka, "Porovnanie simulacnych a meranych vysledkov prietokoveho ventila," in: *Riadenie tekutinových systemov 2010*, pp. 8-15, ISBN 978-80-968150-6-7, Vysne Ruzbachy, Slovakia, 2010.
7. P. Zavadinka, "Simulation of vehicle transport duty cycle with using of hydrostatic units control algorithm," in *Mechatronics 2011*, pp. 395-402, ISBN 978-3-642-23243-5, Warsaw, Poland 2011.
Scopus link: <http://www.scopus.com/inward/record.url?eid=2-s2.0-84903790828&partnerID=40&md5=884021d6fd52afe62692932cf4c0d48f>
8. P. Zavadinka and P. Krissak, "Simulation of vehicle working conditions with hydrostatic pump and motor control algorithm," *JAMRIS (Journal of Automation, Mobile Robotics & Intelligent Systems)*, pp. 40-46, ISSN 1897-8649, 3/2012.
9. P. Zavadinka and R. Grepl, "Simulation based optimization methodology of Port Plates for Roller Pumps," in *7th FPNI PhD Symposium on Fluid Power*, pp. 37-54, ISBN 978-88-7559-069-7, Regio Emilia, Italy, 2012.
10. P. Zavadinka and R. Grepl, "Cam Ring Force Simulation for Variable Roller Pump," in *Mechatronics 2013*, Brno, pp. 199-206, ISBN 978-3-319-02293-2, Czech Republic, 2013.
Scopus link: <http://www.scopus.com/inward/record.url?eid=2-s2.0-84903790828&partnerID=40&md5=884021d6fd52afe62692932cf4c0d48f>
11. P. Krissak, J. Jakubovic and P. Zavadinka, "Transport Duty Cycle Simulation of Electro-hydro-mechanical Drive Unit for mixing Drum," in: *Mechatronics 2013*, pp. 235-241, ISBN 978-3-319-02293, Brno, Czech Republic, 2013.
Scopus link: <http://www.scopus.com/inward/record.url?eid=2-s2.0-84903790213&partnerID=40&md5=f772bde485a2c5323a2ab13f2d5f6884>
12. P. Zavadinka and R. Grepl, "Energy Power Saving Potential of Hydrostatic Drivetrain with Variable Charge Pump," in *8th FPNI PhD Symposium on Fluid Power*, p. 7, ISBN 978-0-7918-4582-0, Lappeenranta, Finland, 2014.
Scopus link: <http://www.scopus.com/inward/record.url?eid=2-s2.0-84912100543&partnerID=40&md5=79fbbe36d3e53684a0543c10659a3ac4>

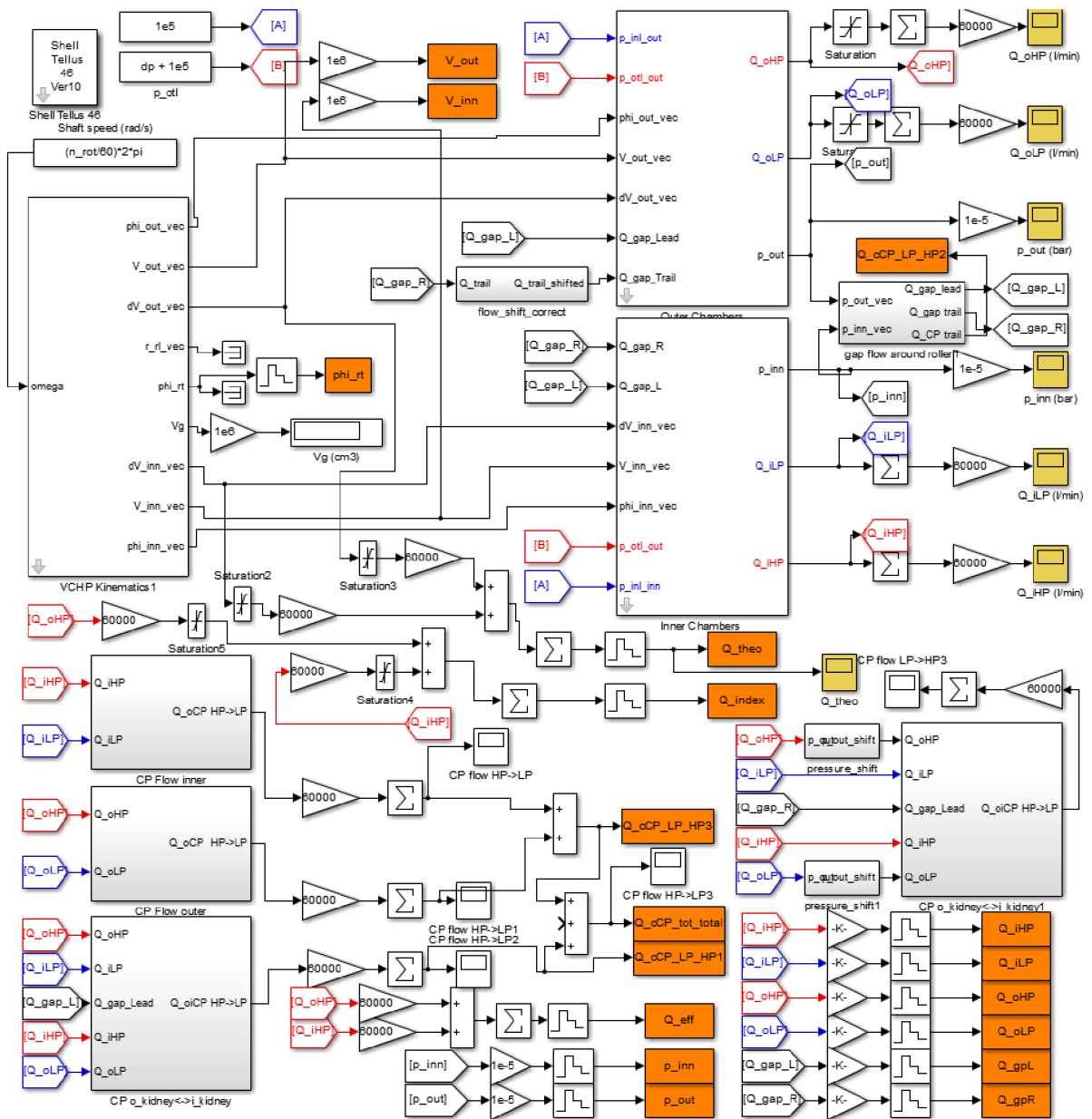
13. L. Jakubovicova, P. Zavadinka and J. Jakubovic, "Transport duty cycle measurement of hybrid drive unit for mixing drum," in *Mechatronics 2015*, Warsaw, Poland, 2015, in print.

Patent Application

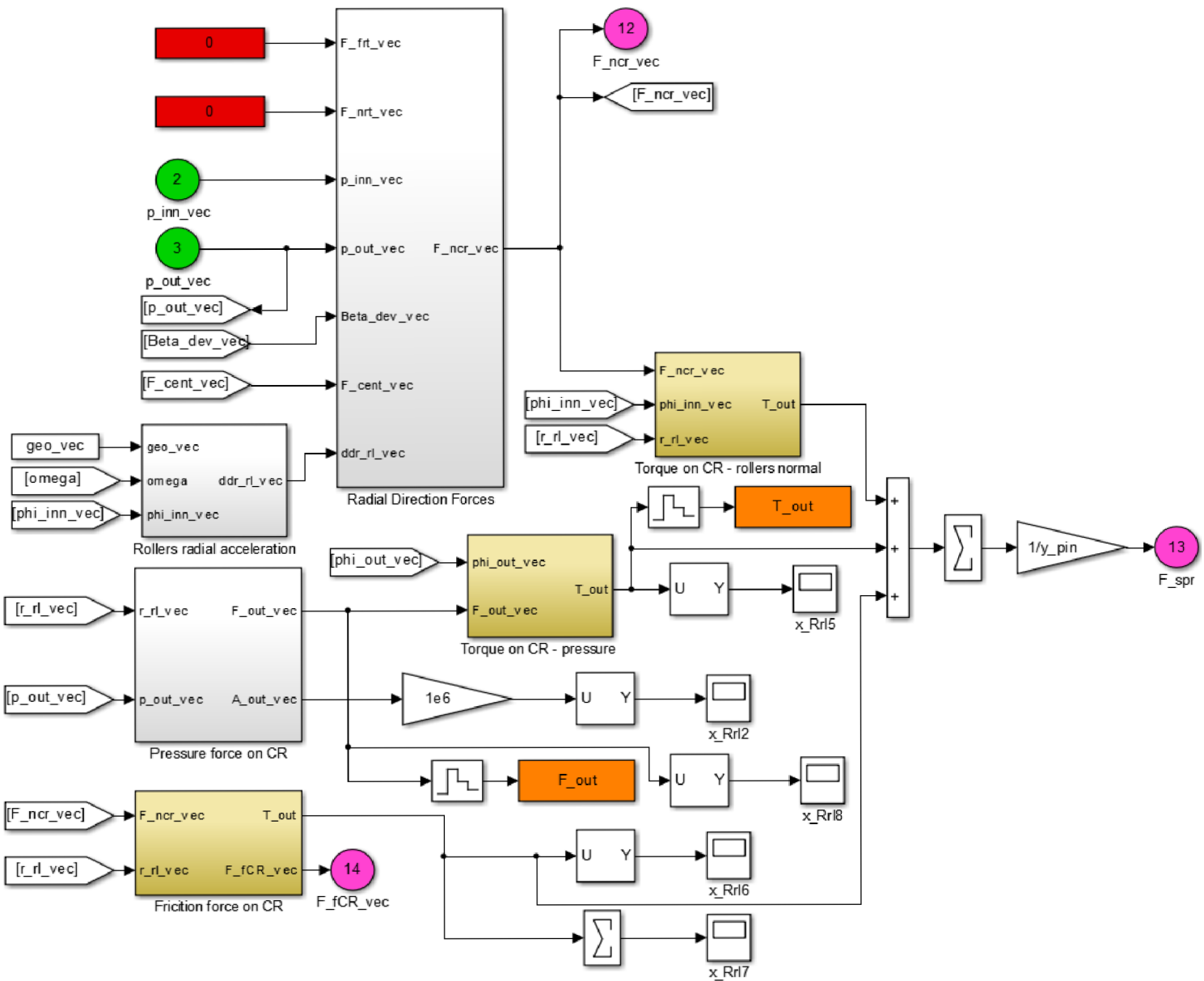
P. Zavadinka, S. Smolka and P. Sedo, "Control unit for hydraulic variable displacement pumps and variable displacement pump with a control unit US20150050165A1", *Patent application*, also published as DE102013216395A1, 2013,
Available at: <http://www.google.com/patents/US20150050165>, [Accessed 12 May 2015]

ATTACHMENTS

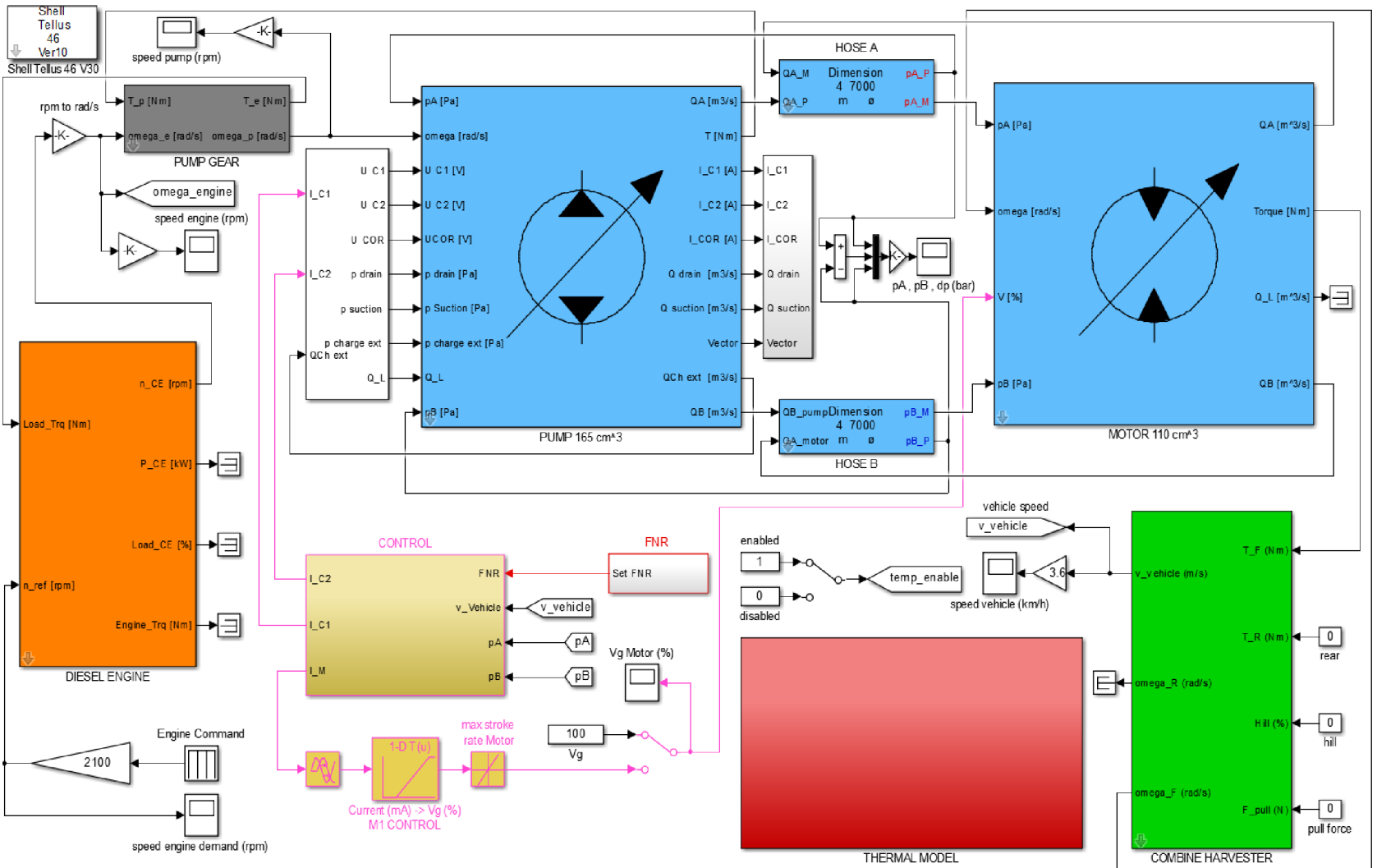
A1: Roller pump simulation model in Simulink (Chapter 5.1).



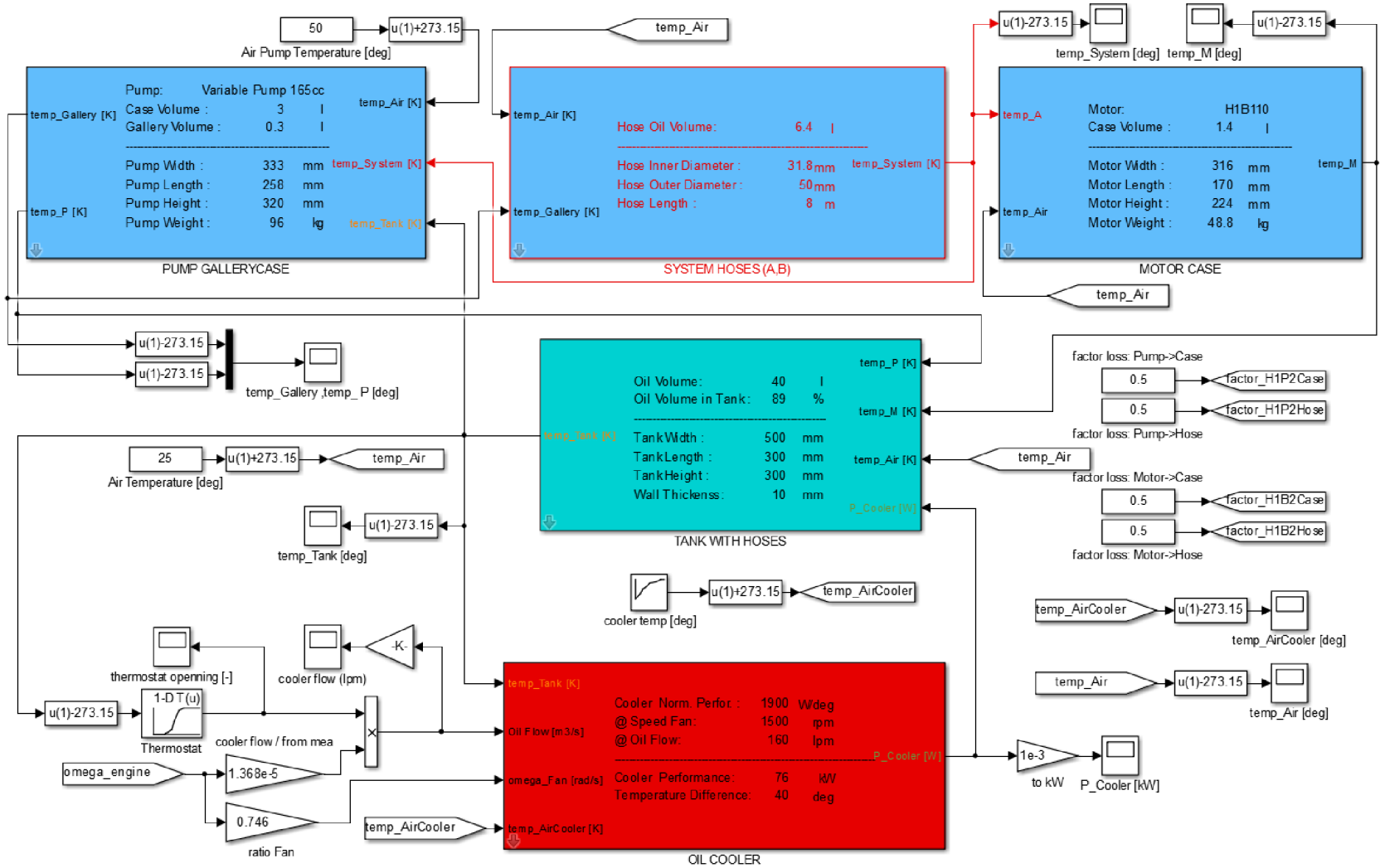
A2: Spring force simulation model in Simulink (Chapter 5.1).



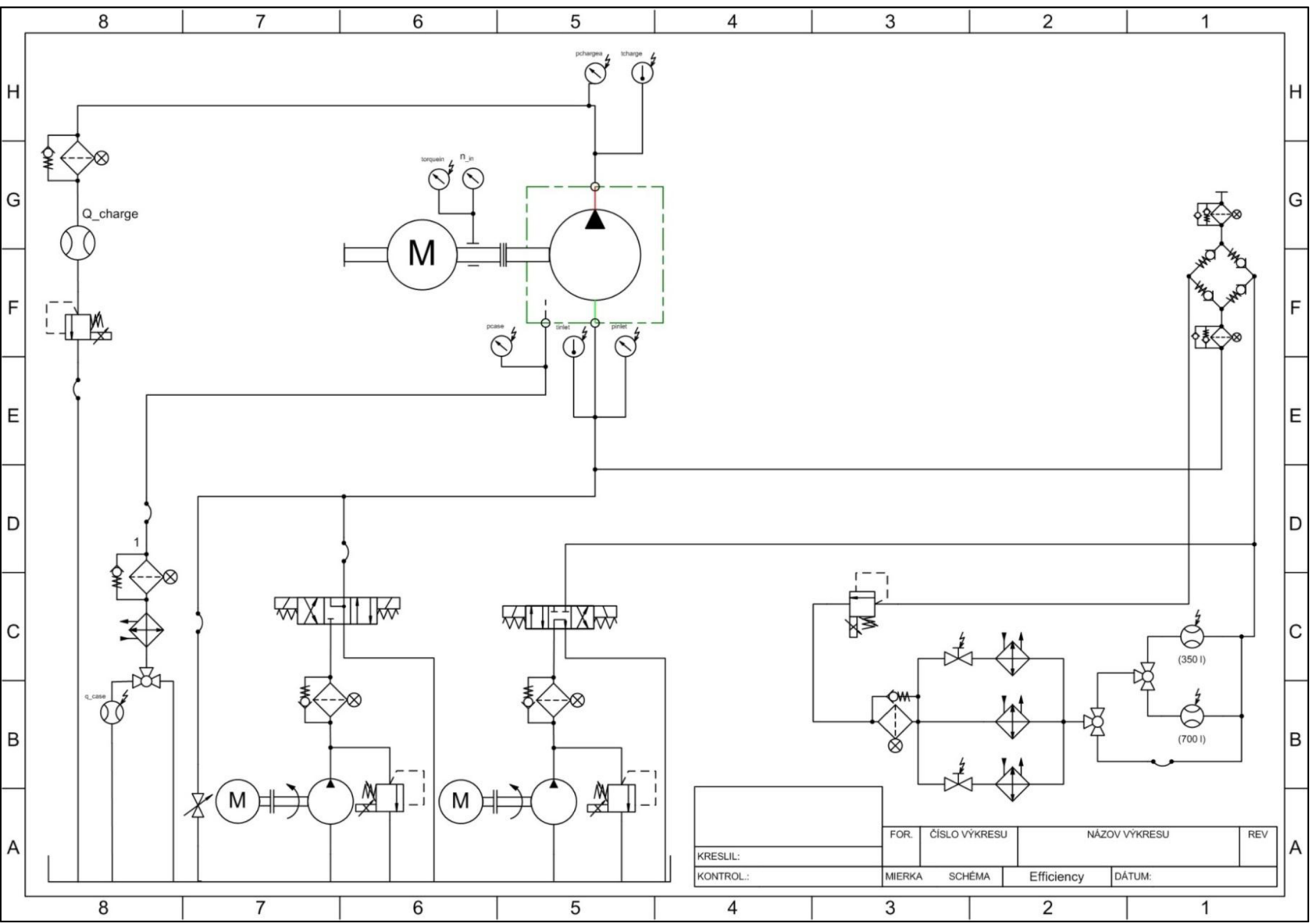
A3: Drivetrain simulation model in Simulink (Chapter 6.2.3).



A4: Thermal simulation model in Simulink (Chapter 6.2.3).



A5: Test stand hydraulic diagram for efficiency measurements (Chapter 5.4.1).



A6: Test stand hydraulic diagram for spring force measurements (Chapter 5.4.2).

